Journal Pre-proof

Intestinal host response to SARS-CoV-2 infection and COVID-19 outcomes in patients with gastrointestinal symptoms

Alexandra E. Livanos, Divya Jha, Francesca Cossarini, Ana S. Gonzalez-Reiche, Minami Tokuyama, Teresa Aydillo, Tommaso L. Parigi, Mark S. Ladinsky, Irene Ramos, Katie Dunleavy, Brian Lee, Rebekah Dixon, Steven T. Chen, Gustavo Martinez-Delgado, Satish Nagula, Emily A. Bruce, Huaibin M. Ko, Benjamin S. Glicksberg, Girish Nadkarni, Elisabet Pujadas, Jason Reidy, Steven Naymagon, Ari Grinspan, Jawad Ahmad, Michael Tankelevich, Yaron Bram, Ronald Gordon, Keshav Sharma, Jane Houldsworth, Graham J. Britton, Alice Chen-Liaw, Matthew P. Spindler, Tamar Plitt, Pei Wang, Andrea Cerutti, Jeremiah J. Faith, Jean-Frederic Colombel, Ephraim Kenigsberg, Carmen Argmann, Miriam Merad, Sacha Gnjatic, Noam Harpaz, Silvio Danese, Carlos Cordon-Cardo, Adeeb Rahman, Robert E. Schwartz, Nikhil A. Kumta, Alessio Aghemo, Pamela J. Bjorkman, Francesca Petralia, Harm van Bakel, Adolfo Garcia-Sastre, Saurabh Mehandru

PII: S0016-5085(21)00461-3
DOI: https://doi.org/10.1053/j.gastro.2021.02.056
Reference: YGAST 64177

To appear in: *Gastroenterology*
Accepted Date: 23 February 2021

Please cite this article as: Livanos AE, Jha D, Cossarini F, Gonzalez-Reiche AS, Tokuyama M, Aydillo T, Parigi TL, Ladinsky MS, Ramos I, Dunleavy K, Lee B, Dixon R, Chen ST, Martinez-Delgado G, Nagula S, Bruce EA, Ko HM, Glicksberg BS, Nadkarni G, Pujadas E, Reidy J, Naymagon S, Grinspan A, Ahmad J, Tankelevich M, Bram Y, Gordon R, Sharma K, Houldsworth J, Britton GJ, Chen-Liaw A, Spindler MP, Plitt T, Wang P, Cerutti A, Faith JJ, Colombel J-F, Kenigsberg E, Argmann C, Merad M, Gnjatic S, Harpaz N, Danese S, Cordon-Cardo C, Rahman A, Schwartz RE, Kumta NA, Aghemo A, Bjorkman PJ, Petralia F, van Bakel H, Garcia-Sastre A, Mehandru S, Intestinal host response to SARS-CoV-2 infection and COVID-19 outcomes in patients with gastrointestinal symptoms, *Gastroenterology* (2021), doi: https://doi.org/10.1053/j.gastro.2021.02.056.

during the production process, errors may be discovered which could affect the content, and all legal disclaimers that apply to the journal pertain.

Title: Intestinal host response to SARS-CoV-2 infection and COVID-19 outcomes in patients with gastrointestinal symptoms

Authors: Alexandra E. Livanos[1,2]*, Divya Jha[1,2]*, Francesca Cossarini[1,3]*, Ana S. Gonzalez-Reiche[4]* Minami Tokuyama[1,2]*, Teresa Aydillo[5,21]*, Tommaso L. Parigi[6]*, Mark S. Ladinsky[7], Irene Ramos[8], Katie Dunleavy[9], Brian Lee[10], Rebekah Dixon[2], Steven T. Chen[1,11], Gustavo Martinez-Delgado[1,2], Satish Nagula[2], Emily A. Bruce[12], Huaibin M. Ko[13,2], Benjamin S. Glicksberg[4,14], Girish Nadkarni[9,14,15,16] , Elisabet Pujadas[13], Jason Reidy[13], Steven Naymagon[2], Ari Grinspan[2], Jawad Ahmad[2], Michael Tankelevich[1,2], Yaron Bram[20], Ronald Gordon[13], Keshav Sharma[1,2], Jane Houldsworth[13], Graham J. Britton[1,18], Alice Chen-Liaw[1,18], Matthew P. Spindler[1,18], Tamar Plitt[1,18], Pei Wang[4], Andrea Cerutti[1,19,20], Jeremiah J. Faith[1,18], Jean-Frederic Colombel[1,2], Ephraim Kenigsberg[1,4], Carmen Argmann[4], Miriam Merad[1,9,10,11], Sacha Gnjatic[1,9,10,11,13], Noam Harpaz[13], Silvio Danese[6], Carlos Cordon-Cardo[4,11,13], Adeeb Rahman[1,4,10,11], Robert E. Schwartz[20], Nikhil A. Kumta[2], Alessio Aghemo[6], Pamela J. Bjorkman[7], Francesca Petralia[4†], Harm van Bakel[4,17†], Adolfo Garcia-Sastre[3,5,21†] and Saurabh Mehandru[1,2†]

* These authors contributed equally to this work.

Affiliations:

[1]Precision Immunology Institute, Icahn School of Medicine at Mount Sinai, New York, NY 10029, USA

[2]The Dr. Henry D. Janowitz Division of Gastroenterology, Department of Medicine, Icahn School of Medicine at Mount Sinai, New York, NY 10029, USA

[3]Division of Infectious Disease, Department of Medicine, Icahn School of Medicine at Mount Sinai, New York, NY 10029, USA

[4]Department of Genetics and Genomic Sciences, Icahn School of Medicine at Mount Sinai, New York, NY 10029, USA

[5]Department of Microbiology, Icahn School of Medicine at Mount Sinai, New York, NY 10029, USA

[6]Department of Biomedical Sciences, Humanitas University, Milan, Italy

[7]Division of Biology and Biological Engineering, California Institute of Technology, Pasadena, CA 91125, USA

[8]Department of Neurology and Center for Advanced Research on Diagnostic Assays, Icahn School of Medicine at Mount Sinai, New York, NY 10029, USA

[9]Department of Medicine, Icahn School of Medicine at Mount Sinai, New York, NY 10029, USA

[10]Human Immune Monitoring Center (HIMC) Icahn School of Medicine at Mount Sinai New York, New York, NY 10029, USA
[11]Department of Oncological Sciences, Icahn School of Medicine at Mount Sinai, New York, NY 10029, USA
[12]Division of Immunobiology, Department of Medicine, University of Vermont, Larner College of Medicine, 89 Beaumont Avenue, Burlington, VT 05405
[13]Department of Pathology, Molecular and Cell Based Medicine Icahn School of Medicine at Mount Sinai, New York, NY 10029, USA
[14]The Hasso Plattner Institute for Digital Health at Mount Sinai, Icahn School of Medicine at Mount Sinai, New York, NY 10029, USA
[15]The Charles Bronfman Institute of Personalized Medicine, Icahn School of Medicine at Mount Sinai, New York, NY 10029, USA
[16]The Mount Sinai Clinical Intelligence Center, Icahn School of Medicine at Mount Sinai, New York, NY 10029, USA
[17]Icahn Institute for Data Science and Genomic Technology, Icahn School of Medicine at Mount Sinai, New York, NY 10029, USA
[18]Catalan Institute for Research and Advanced Studies (ICREA), Barcelona, Spain
[19]Program for Inflammatory and Cardiovascular Disorders, Institut Hospital del Mar d'Investigacions Mèdiques (IMIM), Barcelona, Spain
[20]Division of Gastroenterology and Hepatology, Department of Medicine, Weill Cornell Medicine, New York, NY 10021, USA
[21]Global Health and Emerging Pathogens Institute, Icahn School of Medicine at Mount Sinai, New York, NY 10029, USA

Please address correspondence to:
saurabh.mehandru@mssm.edu,
adolfo.Garcia-Sastre@mssm.edu,
harm.vanbakel@mssm.edu, or
francesca.Petralia@mssm.edu

Authors' contributions

A.E.L., D.J., F.C.: Conceptualization, data curation, formal analysis, writing

A.S.G-R., M.T.: Data curation, formal analysis, writing

T.A., T.L.P.: Data curation, writing

M.S.L, I.R., K.D., B.L., R.D., S.T.C., G.M.D., S.N., E.A.B., H.M.K., B.S.G., G.N., E.P., J.R., S.N., A.G., J.A., M.T., Y.B., R.G., K.S., J.H., G.J.B., A.C.L., M.P.S., T.P., P.W.: data curation

A.C., J.J.F., J.F.C., E.K., C.A., M.M., S.G., N.H., S.D., C.C.C, A.R., R.E.S., N.A.K., A.A., P.J.B., E.A.B.: Data curation, review and editing

F.P., H.V.B., A.G.S., S.M.: Conceptualization, supervision, writing

Conflicts of Interest/Disclosures

A.E.L.: none, D.J.: none, F.C.: none, A.S.G-R.: none, M.T.: none, T.A.: none, T.L.P.: none, M.S.L: none, I.R.: none, K.D.: none, B.L.: none, R.D.: none, S.T.C.: none, G.M.D.: none, S.N.: none, H.M.K.: none, B.S.G.: none, G.N.: reports employment with, consultancy agreements with, and ownership interest in Pensieve Health and Renalytix AI; receiving consulting fees from AstraZeneca, BioVie, GLG Consulting, and Reata; and serving as a scientific advisor or member of Pensieve Health and Renalytix AI. E.P: none. J.R.: none, S.N.: none, A.G.: none, J.A.: none, M.T.: none, Y.B.: none, R.G.: none, K.S.: none, J.H.: none, G.J.B.: none, A.C.L.: none, M.P.S.: none, T.P.: none, P.W.: none, A.C.: none J.J.F.: Serves on the scientific advisor board of Vedanta Biosciences and has received grants from Janssen (unrelated to this work), J.F.C.: Serves as a consultant for the following companies (all unrelated to this work): Abbvie, Amgen, Arena Pharmaceuticals, Boehringer Ingelheim, Celgene Corporations, Celltrion, Eli Lilly, Enterome. E.K.: none, C.A.: none, M.M.: Discloses the following (unrelated to this work): Takeda, Genentech, Regeneron, Compugen, Myeloid Therapeutics, S.G.: Discloses receiving research grants from the following: Bristol Myers Squibb, Genentech, Immune Design, Agenus, Janssen. Also discloses serving as consultant for Merck, OncoMed and Neon Therapeutics. N.H.: Discloses serving as consultant for Lilly USA and pathology service contract with Abbvie and Celgene. S.D.: Discloses serving as a consultant for Ely Lilly, Enthera, Ferring Pharmaceuticals, Gilead, Hospira, Inotrem, Janssen, Johnson & Johnson, MSD, Mundipharma, Mylan, Pfizer, Roche, Sandoz, Sublimity Therapeutics, Takeda, TiGenix, UCB, Vifor. C.C.C: none, A.R.: none, R.E.S.: Discloses serving on the scientific advisory board of Miromatrix Inc. and is a consultant and speaker for Alnylam Inc, N.A.K.: Discloses serving as a consultant for Apollo Endosurgery, Boston Scientific, Gyrus AMCI, Olympus. A.A.: none, P.J.B.: none, E.A.B.: none, F.P.: none, H.V.B.: none, A.G.S.: none, S.M.: Discloses the following (unrelated to this work): Takeda, Genentech, Morphic and discloses receiving research grants from the following: Takeda, Genentech

Abstract

Background and Aims: Given gastrointestinal (GI) symptoms are a prominent extrapulmonary manifestation of COVID-19, we investigated intestinal infection with SARS-CoV-2, its effect on pathogenesis, and clinical significance.

Methods: Human intestinal biopsy tissues were obtained from COVID-19 patients (n=19) and uninfected controls (n=10) for microscopic examination, CyTOF analyses and RNA sequencing. Additionally, disease severity and mortality were examined in patients with and without GI symptoms in two large, independent cohorts of hospitalized patients in the United States (n=634) and Europe (n=287) using multivariate logistic regressions.

Results: COVID-19 cases and controls in the biopsy cohort were comparable for age, gender, rates of hospitalization and relevant comorbid conditions. SARS-CoV-2 was detected in small intestinal epithelial cells by immunofluorescence staining or electron microscopy, in 14 of 16 patients studied. High dimensional analyses of GI tissues revealed low levels of inflammation, including downregulation of key inflammatory genes including *IFNG*, *CXCL8*, *CXCL2* and *IL1B* and reduced frequencies of proinflammatory dendritic cells compared with controls. Consistent with these findings, we found a significant reduction in disease severity and mortality in patients presenting with GI symptoms that was independent of gender, age, and comorbid illnesses and despite similar nasopharyngeal SARS-CoV-2 viral loads. Furthermore, there was reduced levels of key inflammatory proteins in circulation in patients with GI symptoms.

Conclusion: These data highlight the absence of a proinflammatory response in the GI tract despite detection of SARS-CoV-2. In parallel, reduced mortality in COVID-19 patients

presenting with GI symptoms was observed. A potential role of the GI tract in attenuating SARS-CoV-2 associated inflammation needs to be further examined.

Introduction

Gastrointestinal (GI) symptoms comprising nausea, vomiting, and / or diarrhea[1] are a common extrapulmonary manifestation in Coronavirus disease 2019 (COVID-19). Additionally, the presence of GI involvement by severe acute respiratory syndrome coronavirus-2 (SARS-CoV-2) has also been suggested by clinical[2], non-human primate[3] and *in vitro*[4, 5] data. However, to date, there is limited evidence of SARS-CoV-2 infection of human intestinal epithelial cells[6] and there are no studies on the response of the GI immune system in COVID-19 patients.

Given the immune dysregulation seen in COVID-19[7, 8], we aimed to document infection of the GI tract in patients with COVID-19, to define the cellular and transcriptomic changes within the GI tract, and to determine the impact of GI symptoms on COVID-19 outcomes. Here, we present findings from well-characterized cohorts of COVID-19 patients hospitalized in tertiary care centers, from both New York City, USA and Milan, Italy, where we conducted high dimensional analyses of mucosal and systemic immune parameters and investigated disease outcomes associated with GI involvement in COVID-19 patients.

Materials and Methods

Clinical cohorts

1. Intestinal Biopsy Cohort

Endoscopic biopsies were obtained from 20 COVID-19 and 10 control patients undergoing clinically indicated endoscopic procedures after informed consent with Mount Sinai Hospital (MSH) IRB approved protocol (IRB 16-0583). The demographic characteristics of these patients

and controls are provided in Supplementary Table 1 and 2. COVID-19 severity is defined in Supplementary Table 3 and Supplementary Methods.

2. Discovery Cohort

634 subjects with COVID-19, admitted to MSH between April 1, 2020 and April 15, 2020, who met study inclusion criteria were enrolled in a Discovery Cohort under an IRB approved protocol (IRB-20-03297A) (Supplementary Methods).

3. External Validation Cohort

We analyzed a cohort of 287 patients admitted to a tertiary care center in Milan, Italy between February 22, 2020 and March 30, 2020 with COVID-19 (Supplementary Methods).

4. Internal Validation Cohort

A distinct 'Internal Validation Cohort' of patients who were hospitalized at MSH between April 16, 2020 and April 30, 2020 (Supplementary Methods) was analyzed using a predictive model.

Immunofluorescent (IF) microscopy

Formalin fixed, paraffin embedded tissue was analyzed (Supplementary Methods). Primary and secondary antibodies are summarized in Supplementary Table 16.

Transmission Electron Microscopy (TEM) and Electron Tomography (ET)

Biopsy specimens and infected Vero E6 cells (positive control) were examined by electron microscopy (Supplementary Methods).

Cell Culture Experiments, Virus Isolation, and Viral RNA Detection from GI biopsy tissues

Endoscopic biopsy tissue samples were homogenized, inoculated on Vero E6 monolayers under biosafety level 3 (BSL-3) conditions and monitored daily for potential cytopathic effect (CPE). Biopsy homogenate supernatants were assessed for presence of infective particles by plaque

assay (Supplementary Methods). To detect SARS-CoV-2 RNA from intestinal biopsies, a modified version of the CDC 2019-nCoV RT-qPCR was used (Supplementary Methods).

Biopsy collection and processing for Mass cytometry (CyTOF)

Endoscopic biopsies were processed in BSL-3 facility within 2 hours of collection to obtain suspension of the epithelial compartment (EC) and lamina propria (LP) (Supplementary Methods).

CyTOF processing, data acquisition, and data analysis

Cells were processed as previously described[9], acquired on a Helios Mass Cytometer, and de-multiplexed using the Zunder single cell debarcoder. De-barcoded files were uploaded to Cytobank for analyses, followed by annotation using Astrolabe Cytometry Platform (Astrolabe Diagnostics, Inc.) and clustering using Clustergrammer2's interactive heatmap (Supplementary Methods).

Blood collection and processing for CyTOF

Phlebotomy was performed on the Intestinal Biopsy Cohort patients at the time of endoscopic evaluation. Blood samples from COVID-19 patients were processed in enhanced BSL2 conditions (Supplementary Methods).

Specimen Processing for Nucleic Acid Extraction and RNA sequencing

Total RNA was extracted from the cells isolated from both the intestinal compartments, EC and LP cellular fractions, using Direct-zol RNA Miniprep Plus (Zymo) kit according to the manufacturer's instructions. RNA from cases and controls was then used for qRT-PCR and RNA sequencing (Supplementary Methods).

RNA Sequencing

Library preparation and sequencing

RNA-sequencing (RNA-seq) was performed on RNA isolated from the EC and LP samples obtained from COVID-19 cases and controls (Supplementary Methods).

Computational analyses

Descriptive statistics

For univariable statistical analyses, Graph Pad Prism (version 8) was used to calculate unpaired two tailed t-test for continuous variables and either Fisher's exact test or the Chi-square test for categorical variables.

Multivariate model based on Discovery Cohort and External Validation cohort

A multivariate logistic regression was utilized to model each outcome as function of GI symptoms and clinical variables including age, gender, body mass index (BMI) and comorbidities. Significant associations were determined based on 95% confidence interval (CI) based on 1000 bootstrap iterations (Supplementary Methods).

Predictive performance based on the Internal Validation Cohort

Only age and BMI were adjusted for, since they were the only variables significantly associated with both outcomes across different GI symptoms models in the Discovery Cohort (Supplementary Table 9). Then, the estimated model was utilized to predict the outcome of patients in the Internal Validation Cohort.

Average treatment effect (ATE)

ATE of GI symptoms on COVID-19 outcomes was estimated via the TMLE (Target Maximum Likelihood Estimation) package available in R Cran[10].

Quantification of SARS-CoV-2 nasopharyngeal (NP) viral loads

SARS-CoV-2 viral loads were determined as previously reported[11] (Supplementary Methods).

ELLA Cytokine panel and defining associations with GI symptoms

The ELLA cytokine platform measured TNF-α, IL-6, IL-8, and IL-1β[8]. Unpaired two-tailed t-tests were used to compare individual cytokines quantified by the ELLA panel between GI symptomatic and asymptomatic groups. P-values were adjusted via Benjamini-Hochberg[12].

Multiplexed proteomic assay (Olink)

Multiplexed proteomic inflammation panel (Olink, 92 inflammation-related proteins) was used to quantify circulating cytokines using an antibody-mediated proximity extension-based assay. The Benjamini-Hochberg procedure was used to adjust P values for multiple testing.

Consensus Clustering of Olink Data and defining associations with GI symptoms

Consensus clustering was performed on the abundance of the 92 cytokines across all 238 samples using the R package ConsensusClusterPlus[13]. Associations between GI symptoms and Olink proteomic data were derived using unpaired t-test comparing the symptomatic and asymptomatic groups. P-values were adjusted via Benjamini-Hochberg (10% FDR threshold of significance).

Results

The gastrointestinal tract was endoscopically uninflamed in COVID-19 cases

Twenty COVID-19 patients and 10 uninfected controls underwent esophagogastroduodenoscopy, colonoscopy or both (Supplementary Table 1 and 2). Patient 10 was excluded after multiple negative SARS-CoV-2 NP PCR tests and negative COVID-19 antibody test. COVID-19 cases and controls in the biopsy cohort were comparable for age, gender, rates of hospitalization and relevant comorbidities (Supplementary Table 1). Of the COVID-19 cases, 12 were classified as asymptomatic / mild / moderate and 7 as severe (Supplementary Table 1 and 2). GI biopsies were performed after 25.9 ± 30.3 days from last

positive NP swab. Of the 19 patients, 12 (63%) had a positive SARS-COV-2 PCR swab most proximal to their biopsy while 7 (37%) had a negative swab (after previously being positive) (Figure 1A, Supplementary Table 2). COVID-19 treatment regimens and presence of GI symptoms are detailed in Supplementary Table 2. Sample allocation for different assays is detailed in Supplementary Table 2 and Supplementary Figure 1.

The GI mucosa was endoscopically uninflamed in all subjects (Figure 1B), except for one case where inflammation was attributed to transplant rejection. Histology was normal in 7 of the 17 cases examined, while the remaining (n=10) cases had a mild increase in intraepithelial lymphocytes (IEL) and / or a scant neutrophilic infiltration (Figure 1C and D, Supplementary Figure 2). $CD3^+CD8^+$ IELs and $CD3^+CD8^-$ IELs were not significantly different in patients (n=12, 10 duodenum, 2 ileum) compared to controls (n=9, 5 duodenum, 4 ileum) (Supplementary Figure 3).

Small bowel intestinal epithelial cells have robust expression of Angiotensin converting enzyme-2 (ACE2) and harbor SARS-CoV-2 antigens

Robust expression of ACE2 was noted on the small intestinal brush border in both controls and COVID-19 patients (Figure 2, A to D). Additionally, we detected SARS-CoV-2 nucleocapsid protein in small intestinal epithelial cells of 10 of 11 COVID-19 patients tested (Figure 2, E to H and J to M, Supplementary Figure 4 and Supplementary Table 4) indicative of virus infection in these cells. When present, the distribution of viral antigens was exclusively seen in the epithelium and was patchy in the upper small intestines (duodenum; Figure 2, E to H), but diffuse in the lower small intestines (ileum; Figure 2, J to M). The presence of viral antigens on IF did not correlate with the presence of histologic abnormalities. To further define viral nucleocapsid protein positive cells, co-staining with MUC2 to define goblet cells[14] was

performed. Viral nucleocapsid primarily co-localized with MUC2 representing infected goblet cells (Figure 2, O to Q). There were a few cells positive for the viral nucleocapsid protein but negative for MUC2 which tended to be located at the base of the crypts (Figure 2, P to Q). The more diffuse viral antigen staining in the ileum as compared to the duodenum is not explained by apparent differences in ACE-2 protein expression (Figure 2, A to D), however, may be explained by increased goblet cells in the ileum[15] and this data appears to be consistent with organoid cultures[4]. As negative controls, 5 duodenal and 6 ileal biopsies from 10 patients collected prior to the pandemic (Supplementary Table 5) showed no evidence of viral antigens (Figure 2, I and N, Supplementary Figure 5).

Ultrastructural analyses of GI tissues reveal viral particles in small intestinal epithelial cells

Next, we performed TEM in 16 patients. Eight of these patients showed presence of 70-110 nm viral particles in the intestinal epithelial cells of the duodenum and/or ileum by TEM (Supplementary Table 4). Representative ET images (Figure 2, R to W) showed the presence of viral particles morphologically suggestive of SARS-CoV-2 in the duodenum (Figure 2, R, S, V) and the ileum (Figure 2, T, U, W), confirmed with Immuno-EM using mouse polyclonal antiserum against SARS-CoV-2 RB (Figure 2, X, Y). These particles in the exit vesicles of duodenal goblet cells (Figure 2, R, S, V) are consistent with the co-localization of MUC2 staining using IF.

No infectious virions identified in the GI tissues of COVID-19 patients

We inoculated Vero E6 cells with the supernatants of homogenized intestinal tissues, but did not observe any apparent cytopathic effects or plaque formation after 7-days culture. In addition, cell culture supernatants did not reveal the presence of viral RNA by RT-qPCR.

GI lamina propria dendritic cells are depleted in COVID-19 patients

Next, we performed mass cytometry (CyTOF) based immunophenotypic analysis on GI tissue and peripheral blood from a subset of COVID-19 cases (GI tissue, n = 13; blood, n = 10) and controls (GI tissue, n = 9; blood, n = 9) (Supplementary Table 1 and 2, Supplementary Figure 1). Lamina propria (LP) and epithelial compartment (EC) were analyzed separately. Immune populations were clustered on the basis of cell-type specific markers for both the intestinal compartments (LP and EC) and blood (Figure 3, A, C and G, Supplementary Figure 8A and 9A, Data file 1). While the overall distribution of canonical immune cell subsets in the GI LP were comparable between patients and controls (Figure 3, A and B (left panel)), few immune populations showed differences as detailed below. No clear differences in the LP could be discerned based on severity (Figure 3B (right panel), Data file 2).

In the LP, $CD206^{+}CD1c^{+}$ cDC2 (conventional DCs-0.4-fold decrease, p=0.01) and plasmacytoid DCs (pDCs) were reduced in COVID-19 cases (0.5 fold decrease, p=0.07) (Figure 3, D and E), analogous to changes described in the blood[16]. Effector ($PD\text{-}1^{+}CD38^{+}$) $CD4^{+}$ and $CD8^{+}$ T cells (Figure 3F) as well as $CD8^{+}CD103^{+}$ T cells (tissue resident memory) (Supplementary Figure 7A) were increased in patients compared to controls (1.7-fold increase, p=0.06). In the EC, there was decrease in $CD206^{+}$cDC2 (0.4-fold decrease, p=0.05) and an increase in $CD4^{-}CD8^{-}$ IELs (1.6-fold-increase, p=0.03) in patients compared to controls (Figure

3H). Alterations in other immune populations in the LP and EC are shown in Supplementary Figure 7 and 8, respectively.

Among PBMCs, effector ($PD\text{-}1^{+}CD38^{+}$) CD4+ and CD8+ T cells were significantly increased in patients (Figure 3I). Alterations in monocytes, T_{REG} and IgG^{+} plasma cells are shown in Supplementary Figure 9. Finally, a significant increase in activated ($CD29^{+}CD38^{+}$) CD4+ T cells was noted in PBMCs (Supplementary Figure 10A**)** and a non-significant increase of these activated T cells in the LP of patients compared to controls (Supplementary Figure 10B**).** Details of all immune population changes are provided in Data file S2.

Altogether, intestinal tissues of COVID-19 patients showed altered distribution of immune cell subsets, most notable for reduced frequencies of $CD206^{+}CD1c^{+}$ cDC2 and pDCs and an increased frequency of effector T cells.

GI lamina propria pro-inflammatory pathways are downregulated in COVID-19 patients

Next, we performed RNA-Seq on the EC and LP in 13 COVID-19 patients and 8 controls. The EC and LP clustered separately on the basis of their top transcriptional signatures, demonstrating distinctness of the two compartments (Supplementary Figure 11, Data file 3). 1063 differentially expressed genes (DEG) were identified out of total 11419 genes detected (Figure 4A, Data file 3). The majority of DEGs were detected in the LP (1061, false discovery rate[17] ≤ 0.05), compared to 12 DEGs in the EC that largely overlapped with the LP (Figure 4A). Both LP and EC showed upregulation of genes involved in immunomodulation, including the anti-microbial peptide *LCN2*, and the metallothioneins *MT1E*, *MT1F*, *MT1H*, *MT1M*, *MT1X*, *MT2A* and *TMEM107*. In addition, heat shock proteins, *HSPA1A* and *HASPA1B*, were downregulated in both compartments. Pathway enrichment analysis of DEGs ranked by significance revealed

several KEGG pathways that were depleted in patients compared to controls (Figure 4B) including pathways linked to T_H17 cell differentiation and inflammatory bowel diseases (IBD) which are characterized by the depletion of *RORA, IL4R, IFNG, IL18R1, IL1B, STAT4* and *HLA-DRA*. Pathways linked to antigen processing, T_H1 and T_H2 cell differentiation, and MAPK signaling were significantly downregulated in the LP from patients. In contrast, genes associated with amino acid metabolism (*NOS2, SMS, ALDH2, GOT2*), mineral absorption (*MT1G, MT2A, MT1E*), and mucin biosynthesis (*GALNT7, GALNT3, GALNT8*) were significantly upregulated in patients compared to controls (Figure 4B).

We considered the possibility that the observed expression changes could imply alterations in relative cell type proportions (in addition to transcriptional alterations within cells). Therefore, we interrogated data derived from single-cell RNA-seq[18] for enrichment of cell type-specific gene expression signatures. Consistent with our CyTOF data (Figure 3 and Data files 1 and 2), genes associated with DCs and eosinophils were reduced in patients compared to controls (Figure 4C). Additionally, signatures related to the size of endothelial cell and mast cell pools were reduced, while genes linked to goblet cells, proliferating epithelial cells, enteroendocrine cells and epithelial stem cells were increased, possibly reflecting the sequelae of intestinal epithelial infection by SARS-CoV-2 and subsequent recovery (Figure 4C).

We probed myeloid gene signatures further, and found significant downregulation of genes associated with pDC *(DAPK1, IRF7, ICAM1* and *GM2A*), activated DCs (*TNFAIP2, CD86, CD83*), cDC1 (*RELB, IRF8* and *HLA-DRA*) and cDC2 (*CLEC7A* and *CLEC10A*). Additionally, LP genes associated with inflammatory DCs (monocyte-derived DCs, MoDCs) (*TGFBI, TGFB1, STAB1, SDCBP, RNASET2, MSR1, MRC1, MERTK, DNASE1L3, CD163L1,*

C5AR1, SPI1, CSF1R, AOAH, ABCA) were significantly reduced (Figure 4D), consistent with our CyTOF results.

Next, we looked at the average EC and LP expression of recently reported gene signatures linked to the antiviral response against SARS-CoV-2 from post-mortem lung tissue[7], and human intestinal organoids[5]. Although we did not observe a substantial acute SARS-CoV-2 response, there was significant upregulation of *LCN2* in both EC and LP, and *OAS* and *GBP3* in LP only. Notably, we observed a trend towards induction of antiviral response genes in the EC, where expression of canonical antiviral genes such as *IFI44L, IFIT1, IFITM3, IFI44, IFI6* and *OAS3* was increased (Figure 4E, top panel).

Finally, using gene set enrichment analysis (GSEA), we rank ordered the EC DEGs according to effect size (logFC * -logPvalue) and tested for enrichment in the reported SARS-CoV-2 infected organoid gene signatures[5] (Supplementary Figure 12A). The genes upregulated in the EC of patients were significantly enriched in the SARS-COV-2 infected organoid gene datasets. Hallmark pathway enrichment analyses on this ranked EC gene list revealed that the top two processes associated with genes upregulated in EC were interferon alpha response (normalized enrichment score (NES) 1.91, FDR<0.005) and interferon gamma response (NES=1.8, FDR=0.005) (Supplementary Figure 12B), indicative of the host antiviral response against SARS-CoV-2 in the EC.

Projection of our RNA-seq dataset on SARS-CoV-2 infected human bronchial epithelial cells[7] revealed that several inflammatory cytokines and chemokines such as IL-1β, IFN-γ, CCL24 and CXCL8 were downregulated in the intestines of COVID-19 patients (Figure 4E, bottom panel). The only chemokine significantly increased was CCL15 which is structurally similar to antimicrobial peptides and has a role in maintaining intestinal homeostasis[19] (Figure

4E, bottom panel). Key inflammatory genes including *IFNG, IL1B, CXCR4, TNFSF14, CXCL2, CSF-1, CXCL8, IL18R1, NRP1 and IL18BP* were downregulated in LP of patients compared to controls (Figure 4F).

Together, these data reveal a dynamic remodeling of GI tissues by SARS-CoV-2, notably with a significant downregulation of pathways associated with inflammation and antigen presentation in the LP with a concomitant activation of antiviral response signaling genes in the EC.

Clinical impact of GI involvement during COVID-19: frequency of GI symptoms in a Discovery Cohort

Given the observed downregulation of key inflammatory genes, we hypothesized that intestinal involvement in COVID-19 is associated with a milder disease course. We tested this hypothesis in a 'Discovery Cohort' consisting of 634 hospitalized COVID-19 patients at MSH meeting inclusion criteria (Supplementary Figure 13). Demographics (gender, age and race/ethnicity) and clinical variables including the presence of comorbidities and COVID-19 severity were analyzed (Supplementary Table 6). Next, we recorded the presence of GI symptoms (diarrhea, nausea, vomiting) present at the time of hospital admission, to avoid iatrogenic confounders. 299 patients (47%) reported any of the GI symptoms (nausea, vomiting and/or diarrhea) with diarrhea being the most common (245 patients, 39%), followed by nausea (157 patients, 25%), and then vomiting (82 patients, 13%) (Supplementary Table 6).

COVID-19 severity is significantly reduced in patients with GI symptoms when compared to those without GI symptoms in multivariate analysis

Among the Discovery Cohort, 54 (9%) patients had mild disease, 361 (57%) moderate, 158 (25%) severe and 61 (10%) had severe COVID-19 with end organ damage (EOD) (Supplementary Table 3 and 6). 110 patients were admitted to the ICU (17%) and 151 patients (24%) died by the end of data collection (Supplementary Table 6). Patients presenting with GI symptoms had less severe disease than patients without GI symptoms ($p<0.001$ Chi-square test, Table 1). Notably, only 54 (9%) patients in the entire cohort [31(10.3%) with and 23(6.8%) without GI symptoms respectively] had mild disease on presentation (i.e. not requiring any type of supplemental oxygen (SpO2>94% on room air) and with no evidence of pneumonia), therefore, a majority of patients with GI symptoms had concomitant respiratory symptoms. Mortality was significantly lower in COVID-19 patients with GI symptoms (15.7%) than those without GI symptoms (31.0%; $p<0.0001$ Fisher's exact test) (Table 1). Furthermore, each individual GI symptom (nausea, vomiting and diarrhea) was associated with less severe disease ($p<0.02$ Fisher's exact test) and lower mortality ($p<0.001$ Fisher's exact test) (Supplementary Table 7). These findings were further emphasized by Kaplan-Meier estimates of survival over short-term follow-up of 25 days ($p<0.001$ log-rank test) (Figure 5A and Supplementary Figure 14, A and B). Consistent with prior reports[8] older age and higher disease severity were associated with higher mortality (Supplementary Table 8).

Next, we created a multivariate model, adjusting for age, BMI, gender, race/ethnicity, diabetes, HTN, chronic lung disease and heart disease to determine the impact of GI symptoms on COVID-19 outcomes (Table 1). Consistent with published literature[20] age and BMI were positively associated with COVID-19 severity and mortality (Supplementary Table 9). The presence of any GI symptoms, as well as diarrhea, nausea, and vomiting individually, were inversely associated with COVID-19 severity and mortality (Figure 5B, Supplementary Table 9).

Patients who presented with GI symptoms had 50% reduced odds of having severe disease (odds ratio (OR) of 0.56) and death from COVID-19 (OR of 0.54), compared to the patients who presented without GI symptoms (Figure 5B, Supplementary Table 9).

An External Validation Cohort further confirms decreased mortality in COVID-19 patients with GI symptoms on multivariate testing

Next, we confirmed our findings in an External Validation Cohort in which GI symptoms on admission were characterized as presence or absence of diarrhea (Supplementary Table 10). Consistent with the Discovery Cohort, patients with diarrhea on admission had significantly lower mortality (10.0%) compared to patients without diarrhea (23.7%, p=0.008). Additionally, patients with diarrhea had lower composite outcome of mortality or ICU admission compared to those without diarrhea (20% vs 40%, p=0.001) (Supplementary Table 10). On multivariate logistic regression analyses, adjusting for age, gender, BMI, diabetes, chronic heart and lung disease and other confounders, we observed that the presence of diarrhea on admission was significantly inversely associated with mortality with a median OR of 0.33 over 1000 bootstrap iterations (Figure 5C). In 270 patients in which treatment data was available, no specific treatment was associated with GI symptoms (p-values > 0.05) (Supplementary Table 11). In addition, diarrhea was significantly associated with mortality after adjusting for all treatments (Supplementary Table 11). Thus, our observations from this External Validation Cohort were in alignment with those from the Discovery Cohort.

Presence of GI symptoms can be used to predict reduced disease severity and mortality in COVID-19 patients

Next, we developed a predictive model based on the Discovery Cohort and applied it to a distinct Internal Validation Cohort. The inclusion of 'any GI symptoms' to a model consisting of age and BMI, improved the ability to predict severity and mortality with a median area under the curve (AUC) of 0.64 (age + BMI + any GI symptoms) vs 0.59 (age + BMI) for disease severity and 0.73 (age + BMI + any GI symptoms) vs 0.70 (age + BMI) for mortality (Figure 5D, Supplementary Table 12). In addition, the effect of GI symptoms, age and BMI on the AUC was evaluated by excluding each variable one at a time from the model and calculating the consequent reduction in AUC. The exclusion of GI symptoms resulted in a significant reduction in AUC with a median value of 0.054 for disease severity and 0.03 for mortality. Notably, the effect of GI symptoms on the AUC was more dramatic than that of age (AUC reduction of 0.054 versus 0.025) for disease severity (Figure 5E, Supplementary Table 12)**.**

Average treatment effect (ATE) of GI symptoms on COVID-19 outcomes

Using causal inference methodology, we quantified the ATE of GI symptoms on COVID-19 outcomes while accounting for potential confounders. We performed this analysis on the MSH Cohort combining Discovery and Internal Validation Cohort and on the External Validation Cohort. The marginal effect of GI symptoms in the MSH cohort was significant for both severity and mortality after adjusting for all confounders (Data file 4). Additionally, based on the External Validation Cohort, the ATE for diarrhea was significant for mortality and combined outcome of ICU admission or death, but not for ICU admission alone (Data file 4). The OR for the marginal treatment effect of diarrhea was 0.9 for mortality in both the MSH and External Validation Cohort.

Nasopharyngeal SARS-CoV-2 viral loads are similar in patients with and without GI symptoms.

Given recent reports suggesting that NP SARS-CoV-2 viral loads are correlated with disease outcomes[11], we compared NP viral loads in a subset of Discovery and Internal Validation Cohort (n=329, where data available). Patients with and without GI symptoms had comparable SARS-CoV-2 NP viral loads (mean $\log_{10}$ copies/mL 5.1 (SD 2.3) and 5.6 (SD 2.4), respectively) (p=0.07); furthermore, no significant differences were observed for each individual GI symptom (Figure 5F).

COVID-19 patients with GI symptoms have reduced levels of circulating cytokines associated with inflammation and tissue damage.

To correlate the observed mortality difference with GI symptoms with known biomarkers for severe COVID-19, we examined IL-6, IL-8, TNF-α, and IL-1β levels measured on admission. IL-6 and IL-8, which are known to be directly associated with poor survival[8], were found to be significantly reduced in circulation of patients with GI symptoms (FDR 10%) (Supplementary Figure 15, Supplementary Table 13).

Next, we performed a validated, multiplexed proteomic assay (Olink), in 238 patients (from among the Discovery and Internal Validation Cohorts; GI symptoms (n=104), no GI symptoms (n=134)) where serum samples were available for analyses. Unsupervised consensus clustering of 92 analytes revealed six groups of analytes with similar expression patterns across all patients (Figure 6A, Supplementary Table 14). Analytes in clusters 5 and 6 displayed less correlation in patients with GI symptoms compared to those without GI symptoms (Figure 6A, Supplementary Figure 16). “KEGG Jak/Stat Signaling Pathway” was significantly enriched in Cluster 5; while the "Hallmark Inflammatory Response" pathway was significantly enriched in

Cluster 4 (Fisher's exact test 10% FDR). These pathways were downregulated in patients with diarrhea ($p<0.05$ from t-test) (Figure 6B), suggesting a reduced inflammatory response in patients with GI symptoms. Additionally, Clusters 1, 2, 3, 5 and 6 were significantly downregulated in patients with GI symptoms compared to those without (FDR 15%) (Figure 6C). This seemed to be driven mostly by diarrhea since the same clusters were significantly downregulated in patients with diarrhea (FDR 10%). We observed a similar, albeit a reduced signal for nausea and vomiting likely due to the smaller sample size (n=29 for vomiting, n=54 for nausea).

Key inflammatory cytokines and chemokines were significantly downregulated (IL-8, TGF-α, IL-17C, IL-15RA, IL-10RB, MMP10, TNFRSF9, OPG, IL-6, LIF, GDNF, IL-17A, ARTN and CCL28) while TNF-Related Apoptosis Inducing Ligand (TRAIL), a cytokine with immune regulatory properties[21] and IL-7, a cytokine associated with T cell development[22] were significantly upregulated in patients with GI symptoms (t-test FDR 10%) (Figure 6, D and E, Supplementary Table 15).

Overall, GI symptoms are associated with significantly reduced levels of key inflammatory cytokines including IL-6, IL-8, IL-17 and CCL28 that are known to be associated with poor COVID-19 outcomes.

Discussion

Given the robust expression of ACE2 on the small intestinal epithelium, we hypothesized that the intestines would be susceptible to SARS-CoV-2 infection. Here, we detailed for the first time SARS-CoV-2 infection of human intestinal epithelial cells *in vivo* using IF and EM. Specifically, infected intestinal cells were primarily goblet cells. We also observed a mild

inflammatory response in the intestinal tissues despite the presence of SARS-CoV-2 antigens. Finally, we found reduced systemic inflammation as well as mortality in hospitalized COVID-19 patients presenting with GI symptoms.

Using multiple approaches, we observed evidence of reduced inflammatory response within the GI tract. This includes a lack of inflammatory monocytes and macrophages and a depletion of DC subsets in the GI tract which is in contrast to the significant inflammatory response observed in the blood and lungs of severe COVID-19 patients[23]. Additionally, a downregulation of several proinflammatory genes that were found to be elevated in the lungs during SARS-CoV-2 infection[24] was observed in GI tissues. Lastly, systemic levels of IL-6 and IL-8 as well as IL-17[20] and CCL28[25] were lower in hospitalized patients presenting with GI symptoms, despite comparable NP SARS-CoV-2 viral loads. Notably, the reduced circulating IL-17 and CCL28 (by Olink) is consistent with our RNAseq data. The observed attenuation of GI inflammation is in alignment with data from the 2003 SARS epidemic[26], autopsy studies from COVID-19 patients[27] and from animal models[28, 29].

In two distinct and large cohorts of COVID-19 patients, we observed a significant reduction in mortality in patients presenting with GI symptoms compared to those without GI symptoms, even after adjusting for multiple confounders including age and comorbidities, which is consistent with findings in two smaller cohorts[30, 31]. Notably this finding is different from early reports suggesting increased severity with GI symptoms[32], likely attributable to the inclusion of abnormal liver function tests which are associated with poor outcomes.

We duly acknowledge some limitations of our study. GI biopsies were performed on a distinct set of patients undergoing clinically indicated procedures and therefore, they were not all in the acute phase of illness. Furthermore, given only 3 patients in the biopsy cohort had GI

symptoms, we were unable to perform comparisons between those with and without GI symptoms. Although we could not isolate infectious virus from intestinal biopsies (possibly due to culture methods, low multiplicity of infection or inactivation of virus following contact with enteric secretions) we demonstrate presence of virus in intestinal tissue using two parallel methods, IF and EM/ET. One of the possible reasons why SARS-CoV-2 induced less severe inflammation in the gut could be through the induction of potent neutralizing IgA antibodies which are predominantly produced in the intestines and do not fix complement unlike IgG antibodies mainly induced in the lungs[33, 34]. Furthermore, dimeric IgA (as would be induced in the gut) is more potent in viral neutralization than IgG[35]. Finally, we acknowledge that reporting of GI symptoms can be subject to individual variation and has the potential for being under reported.

In summary, our data detail the previously unappreciated GI tissue response to SARS-CoV-2 and provide the rationale for future mechanistic studies to understand a possible attenuation of SARS-CoV-2 pathogenicity by the intestinal environment.

Figures and Table Legends

Figure 1 Clinical timing, endoscopic findings and histologic features in the small intestines of COVID-19 patients. (**A**) Timing of GI evaluation with respect to COVID-19 disease course. (**B**) Representative endoscopic images of the duodenum in COVID-19 (left) and control (right) patients. (**C**) Histologically normal duodenal tissue in a COVID-19 patient. (**D**) Histologic signs of inflammation detected in duodenal biopsies of COVID-19 patients including neutrophils (arrow) and increased intraepithelial lymphocytes (*). Scale bar; 100 µm.

Figure 2 SARS-CoV-2 viral particles and protein are detectable in intestinal tissues of COVID-19 patients. (**A-H**) Immunofluorescence (IF) staining of duodenal (**A, B**) and ileal (**C, D**) biopsies of COVID-19 patients (**B, D**) and controls (**A, C**) with ACE2 (green), EPCAM (red) and DAPI (blue). (**E-N**) IF staining of duodenal (**E-I**) and ileal (**J-N**) biopsies from patients (**E-H, J-M**) and controls (**I, N**) with SARS-CoV-2 nucleocapsid (green), EPCAM (red) and DAPI (blue) including isotype (**G, L**) and no primary (**H, M**) controls. **(O-Q)** IF staining of duodenal **(O, P)** and ileal **(Q)** biopsies of patients with SARS-CoV-2 nucleocapsid (green), MUC2 (red) and DAPI (blue) showing SARS-CoV-2 nucleocapsid in goblet cells (*, MUC2+) and non-goblet epithelial cells (arrows, MUC2-). (**R-W**) Electron tomography (ET) of a duodenal biopsy (**R**, montaged projection overview; **S**, Tomographic reconstruction of the region indicated by the rectangle in **R** showing the goblet cell Golgi region; **V**, Detail of the presumptive virion indicated by the red arrow in **S**. Note dark nucleocapsid puncta and surface spikes (arrows). ET of an ileal biopsy from a COVID-19 patient (**T)**, montaged tomographic reconstruction of a goblet cell Golgi region; **U,** Detail of the region indicated by the rectangle in **T**, showing a presumptive exit compartment containing 5 presumptive SARS-CoV-2 virions; **W**, Detail of a presumptive virion from **U**, membrane bilayer and surface spikes are evident. The virion structures in **R-W** are comparable with those from a SARS-CoV-2–infected cultured cell (Supplementary Figure 6 and Supplementary Movies 1-2). Projection image (**X**) of a presumptive SARS-CoV-2 virion within an intestinal epithelial cell of CGI-115, labeled with a mouse polyclonal antiserum against SARS-CoV-2 RBD[36] and 10 nm gold conjugated anti-mouse secondary antibodies. Detail of the presumptive virion itself is not apparent in the projection image. A single slice (**Y**) (~10 nm) from a tomographic reconstruction of the same area shown in **X**. The spherical shape and membrane bilayer of the presumptive CoV-2 virion (indicated by *)

are discernible, with gold particles connoting anti-S labeling localized to the presumptive virion's outer periphery. Scale bars; 100 µm (**A-N**), 10 µm (**O-Q**), 5 µm (**R**), 0.2 µm (**S, U**), 1 µm (**T**), 0.05 µm (**V, W**), 0.025 µm (**X**,**Y**).

Figure 3 CyTOF-based analysis identified immune cell signatures in intestinal biopsies and blood from COVID-19 patients and controls. Uniform Manifold Approximation and Projection (UMAP) presentation of the eight clusters of LP immune populations based on 38 markers (**A**), by infection status (**B**, left panel) with COVID-19 patients (red) and controls (blue), and by disease severity (**B,** right panel) with controls (blue), severe (red) and asymptomatic/mild/moderate (green) COVID-19 patients. (**C**) The heatmap depicting immune populations in the LP based on specific cell type markers. (**D**) Representative histograms comparing $CD206^+$ and $CD123^+$ in DC subsets in patients (red) and controls (blue). (**E**) Relative frequencies of $CD206^+$ cDC2 and plasmacytoid DCs in LP of patients and controls (unsupervised analysis). (**F**) Relative frequencies of $PD\text{-}1^+$ $CD38^+$ (effector) CD4+ and CD8+ T cells in LP of control and patients (supervised analysis). (**G**) UMAP presentation of the eight clusters of immune populations based on 38 markers in the EC of intestinal biopsies. (**H**) Relative frequencies of $CD206^+$ cDC2 and $CD4^-CD8^-$ T cells in the EC of controls and patients (unsupervised analysis). (**I**) Relative frequencies of $PD\text{-}1^+CD38^+$ (effector) $CD4^+$ and $CD8^+$ T cells in blood of controls and patients (supervised analysis). Open red circles denote patients with asymptomatic/mild/moderate disease while filled red circles denote patients with severe COVID-19. Bar plots represent median values.

Figure 4 Transcriptional changes in intestinal biopsies from COVID-19 patients compared with controls. (**A**) Hierarchical clustering of average expression changes for 1,063 genes (rows) with induced (red) or depleted (blue) expression (FDR ≤ 0.05) in the EC and LP of intestinal biopsies from COVID-19 patients. The panel on the left indicates significant genes for each tissue fraction in yellow. The color bar indicates the average log2 fold-change (FC). (**B**) Top enriched pathways (KEGG) that are induced (red) or depleted (blue) in LP of COVID-19 patients are displayed. The dash line indicates the $P \leq .05$ cutoff. Gene names are indicated for main pathways. (**C**) Deconvolution of main gastrointestinal cell types enriched or depleted in the LP of COVID-19 patients compared with controls. Reference scRNA-seq cell type signatures were taken from *Smillie et al. 2019*. ($P \leq .05$, Fisher's exact test). (**D**) Average expression changes for dendritic cell markers in the EC and LP. Reference scRNA-seq cell type signatures were taken from *Martin et al. 2019*. The color bar indicates the average log2 FC. (**E**) Hierarchical clustering of average expression changes (columns) in the EC and LP for genes related to antiviral response to SARS-CoV-2 in post-mortem lung tissue of COVID-19 patients as described by *Blanco-Mello et al. 2020* (top panel) and for cytokines and chemokines (bottom panel). The color bar indicates the average log2 FC. (**F**) The gene expression levels for the top 10 significant chemokines and cytokines in the LP of COVID-19 patients and controls. * $P < .05$, ** $P < .01$.

Figure 5 COVID-19 patients with GI symptoms had reduced severity and mortality despite similar nasopharyngeal viral loads compared to those without GI symptoms. (**A**) Kaplan-Meier (KM) curves for survival stratified by any GI Symptoms (left panel) and diarrhea (right panel) for patients in the Discovery Cohort. P-values from log-rank test and 95% confidence intervals of KM curves are shown. The number of patients at risk are reported for the respective

timepoints. (**B**) Confidence intervals (CI) of odds ratio (95%) of GI symptoms based on 1000 bootstrap iterations in a multivariate logistic regression for severity (blue) and mortality (red). (**C**) Validation based on the External Cohort. CI of odds ratio (95%) of diarrhea covariate based on 1000 bootstrap iterations to capture mortality, ICU admission and composite outcome of ICU admission or death. Results are based on multivariate models after accounting for confounders including BMI, age, gender, lung disease, heart disease and hypertension. (**D**) Validation based on the Internal Cohort. Boxplot of AUC over 1000 bootstrap iterations to predict mortality and disease severity in the Internal Validation Cohort. (**E**) CI of the reduction in AUC (95%) based on 1000 bootstrap iterations for the model "Age + BMI + Any GI Symptoms" after removing age (blue), GI symptoms (red) and BMI (green). (**F**) SARS-CoV-2 viral load copies per mL (log_{10} transformed based on N2 primer with the addition of a constant) stratified by GI symptoms. The square corresponds to the average viral load and the error bars show one standard deviation of uncertainty from the mean. P-values from two-tailed unpaired t-tests are reported.

Figure 6 COVID-19 patients with GI symptoms have reduced levels of circulating inflammatory cytokines. (**A**) Correlation matrix (Pearson's) for 92 markers in the Olink panel across patients with any GI symptoms (top left panel) compared with no GI symptoms (top right panel) and patients with diarrhea (bottom left panel) compared with patients without diarrhea (bottom right panel). Cluster assignment is reported on the top of the heatmap. (**B**) Boxplot of "Hallmark Inflammatory Response" and "KEGG JAK/STAT Signaling pathway" z-scores stratified by GI symptoms which were significantly enriched at 10% FDR in Cluster 4 and Cluster 5, respectively. (**C**) Significant associations between proteomic clusters and GI symptoms at 10% (dark blue) and 15% (light blue) FDR based on unpaired two-tailed t-test. (**D**)

Analytes associated with GI symptoms at 10% FDR based on unpaired t-test. The intensity of the color is proportional to the -log10 p-value. Negative associations are in blue, while positive associations in red. On the right side of the heatmap, the cluster assignment for each marker is reported. (**E**) Boxplots represent median and interquartile range of select differentially expressed markers stratified by GI symptoms. P-values from unpaired t-test are reported.

Table 1 Basic demographics, clinical characteristics and outcomes in patients with and without GI symptoms. For age, the mean ± standard deviation is listed and an unpaired two-tailed t-test was performed. For categorical variables, the number of patients followed by the percent of patients in parentheses is listed and the Fisher's exact test or the Chi-square test was used as appropriate.

References:

1. Gupta A, Madhavan MV, Sehgal K, et al. Extrapulmonary manifestations of COVID-19. Nat Med 2020;26:1017-1032.
2. Sultan S, Altayar O, Siddique SM, et al. AGA Institute Rapid Review of the GI and Liver Manifestations of COVID-19, Meta-Analysis of International Data, and Recommendations for the Consultative Management of Patients with COVID-19. Gastroenterology 2020.
3. Munster VJ, Feldmann F, Williamson BN, et al. Respiratory disease in rhesus macaques inoculated with SARS-CoV-2. Nature 2020.

4. Zang R, Gomez Castro MF, McCune BT, et al. TMPRSS2 and TMPRSS4 promote SARS-CoV-2 infection of human small intestinal enterocytes. Sci Immunol 2020;5.
5. Lamers MM, Beumer J, van der Vaart J, et al. SARS-CoV-2 productively infects human gut enterocytes. Science 2020;369:50-54.
6. Xiao F, Tang M, Zheng X, et al. Evidence for Gastrointestinal Infection of SARS-CoV-2. Gastroenterology 2020;158:1831-1833 e3.
7. Blanco-Melo D, Nilsson-Payant BE, Liu WC, et al. Imbalanced Host Response to SARS-CoV-2 Drives Development of COVID-19. Cell 2020;181:1036-1045 e9.
8. Del Valle DM, Kim-Schulze S, Hsin-Hui H, et al. An inflammatory cytokine signature helps predict COVID-19 severity and death. medRxiv 2020.
9. Geanon D, Lee B, Kelly G, et al. A Streamlined CyTOF Workflow To Facilitate Standardized Multi-Site Immune Profiling of COVID-19 Patients. medRxiv 2020.
10. Gruber S, van der Laan M. tmle: An R Package for Targeted Maximum Likelihood Estimation. Journal of Statistical Software 2012;51:1-35. https://www.jstatsoft.org/v051/i13.
11. Pujadas E, Chaudhry F, McBride R, et al. SARS-CoV-2 viral load predicts COVID-19 mortality. Lancet Respir Med 2020;8:e70.
12. Benjamini Y, Hochberg Y. Controlling the False Discovery Rate: A Practical and Powerful Approach to Multiple Testing. Journal of the Royal Statistical Society. Series B (Methodological) 1995;57:289-300.
13. Wilkerson MD, Hayes DN. ConsensusClusterPlus: a class discovery tool with confidence assessments and item tracking. Bioinformatics 2010;26:1572-3.
14. Chang SK, Dohrman AF, Basbaum CB, et al. Localization of mucin (MUC2 and MUC3) messenger RNA and peptide expression in human normal intestine and colon cancer. Gastroenterology 1994;107:28-36.
15. Barker N, van de Wetering M, Clevers H. The intestinal stem cell. Genes Dev 2008;22:1856-64.
16. Laing AG, Lorenc A, Del Molino Del Barrio I, et al. A dynamic COVID-19 immune signature includes associations with poor prognosis. Nat Med 2020.
17. Hoffmann M, Kleine-Weber H, Schroeder S, et al. SARS-CoV-2 Cell Entry Depends on ACE2 and TMPRSS2 and Is Blocked by a Clinically Proven Protease Inhibitor. Cell 2020.
18. Smillie CS, Biton M, Ordovas-Montanes J, et al. Intra- and Inter-cellular Rewiring of the Human Colon during Ulcerative Colitis. Cell 2019;178:714-730 e22.
19. Kotarsky K, Sitnik KM, Stenstad H, et al. A novel role for constitutively expressed epithelial-derived chemokines as antibacterial peptides in the intestinal mucosa. Mucosal Immunol 2010;3:40-8.
20. Rao X, Wu C, Wang S, et al. The importance of overweight in COVID-19: A retrospective analysis in a single center of Wuhan, China. Medicine (Baltimore) 2020;99:e22766.
21. Falschlehner C, Schaefer U, Walczak H. Following TRAIL's path in the immune system. Immunology 2009;127:145-54.
22. Mackall CL, Fry TJ, Gress RE. Harnessing the biology of IL-7 for therapeutic application. Nat Rev Immunol 2011;11:330-42.

23. Zhang H, Zhou P, Wei Y, et al. Histopathologic Changes and SARS-CoV-2 Immunostaining in the Lung of a Patient With COVID-19. Ann Intern Med 2020;172:629-632.
24. Liao M, Liu Y, Yuan J, et al. Single-cell landscape of bronchoalveolar immune cells in patients with COVID-19. Nat Med 2020;26:842-844.
25. Lucas C, Wong P, Klein J, et al. Longitudinal analyses reveal immunological misfiring in severe COVID-19. Nature 2020;584:463-469.
26. Leung WK, To KF, Chan PK, et al. Enteric involvement of severe acute respiratory syndrome-associated coronavirus infection. Gastroenterology 2003;125:1011-7.
27. Skok K, Vander K, Setaffy L, et al. COVID-19 autopsies: Procedure, technical aspects and cause of fatal course. Experiences from a single-center. Pathol Res Pract 2021;217:153305.
28. Sia SF, Yan LM, Chin AWH, et al. Pathogenesis and transmission of SARS-CoV-2 in golden hamsters. Nature 2020;583:834-838.
29. Shi J, Wen Z, Zhong G, et al. Susceptibility of ferrets, cats, dogs, and other domesticated animals to SARS-coronavirus 2. Science 2020;368:1016-1020.
30. Nobel YR, Phipps M, Zucker J, et al. Gastrointestinal Symptoms and Coronavirus Disease 2019: A Case-Control Study From the United States. Gastroenterology 2020;159:373-375 e2.
31. Aghemo A, Piovani D, Parigi TL, et al. COVID-19 Digestive System Involvement and Clinical Outcomes in a Large Academic Hospital in Milan, Italy. Clin Gastroenterol Hepatol 2020;18:2366-2368 e3.
32. Mao R, Qiu Y, He JS, et al. Manifestations and prognosis of gastrointestinal and liver involvement in patients with COVID-19: a systematic review and meta-analysis. Lancet Gastroenterol Hepatol 2020;5:667-678.
33. Cerutti A, Chen K, Chorny A. Immunoglobulin responses at the mucosal interface. Annu Rev Immunol 2011;29:273-93.
34. Cerutti A. The regulation of IgA class switching. Nat Rev Immunol 2008;8:421-34.
35. Wang Z, Lorenzi JCC, Muecksch F, et al. Enhanced SARS-CoV-2 Neutralization by Secretory IgA in vitro. bioRxiv 2020.
36. Cohen AA, Gnanapragasam PNP, Lee YE, et al. Mosaic nanoparticles elicit cross-reactive immune responses to zoonotic coronaviruses in mice. Science 2021;371:735-741.

Author names in bold designate shared co-first authorship

Acknowledgements

We would like to thank the clinical staff, physicians and patients who participated in this study. This research was partly funded by NIH/NIDDK123749 0S1 (S.M.). Additional support was

provided by CRIP (Center for Research for Influenza Pathogenesis), a NIAID supported Center of Excellence for Influenza Research and Surveillance (CEIRS, contract # HHSN272201400008C), and NIAID R01AI113186 (to H.B). Additionally, the work was supported by the generous support of the JPB Foundation, the Open Philanthropy Project (research grant 2020-215611 (5384)), the Defense Advanced Research Projects Agency, and anonymous donors to AG-S. MT was funded by the Digestive Disease Research Foundation (DDRF). A.S.G-R. is supported in part by a Robin Chemers Neustein Postdoctoral Fellowship Award. The research carried out by H.V.B and A.S.G-R was supported by the Office of Research Infrastructure of the National Institutes of Health (NIH) under awards S10OD018522 and S10OD026880. R.E.S is funded by (NCI R01CA234614, NIAID 2R01AI107301 and NIDDK R01DK121072) and is supported as Irma Hirschl Trust Research Award Scholars. E.A.B is supported by the NIH grant P20GM125498 (awarded to UVM Translational Global Infectious Disease Research Center). P.J.B. M.S.L. are supported by George Mason University Fast Grants. S.T.C. is supported by grant F30CA243210. G.J.B. is supported by a Research Fellowship Award from the Crohn's and Colitis Foundation of America. M.P.S. is supported by NIH T32 5T32AI007605. S.G. is supported by grants U24 CA224319, U01 DK124165, and P01 CA190174. We also thank Dr. Randy Albrecht for support with the BSL3 facility and procedures at the Icahn School of Medicine at Mount Sinai (ISMMS).

Authors' abbreviations: A.E.L.: Gastroenterology Fellow, D.J.: Postdoctoral Fellow, F.C.: Assistant Professor, A.S.G-R.: Postdoctoral Fellow, M.T.: MD candidate, T.A.: Instructor, T.L.P.: Gastroenterology Fellow, M.S.L.: Electron Microscopy Specialist, I.R.: Assistant Professor, K.D.: Internal Medicine Resident, B.L.: Computational Scientist, R.D.: Senior Research Coordinator, S.T.C.: MD/PhD candidate, G.M.D.: Research manager, S.N.: Associate Professor, E.A.B.: Faculty Scientist, H.M.K.: Assistant Professor, B.S.G.: Assistant Professor, G.N.: Assistant Professor, E.P: Pathology Resident, J.R.: Electron Microscopist, S.N.: Assistant Professor, A.G.: Assistant Professor, J.A.: Professor, M.T.: Research Coordinator, Y.B.: Postdoctoral Fellow, R.G.: Research Professor, K.S.: Master's candidate, J.H: Associate Professor, G.J.B.: Instructor, A.C.L.: MD/PhD candidate, M.P.S.: MD/PhD candidate, T.P.: PhD candidate, P.W.: Professor, A.C.: Professor, J.J.F.: Associate Professor, J.F.C.: Professor, E.K.: Assistant Professor, C.A.: Associate Professor, M.M.: Professor, S.G.: Associate Professor,

N.H.: Professor, S.D.: Professor, C.C.C.: Professor, A.R.: Associate Professor, R.E.S.: Assistant Professor, N.A.K.: Associate Professor, A.A.: Associate Professor, P.J.B.: Professor, F.P.: Assistant Professor, H.V.B.: Assistant Professor, A.G.S.: Professor, S.M.: Associate Professor.

Data and materials availability: Will be made available upon acceptance.

Table 1 Basic demographics, clinical characteristics and outcomes in patients with and without GI symptoms. For age, the mean ± standard deviation is listed and an unpaired two-tailed t-test was performed. For categorical variables, the number of patients followed by the percent of patients in parentheses is listed and the Fisher's exact test or the Chi-square test was used as appropriate.

	GI symptoms (n=299)	**No GI symptoms (n=335)**	***P*-value**
Age (years)	60.5 ± 15.0	67.2 ± 15.7	**<.0001**
Male	168 (56.2)	201 (60.0)	.33
Race/ethnicities			
Hispanic	85 (28.4)	92 (27.5)	
African-American	66 (22.1)	95 (28.4)	
White	70 (23.4)	67 (20.0)	
Asian	22 (7.4)	13 (3.9)	
Other	56 (18.7)	68 (20.3)	.13
Comorbidities			
HTN	112 (37.5)	117 (34.9)	.51
Diabetes	58 (19.4)	83 (24.8)	.13
Obesity (BMI>30)*	108 (40.6)	103 (34.1)	.12
Chronic lung disease	34 (11.4)	25 (7.5)	.10
Heart disease	48 (16.1)	63 (18.8)	.40
Chronic kidney disease	41 (13.7)	54 (16.1)	.44
Cancer	27 (9.0)	39 (11.6)	.30
HIV	5 (1.7)	6 (1.8)	.99
IBD	4 (1.3)	3 (0.9)	.71
Disease severity			
Mild	31 (10.4)	23 (6.9)	
Moderate	188 (62.9)	173 (51.6)	
Severe	63 (21.1)	95 (28.4)	
Severe with EOD	17 (5.7)	44 (13.1)	**.0004**
Outcomes			
ICU admission	45 (15.1)	65 (19.4)	.17
Mortality	47 (15.7)	104 (31.0)	**<.0001**

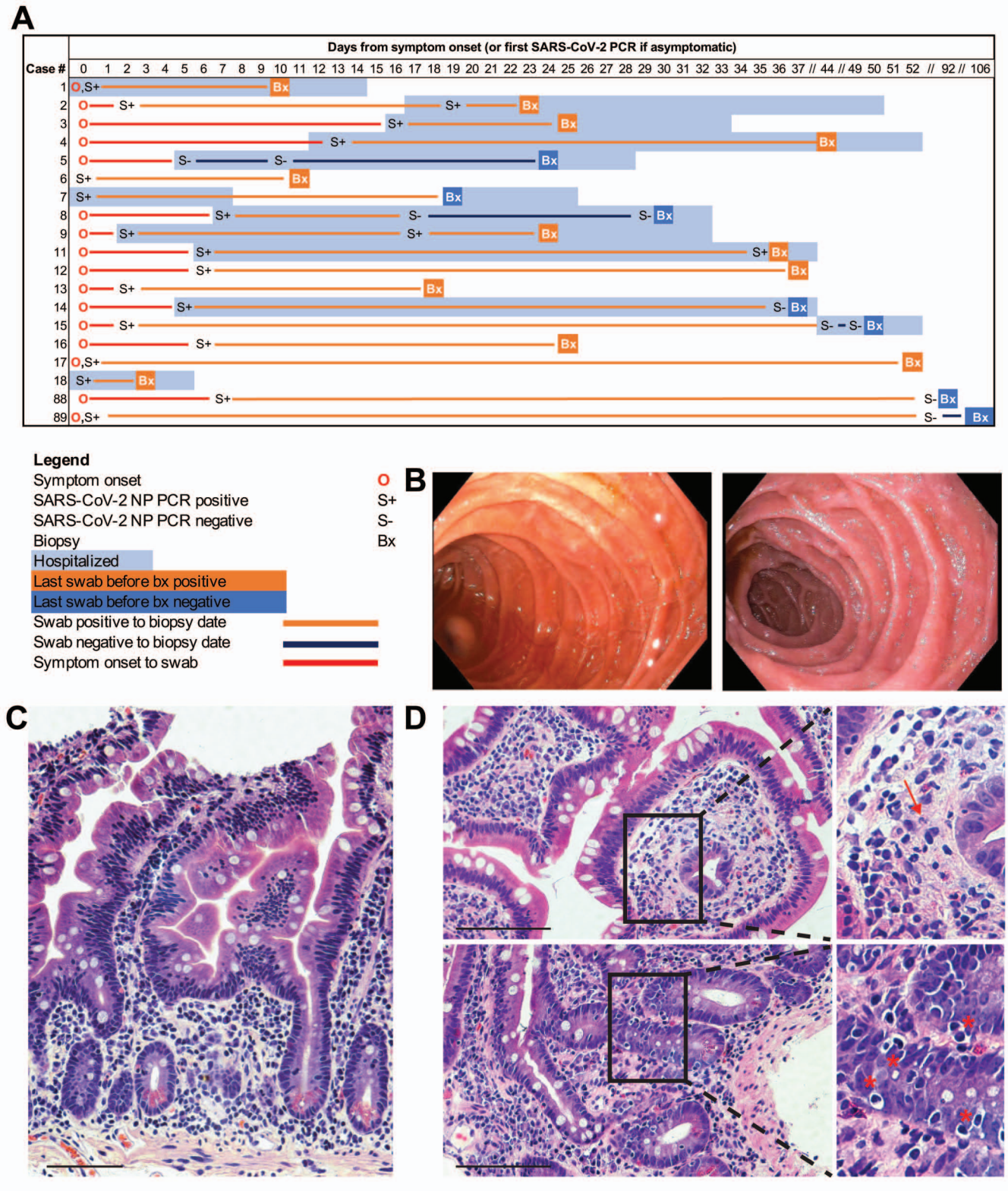
A
Days from symptom onset (or first SARS-CoV-2 PCR if asymptomatic)
Case #
0 1 2 3 4 5 6 7 8 9 10 11 12 13 14 15 16 17 18 19 20 21 22 23 24 25 26 27 28 29 30 31 32 33 34 35 36 37 // 44 // 49 50 51 52 // 92 // 106
1 O,S+ Bx
2 O S+ S+ Bx
3 O S+ Bx
4 O S+ Bx
5 O S- S- Bx
6 S+ Bx
7 S+ Bx
8 O S+ S- S- Bx
9 O S+ S+ Bx
11 O S+ S+ Bx
12 O S+ Bx
13 O S+ Bx
14 O S+ S- Bx
15 O S+ S- S- Bx
16 O S+ Bx
17 O,S+ Bx
18 S+ Bx
88 O S+ S- Bx
89 O,S+ S- Bx
Legend
Symptom onset O
SARS-CoV-2 NP PCR positive S+
SARS-CoV-2 NP PCR negative S-
Biopsy Bx
Hospitalized
Last swab before bx positive
Last swab before bx negative
Swab positive to biopsy date
Swab negative to biopsy date
Symptom onset to swab
B
C
D

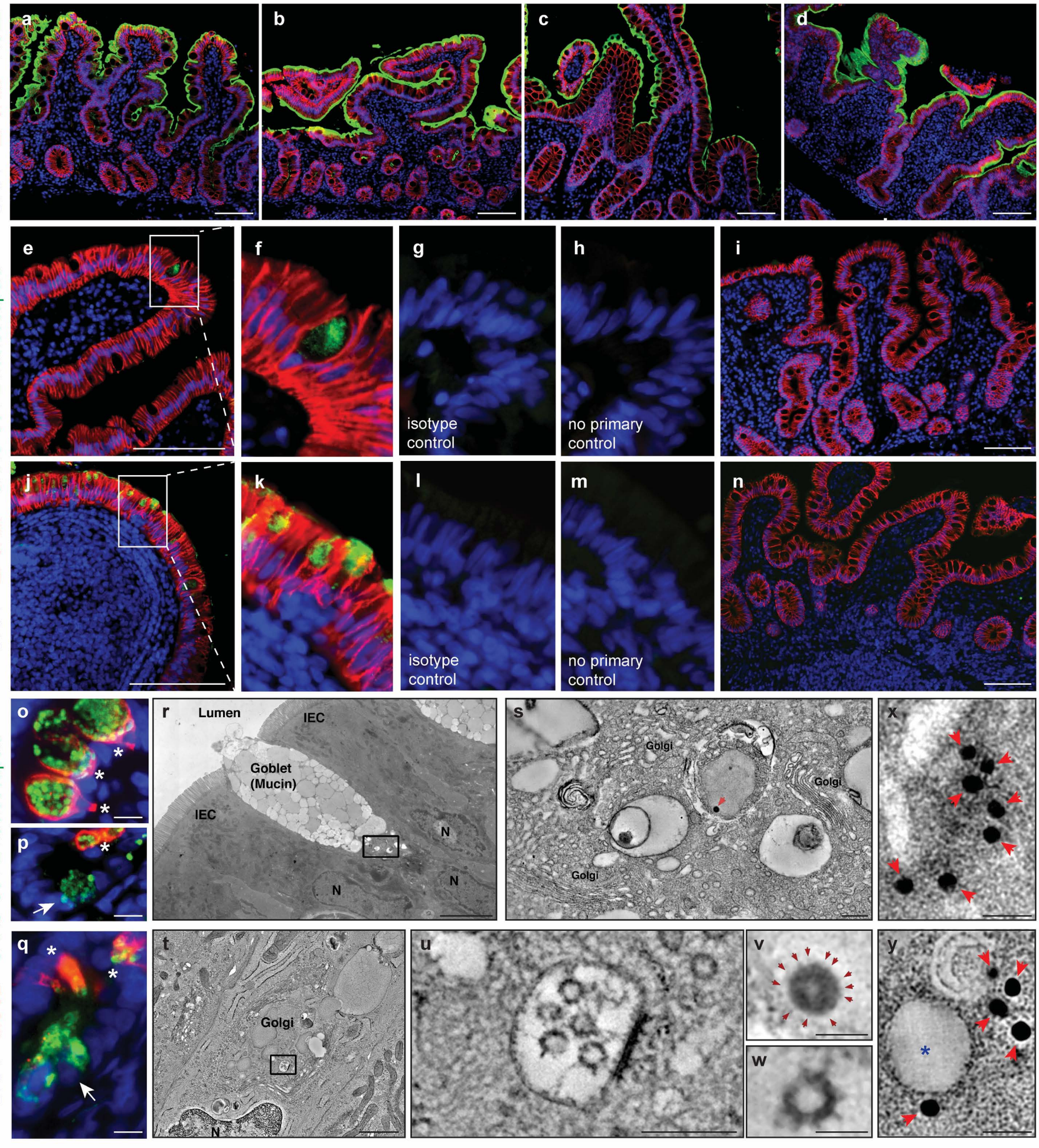
DAPI EPCAM ACE2
a
b
c
d
SARS-CoV-2 nucleocapsid EPCAM DAPI
e
f
g
isotype control
h
no primary control
i
j
k
l
isotype control
m
no primary control
n
SARS-CoV-2 nucleocapsid
o
p
r
Lumen
IEC
Goblet (Mucin)
IEC
N
N
N
s
Golgi
Golgi
Golgi
x
DAPI MUC2 SARS-CoV-2 nucleocapsid
q
t
Golgi
N
u
v
w
y

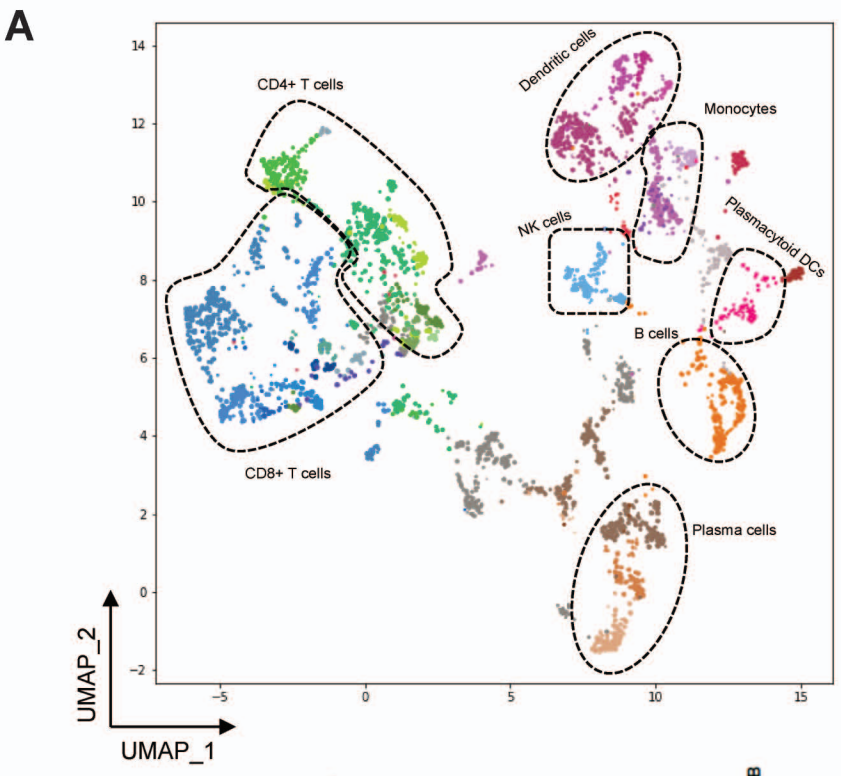
A
CD4+ T cells
Dendritic cells
Monocytes
NK cells
Plasmacytoid DCs
B cells
CD8+ T cells
Plasma cells
UMAP_2
UMAP_1

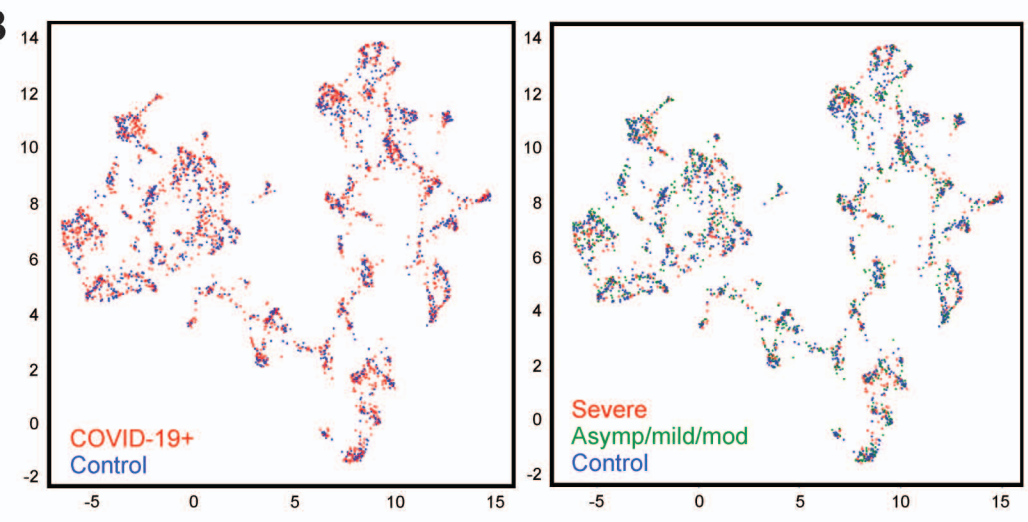
B
COVID-19+
Control
Severe
Asymp/mild/mod
Control

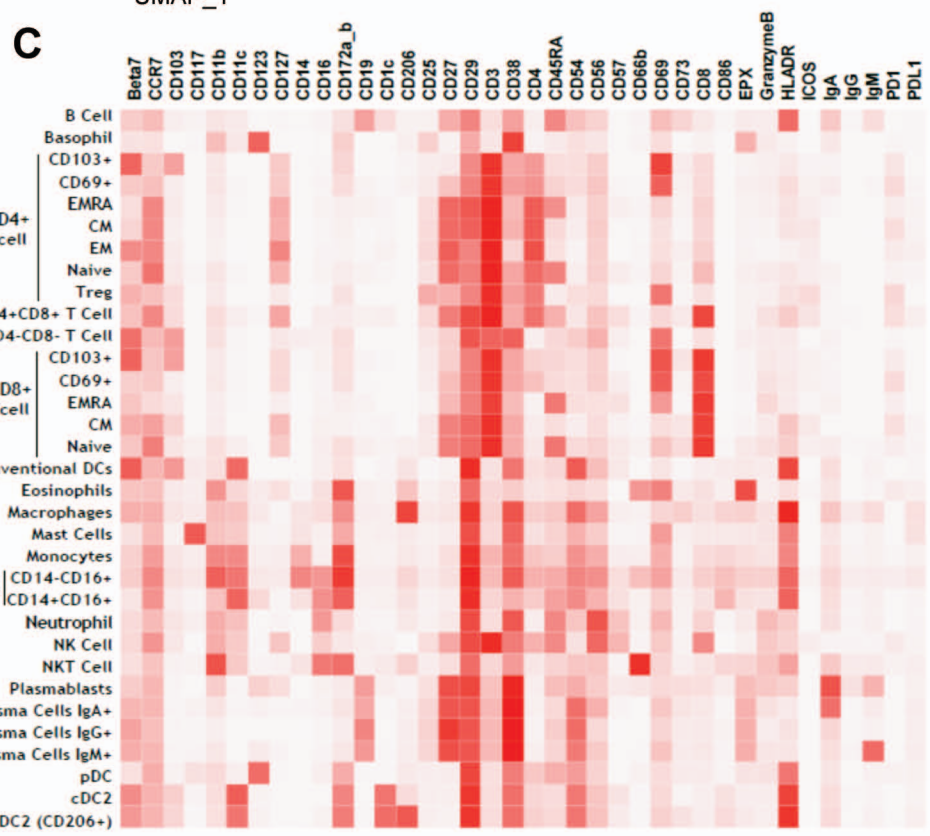
C
Beta7
CCR7
CD103
CD117
CD11b
CD11c
CD123
CD127
CD14
CD16
CD172a_b
CD19
CD1c
CD206
CD25
CD27
CD29
CD3
CD38
CD4
CD45RA
CD54
CD56
CD57
CD66b
CD69
CD73
CD8
CD86
EPX
GranzymeB
HLADR
ICOS
IgA
IgG
IgM
PD1
PDL1
B Cell
Basophil
CD4+ Tcell
CD103+
CD69+
EMRA
CM
EM
Naive
Treg
CD4+CD8+ T Cell
CD4-CD8- T Cell
CD8+ Tcell
CD103+
CD69+
EMRA
CM
Naive
Conventional DCs
Eosinophils
Macrophages
Mast Cells
Monocytes
Monocytes
CD14-CD16+
CD14+CD16+
Neutrophil
NK Cell
NKT Cell
Plasmablasts
Plasma Cells IgA+
Plasma Cells IgG+
Plasma Cells IgM+
pDC
cDC2
cDC2 (CD206+)

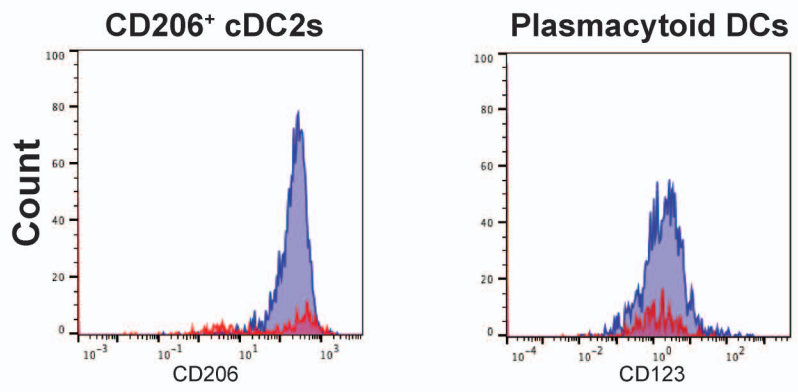
D
CD206⁺ cDC2s
Plasmacytoid DCs
Count
CD206
CD123

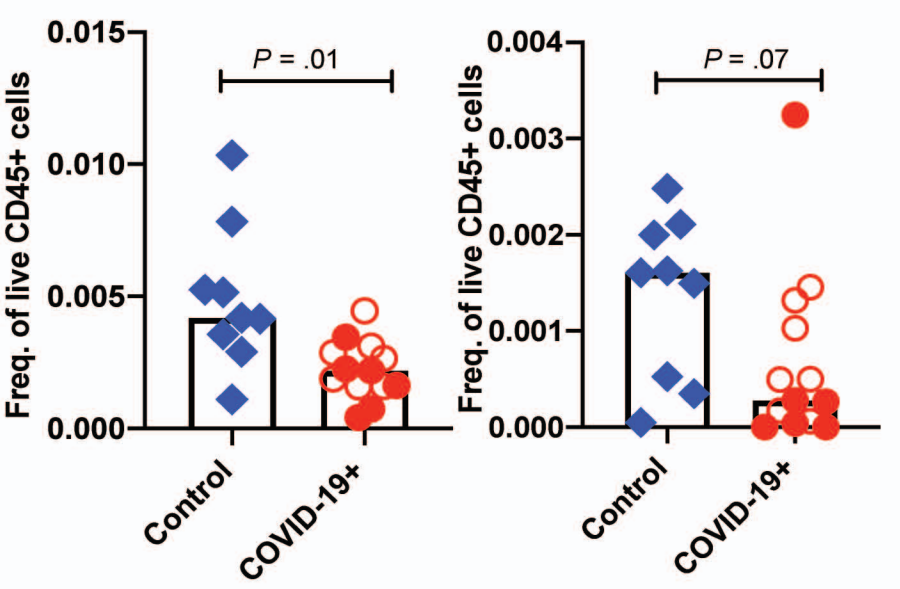
E
Freq. of live CD45+ cells
P = .01
P = .07
Control
COVID-19+

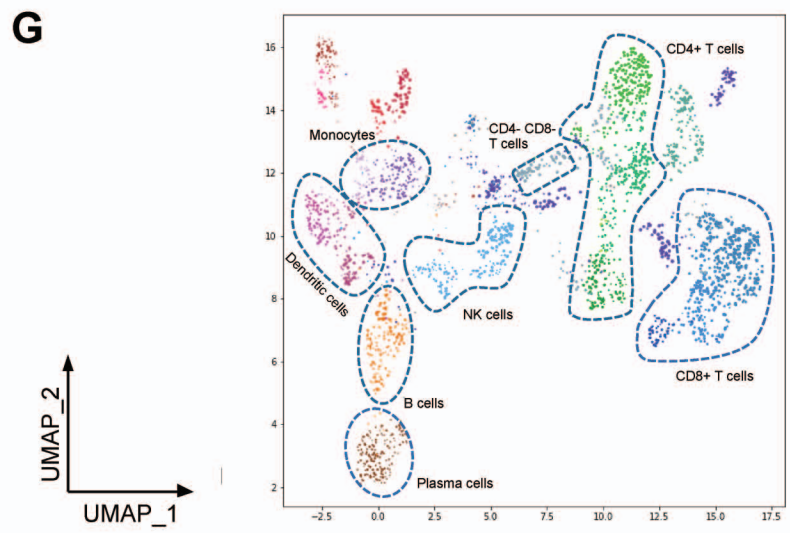
G
Monocytes
CD4- CD8- T cells
CD4+ T cells
Dendritic cells
NK cells
CD8+ T cells
B cells
Plasma cells
UMAP_2
UMAP_1

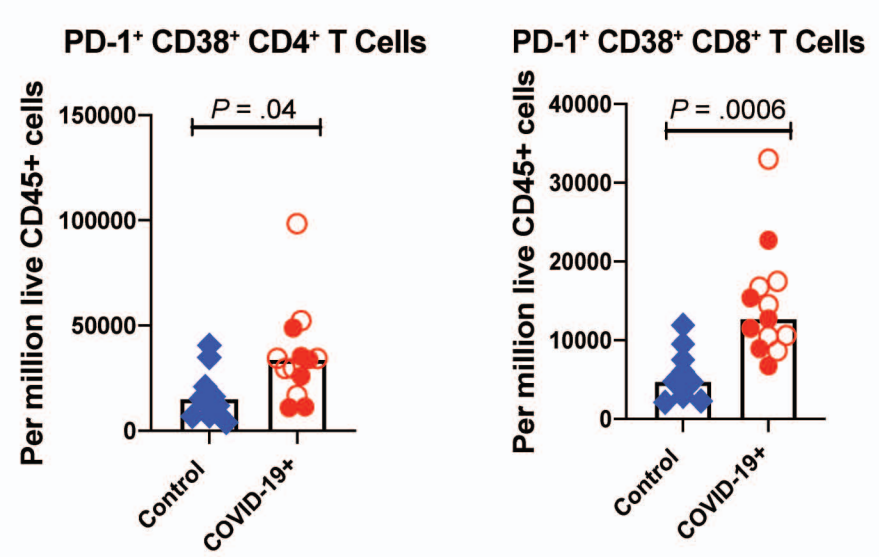
F
PD-1⁺ CD38⁺ CD4⁺ T Cells
PD-1⁺ CD38⁺ CD8⁺ T Cells
Per million live CD45+ cells
P = .04
P = .0006
Control
COVID-19+

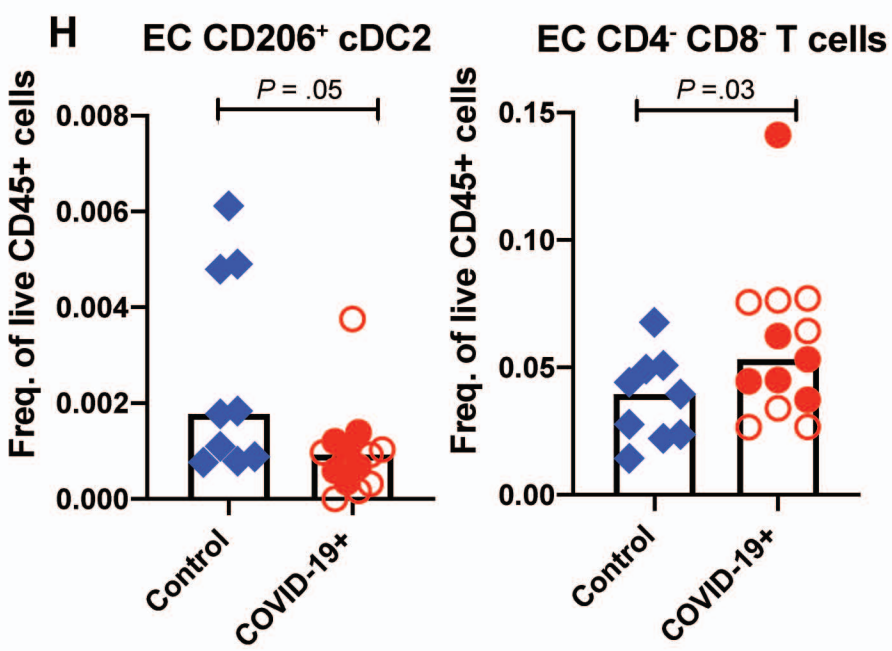
H
EC CD206⁺ cDC2
EC CD4⁻ CD8⁻ T cells
Freq. of live CD45+ cells
P = .05
P =.03
Control
COVID-19+

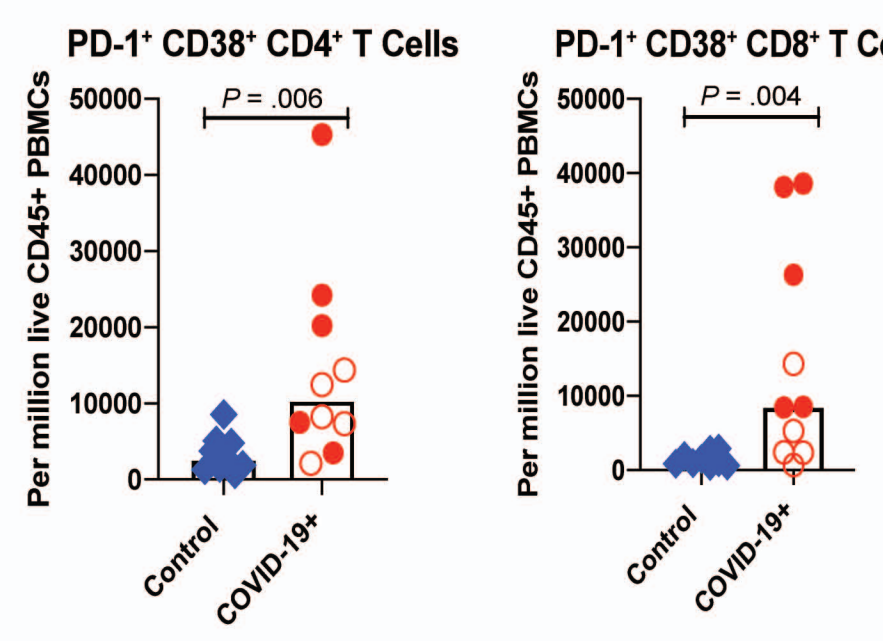
I
PD-1⁺ CD38⁺ CD4⁺ T Cells
PD-1⁺ CD38⁺ CD8⁺ T Cells
Per million live CD45+ PBMCs
P = .006
P = .004
Control
COVID-19+

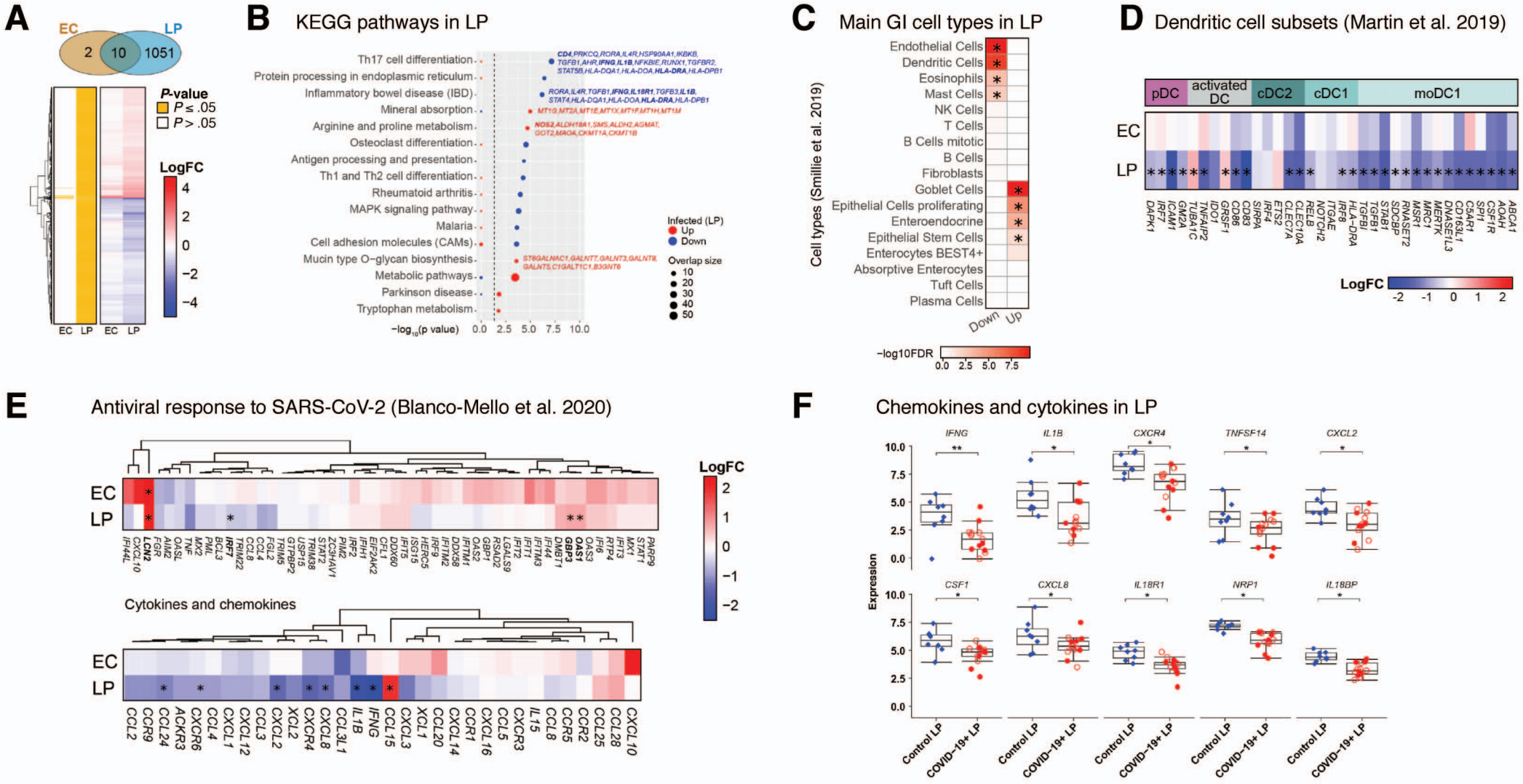
A
EC
LP
2
10
1051
P-value
P ≤ .05
P > .05
LogFC
4
2
0
−2
−4
EC LP EC LP
B
KEGG pathways in LP
Th17 cell differentiation
Protein processing in endoplasmic reticulum
Inflammatory bowel disease (IBD)
Mineral absorption
Arginine and proline metabolism
Osteoclast differentiation
Antigen processing and presentation
Th1 and Th2 cell differentiation
Rheumatoid arthritis
MAPK signaling pathway
Malaria
Cell adhesion molecules (CAMs)
Mucin type O−glycan biosynthesis
Metabolic pathways
Parkinson disease
Tryptophan metabolism
CD4,PRKCQ,RORA,IL4R,HSP90AA1,IKBKB,
TGFB1,AHR,IFNG,IL1B,NFKBIE,RUNX1,TGFBR2,
STAT5B,HLA-DQA1,HLA-DOA,HLA-DRA,HLA-DPB1
RORA,IL4R,TGFB1,IFNG,IL18R1,TGFB3,IL1B,
STAT4,HLA-DQA1,HLA-DOA,HLA-DRA,HLA-DPB1
MT1G,MT2A,MT1E,MT1X,MT1F,MT1H,MT1M
NOS2,ALDH1B1,SMS,ALDH2,AGMAT,
GOT2,MAOA,CKMT1A,CKMT1B
ST6GALNAC1,GALNT7,GALNT3,GALNT8,
GALNT5,C1GALT1C1,B3GNT6
−log10(p value) 0.0 2.5 5.0 7.5 10.0
Infected (LP)
Up
Down
Overlap size
10
20
30
40
50
C
Main GI cell types in LP
Cell types (Smillie et al. 2019)
Endothelial Cells
Dendritic Cells
Eosinophils
Mast Cells
NK Cells
T Cells
B Cells mitotic
B Cells
Fibroblasts
Goblet Cells
Epithelial Cells proliferating
Enteroendocrine
Epithelial Stem Cells
Enterocytes BEST4+
Absorptive Enterocytes
Tuft Cells
Plasma Cells
Down Up
−log10FDR
0.0 2.5 5.0 7.5
D
Dendritic cell subsets (Martin et al. 2019)
pDC
activated DC
cDC2
cDC1
moDC1
EC
LP
DAPK1 IRF7 ICAM1 GM2A TUBA1C TNFAIP2 IDO1 GRSF1 CD86 CD83 SIRPA IRF4 ETS2 CLEC7A CLEC10A RELB NOTCH2 ITGAE IRF8 HLA-DRA TGFBI TGFB1 S100A1 SCIMP SDCBP RNASET2 MSR1 MRC1 MERTK DNASE1L3 CD163L1 C5AR1 SPI1 CSF1R AOAH ABCA1
LogFC
−2 −1 0 1 2
E
Antiviral response to SARS-CoV-2 (Blanco-Mello et al. 2020)
EC
LP
IFI44L CXCL10 LCN2 FGR AIM2 OASL TNF MX2 PML BCL3 IRF7 TRIM22 CCL8 CCL4 FGL2 TRIM5 GTPBP2 USP15 TRIM38 STAT2 ZC3HAV1 PIM2 IRF2 IFIH1 EIF2AK2 CFL1 DDX60 IFIT5 ISG15 HERC5 IRF9 IFITM2 DDX58 IFITM1 OAS2 GBP1 RSAD2 LGALS9 IFIT2 IFIT1 IFITM3 IFI44 DMBT1 GBP3 OAS1 OAS3 IFI6 RTP4 IFI73 MX1 STAT1 PARP9
LogFC
2
1
0
−1
−2
Cytokines and chemokines
EC
LP
CCL2 CCL9 CCL24 ACKR3 CXCR6 CCL4 CCL1 CXCL12 CCL3 CXCL2 XCL2 CXCR4 CXCL8 CCL3L1 IL1B IFNG CCL15 CXCL3 XCL1 CCL20 CXCL14 CCR1 CXCL16 CCL5 CXCR3 IL15 CCL8 CCR5 CCR2 CCL25 CCL28 CXCL10
F
Chemokines and cytokines in LP
IFNG
IL1B
CXCR4
TNFSF14
CXCL2
CSF1
CXCL8
IL18R1
NRP1
IL18BP
Expression
10.0
7.5
5.0
2.5
0.0
Control LP
COVID−19+ LP

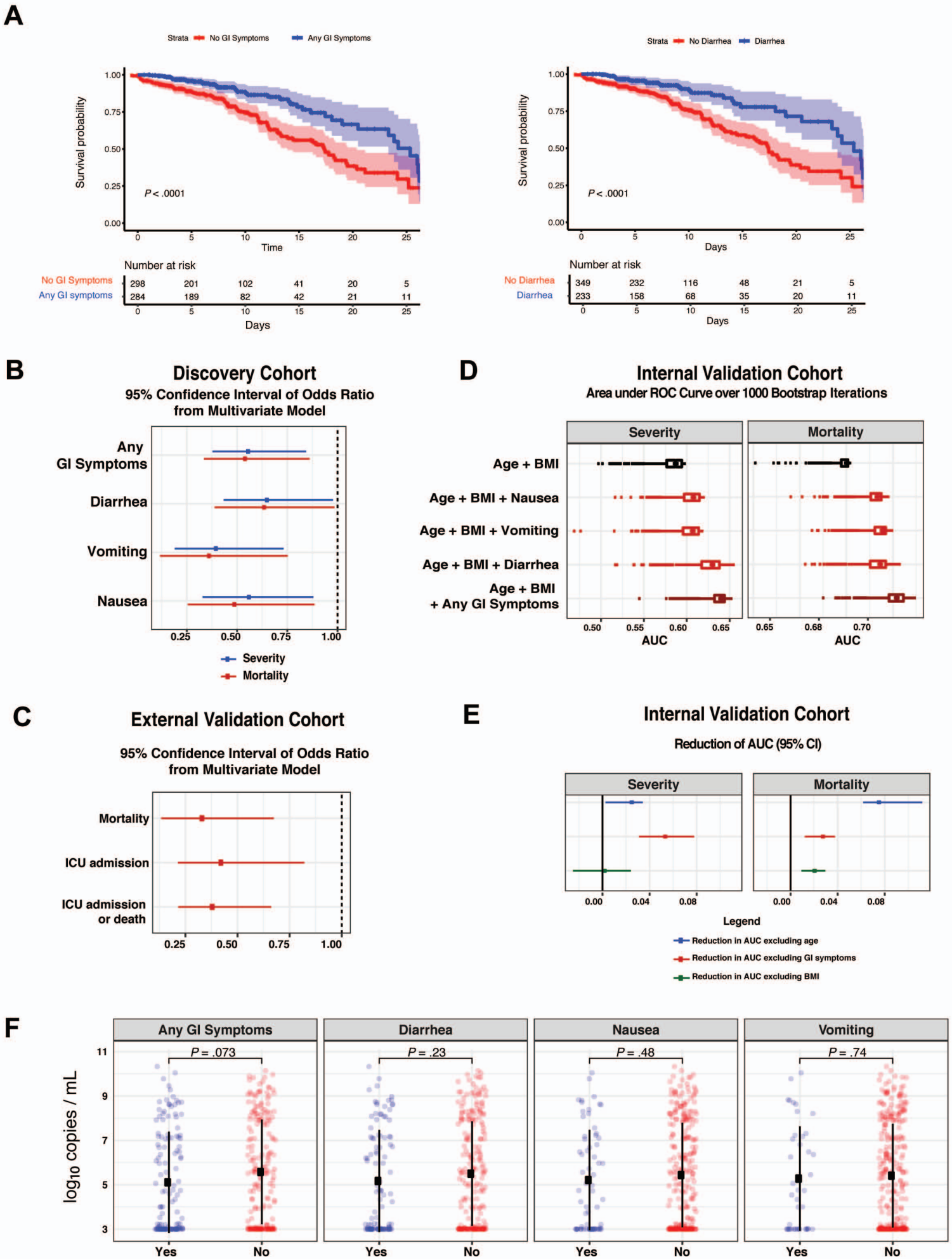
A
Strata No GI Symptoms Any GI Symptoms
Survival probability
1.00
0.75
0.50
0.25
0.00
P < .0001
0 5 10 15 20 25
Time
Number at risk
No GI Symptoms 298 201 102 41 20 5
Any GI symptoms 284 189 82 42 21 11
0 5 10 15 20 25
Days
Strata No Diarrhea Diarrhea
Survival probability
P < .0001
0 5 10 15 20 25
Days
Number at risk
No Diarrhea 349 232 116 48 21 5
Diarrhea 233 158 68 35 20 11
0 5 10 15 20 25
Days
B
Discovery Cohort
95% Confidence Interval of Odds Ratio from Multivariate Model
Any GI Symptoms
Diarrhea
Vomiting
Nausea
0.25 0.50 0.75 1.00
Severity
Mortality
D
Internal Validation Cohort
Area under ROC Curve over 1000 Bootstrap Iterations
Severity
Mortality
Age + BMI
Age + BMI + Nausea
Age + BMI + Vomiting
Age + BMI + Diarrhea
Age + BMI + Any GI Symptoms
0.50 0.55 0.60 0.65
AUC
0.65 0.68 0.70
AUC
C
External Validation Cohort
95% Confidence Interval of Odds Ratio from Multivariate Model
Mortality
ICU admission
ICU admission or death
0.25 0.50 0.75 1.00
E
Internal Validation Cohort
Reduction of AUC (95% CI)
Severity
Mortality
0.00 0.04 0.08
0.00 0.04 0.08
Legend
Reduction in AUC excluding age
Reduction in AUC excluding GI symptoms
Reduction in AUC excluding BMI
F
Any GI Symptoms
Diarrhea
Nausea
Vomiting
P = .073
P = .23
P = .48
P = .74
log10 copies / mL
11
9
7
5
3
Yes No

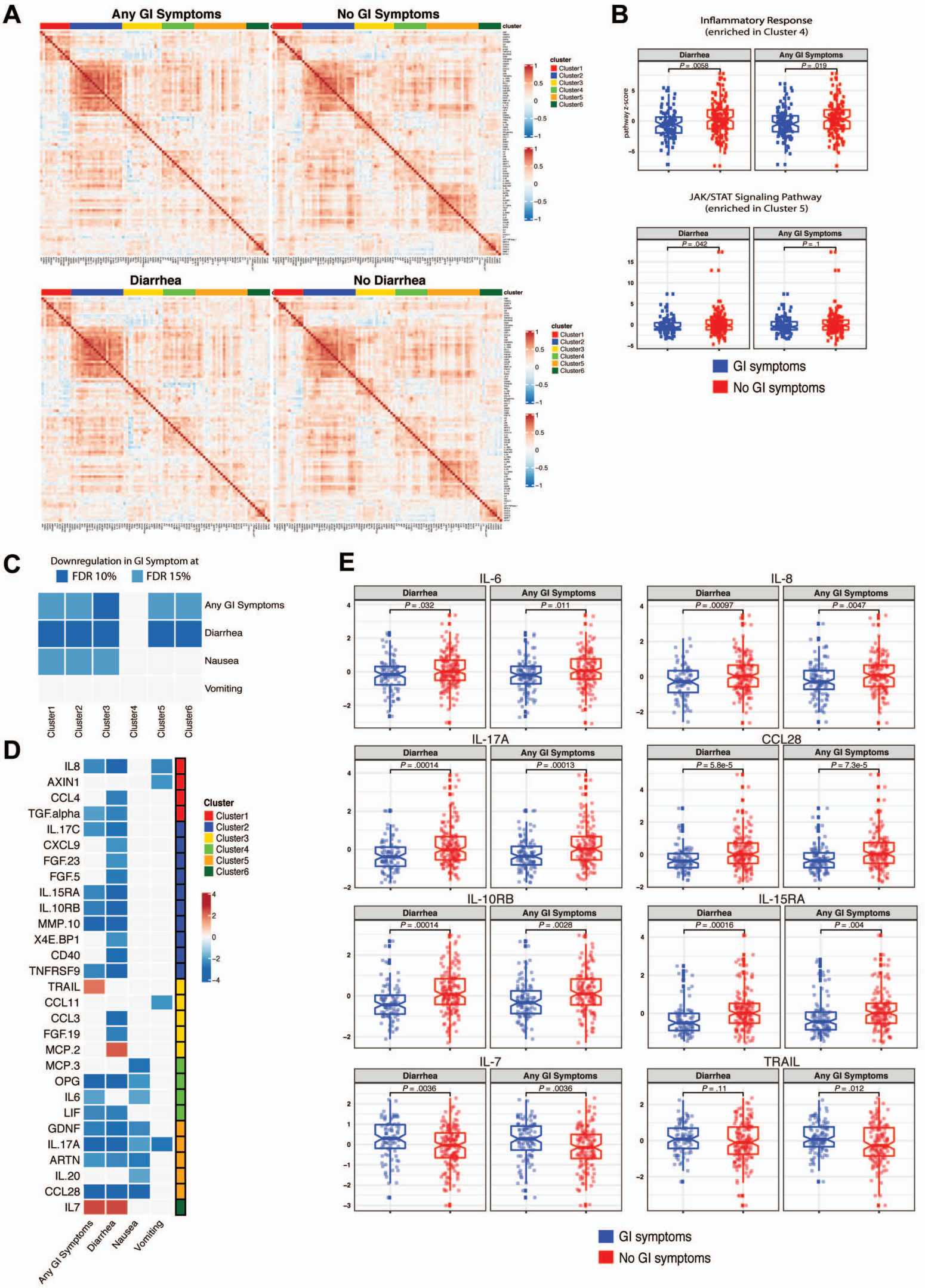
A
Any GI Symptoms
No GI Symptoms
Diarrhea
No Diarrhea
cluster
Cluster1
Cluster2
Cluster3
Cluster4
Cluster5
Cluster6
B
Inflammatory Response
(enriched in Cluster 4)
Diarrhea
Any GI Symptoms
P = .0058
P = .019
pathway z-score
JAK/STAT Signaling Pathway
(enriched in Cluster 5)
P = .042
P = .1
GI symptoms
No GI symptoms
C
Downregulation in GI Symptom at
FDR 10%
FDR 15%
Any GI Symptoms
Diarrhea
Nausea
Vomiting
Cluster1
Cluster2
Cluster3
Cluster4
Cluster5
Cluster6
D
IL8
AXIN1
CCL4
TGF.alpha
IL.17C
CXCL9
FGF.23
FGF.5
IL.15RA
IL.10RB
MMP.10
X4E.BP1
CD40
TNFRSF9
TRAIL
CCL11
CCL3
FGF.19
MCP.2
MCP.3
OPG
IL6
LIF
GDNF
IL.17A
ARTN
IL.20
CCL28
IL7
Any GI Symptoms
Diarrhea
Nausea
Vomiting
Cluster
E
IL-6
P = .032
P = .011
IL-8
P = .00097
P = .0047
IL-17A
P = .00014
P = .00013
CCL28
P = 5.8e-5
P = 7.3e-5
IL-10RB
P = .00014
P = .0028
IL-15RA
P = .00016
P = .004
IL-7
P = .0036
P = .0036
TRAIL
P = .11
P = .012
GI symptoms
No GI symptoms

Short summary: Intestinal infection with SARS-CoV-2 is associated with a mild inflammatory response and improved clinical outcomes.

What you need to know

BACKGROUND AND CONTEXT

Gastrointestinal manifestations are common in COVID-19, however to date, there is limited evidence of SARS-CoV-2 infection of human enterocytes, tissue immune responses and relationship to clinical outcomes.

NEW FINDINGS

Immunofluorescence and electron microscopic detection of SARS-CoV-2 in small intestinal biopsies obtained from patients with COVID-19.

Downregulation of key inflammatory pathways and reduced myeloid cells in intestinal biopsies.

Lower severity and mortality in COVID-19 patients with GI symptoms in a multivariable model in 2 large independent cohorts from the United States and Europe.

LIMITATIONS

Clinical documentation of GI symptoms might vary depending on providers and on the acuity of the patients' presentation.

IMPACT

These data demonstrate *in vivo* GI tract infection by SARS-CoV-2 and the clinical impact of GI symptoms on COVID-19 outcomes in two large patient cohorts.

Intestinal host response to SARS-CoV-2 infection and COVID-19 outcomes in patients with gastrointestinal symptoms

Supplementary materials and methods

Clinical cohorts

1. Intestinal Biopsy Cohort

Subjects included hospitalized patients at Mount Sinai Hospital (MSH) as well as those seen in the outpatient GI practices that underwent endoscopy between April 17, 2020 and June 2, 2020. COVID-19 cases and controls were defined on the basis of nasopharyngeal SARS-CoV-2 swab PCR tests. Inclusion criteria included: (1) A positive nasopharyngeal (NP) SARS-CoV-2 PCR test, relevant clinical symptoms and serological evidence of anti-SARS-CoV-2 antibodies (for cases), and a negative NP SARS-CoV-2 test AND absence of fever, cough, shortness of breath and relevant contact history (for controls); (2) Clinical indication for endoscopic procedure; and (3) The patient and/or his/her health care proxy's ability to provide informed consent. Exclusion criteria included: (1) Comorbid conditions including severe coagulopathy; (2) concomitant anticoagulation use; (3) critical illness and any other clinical parameter which could potentially increase the of risk of additional research biopsies; and (4) Failure to obtain consent. COVID-19 severity was defined based on internal scoring system developed by the Department of Infectious Diseases at MSH. This scoring system was developed according to the WHO Ordinal Clinical Progression/Improvement Scale (https://www.who.int/publications/i/item/covid-19-therapeutic-trial-synopsis) and based on oxygenation status and organ damage, with the following definitions: Mild - SpO2>94% on room air AND no pneumonia on imaging, Moderate - SpO2<94% on room air OR pneumonia on imaging, Severe - high flow nasal cannula (HFNC), non-rebreather mask (NRBM), Bilevel Positive Airway Pressure (non-invasive positive airway

ventilation), or Mechanical ventilation AND no pressor medications AND creatinine clearance > 30 AND ALT < 5x upper limit of normal, Severe with evidence of end organ damage (EOD) - high flow nasal canula (HFNC), non-rebreather mask (NRBM), Bilevel Positive Airway Pressure (non-invasive positive airway ventilation), or Mechanical ventilation AND pressor medications OR creatinine clearance <30 OR new renal replacement therapy OR ALT > 5x upper limit of normal (Supplementary Table 3).

2. Discovery Cohort

Patients admitted to MSH between April 1, 2020 and April 15, 2020 were recruited into the Discovery Cohort if they were SARS-CoV-2 PCR positive, more than 18 years of age and if the "ELLA panel of cytokines" (IL-6, IL-8, IL-1β and TNF-α) was performed as part of clinical care. Clinical details from eligible patients were extracted from Mount Sinai Data Warehouse (MSDW) under an IRB approved protocol (IRB-20-03297A North American registry of the digestive manifestations of COVID-19). Inclusion criteria included (1) A positive NP SARS-CoV-2 PCR test within the Mount Sinai Health System between April 1-15, 2020 and admission to the Mount Sinai Hospital; (2) Age >18 years of age; and (3) Patients who had an ELLA cytokine panel performed during hospitalization. Exclusion criteria included (1) Testing at a site outside of Mount Sinai Hospital in an ambulatory setting or those who were tested in the emergency room but not admitted; (2) Patients <18 years of age; and (3) Patient's without an ELLA cytokine panel.

A total of 634 subjects were included in the Discovery Cohort (Supplementary Figure 11). In addition to demographic information (including race and ethnicity, age and gender), clinical characteristics, laboratory data and outcomes data was extracted from the medical charts. Co-

variates that were studied included: BMI (obesity defined as BMI >30) and comorbid conditions including, hypertension, diabetes, chronic lung disease (including asthma and COPD), heart disease (including coronary artery disease, atrial fibrillation and heart failure), chronic kidney disease, cancer, HIV, and inflammatory bowel disease (IBD).

GI symptoms were defined as more than one episode of either diarrhea, nausea, and/or vomiting at the time of admission. If only one episode of either diarrhea, nausea, and/or vomiting was specifically documented, patients were not considered to have GI symptoms. Additionally, we did not consider GI symptoms that developed during the course of hospitalization, as they could reflect nosocomial or treatment-related effects and only considered the GI symptoms that were present at the time of hospital admission so as to avoid including iatrogenic confounders (treatments or hospital acquired illnesses that can result in diarrhea, nausea and vomiting).

Disease severity (as described above) and mortality were considered as outcomes variables. Mortality was calculated as patient status (dead or alive) at 25 days post admission. If no information was available after discharge, patients were censored at the time of hospital discharge.

3. External Validation Cohort

This cohort consisted of 287 patients admitted to a tertiary care center in Milan, Italy between February 22, 2020 and March 30, 2020, with a confirmed positive SARS-CoV-2 PCR and who did not die or were not transferred to the ICU within 24 hours from admission were studied as detailed in *Aghemo et al*[1]. Presence of vomiting and diarrhea (defined as at least three loose bowel movement per day) on or prior to admission was recorded. Outcomes were analyzed using ICU admission, death or the composite study end-point of ICU admission or death within 20 days of hospitalization.

4. Internal Validation Cohort

The Internal Validation Cohort is a distinct cohort of patients admitted to MSH between April 16, 2020 and April 30, 2020 used to test a predictive model for COVID-19 severity and mortality. The same inclusion and exclusion criteria as in the Discovery Cohort were used with the following differences: (1) A positive SARS-CoV-2 PCR test between April 16, 2020 and April 30, 2020; (2) An additional exclusion of patients that were already included in the Discovery Cohort. From a total of 408 patients, 242 met inclusion criteria and were thus included in the Internal Validation Cohort. Demographic, clinical and outcomes related data was extracted from patients' medical records as described for the Discovery Cohort.

SARS-CoV-2 testing

The SARS-CoV-2 PCR was run in the Clinical Microbiology laboratory as part of routine care on the Roche cobas platform which performs selective amplification of 2 targets ORF-1 gene (Target 1) and the E-gene for pan-Sarbecovirus (Target 2) (detects SARS-CoV-2 as well as SARS or MERS viruses, but not routine seasonal Coronavirus). A positive result indicated that either both Target 1 and Target 2 were detected (majority of cases) or Target 1 alone was detected. A presumptive positive result indicates a negative Target 1 result and a positive Target 2 result which according to the manufacture can be a result of the following: "1) a sample at concentrations near or below the limit of detection of the test, 2) a mutation in the Target 1 target region in the oligo binding sites, or 3) infection with some other Sarbecovirus (e.g., SARS-CoV or some other Sarbecovirus previously unknown to infect humans), or 4) other factors." Patients with a presumptive positive SARS-CoV-2 PCR were included in the analysis if they were treated clinically as having COVID-19.

Immunofluorescent (IF) microscopy

Sections (5μm) of formalin fixed, paraffin embedded tissue were dewaxed in xylene and rehydrated in graded alcohol and then washed in phosphate-buffered saline (PBS). Heat-induced epitope retrieval was performed by incubating slides in a pressure cooker for 15 minutes on high in target retrieval solution (Dako, S1699). Once slides cooled to room temperature, they were washed twice in PBS and then permeabilized for 30 minutes in 0.1% tritonX-100 in PBS. Non-specific binding was blocked with 10% goat serum for 1 hour at room temperature. Sections were then incubated in primary antibodies diluted in blocking solution overnight at 4°C. Primary and secondary antibodies are summarized in Supplementary Table 16. Slides were washed in PBST (0.1% tween 20, PBS) thrice and then incubated in secondary antibody and 4′,6-diamidino-2-phenylindole (1μg/mL) for 1 hour at room temperature. Sections were washed twice in PBST and once in PBS then mounted with Fluoromount-G (Electron microscopy sciences, 1798425). Controls included, omitting primary antibody (no primary control), or substituting primary antibodies with non-reactive antibodies of the same isotype (isotype control). Tissue was visualized and imaged using a Nikon Eclipse Ni microscope and digital SLR camera (Nikon, DS-Qi2).

IEL quantification

Three-10x non-overlapping IF images were taken for each biopsy. Twelve biopsies (10 duodenum, 2 ileum) from 11 COVID-19 patients in the biopsy cohort were analyzed along with 9 uninfected controls (5 duodenum, 4 ileum). CD3+ intraepithelial lymphocytes (IELs) and CD3+ CD8+ (IELs) were quantified for each image. The length of epithelium in each image was measured in ImageJ[2]. Biopsies from COVID-19 patients and controls were compared via unpaired t test.

Routine Clinical Electron Microscopy (EM)

Following post-fixation in 1% osmium tetroxide, tissues were serially dehydrated and embedded in epoxy resin in standard fashion. One-micron toluidine-stained scout sections were prepared for light microscopic orientation; 80 nm ultrathin sections for EM were stained with uranyl acetate and lead citrate and examined in a Hitachi 7650 transmission electron microscope at 80kV.

Infection of cultured cells for EM and Electron Tomography (ET) analyses

Viral infections of cultured cells were conducted at the UVM BSL-3 facility under an approved Institutional Biosafety protocol. SARS-CoV-2 strain 2019-nCoV/USA_USA-WA1/2020 (WA1) was generously provided by Kenneth Plante and the World Reference Center for Emerging Viruses and Arboviruses at the University of Texas Medical Branch and propagated in African green monkey kidney cells (Vero E6) that were kindly provided by J.L Whitton. Vero E6 cells were maintained in complete Dulbecco's Modified Eagle Medium (cDMEM; Thermo Fisher, Cat. #11965–092) containing 10% fetal bovine serum (Gibco, Thermo-Fisher, Cat. #16140–071), 1% HEPES Buffer Solution (15630–130), and 1% penicillin–streptomycin (Thermo Fisher, Cat. #15140–122). Cells were grown in a humidified incubator at 37ºC with 5% CO_2. Vero E6 cells seeded in six well dishes and infected with SARS-CoV-2 at a multiplicity of infection of 0.01 for 48 hours before fixing and preparing for electron microscopy. Cells were pre-fixed with 3% glutaraldehyde, 1% paraformaldehyde, 5% sucrose in 0.1M sodium cacodylate trihydrate,

removed from the plates and further prepared by high-pressure freezing and freeze-substitution as described below.

Electron Microscopy and Dual-Axis Tomography of Intestinal Biopsy Tissue

Tissue samples were fixed with 3% glutaraldehyde to meet biosafety requirements. Tissues were rinsed with cold 0.1M sodium cacodylate trihydrate + 5% sucrose and further dissected to block sizes sufficient for high-pressure freezing. Tissues or cultured cells were rinsed with 0.1M cacodylate buffer containing 10% Ficoll (external cryoprotectant), placed into brass planchettes (Ted Pella, Inc.) and ultra-rapidly frozen with a HPM-010 High Pressure Freezing Machine (Bal-Tec/ABRA, Switzerland). Vitreously frozen samples were transferred under liquid nitrogen to Nalgene cryogenic vials (Thermo-Fisher Scientific) containing a frozen mixture of 2% OsO_4, 0.05% uranyl acetate in acetone. Vials were placed in a AFS-2 Freeze-substitution machine (Leica Microsystems, Vienna) and the samples freeze-substituted for 72 h at -90°C. Samples were then warmed to -20°C over 24 h and held at that temperature for a further 12 h before being warmed to room temperature, rinsed 3x with acetone, then infiltrated into Epon-Araldite resin (Electron Microscopy Sciences). Samples were flat-embedded between two Teflon-coated glass microscope slides and the resin polymerized at 60 °C for 24 h. Embedded tissue blocks were observed by light microscopy to ascertain preservation quality and select regions of interest (i.e., apical epithelium). Blocks were extracted with a scalpel and glued to plastic sectioning stubs prior to sectioning. Semi-thin (150 nm) serial sections were cut with a UC6 ultramicrotome (Leica Microsystems) using a diamond knife (Diatome, Ltd. Switzerland). Sections were placed on formvar-coated copper-rhodium slot grids (Electron Microscopy Sciences) and stained with 3% uranyl acetate and lead citrate. Colloidal gold particles (10 nm) were placed on both surfaces

of the grids to serve as fiducial markers for tomographic image alignment. Grids were placed in a dual-axis tomography holder (Model 2010, E.A. Fischione Instruments, Export PA) and imaged with a Tecnai G2 T12 transmission electron microscope (120 KeV; ThermoFisher Scientific). Images were recorded with a 2k x 2k CCD camera (XP1000; Gatan, Pleasonton, CA). Tomographic tilt series and large-area montages were acquired automatically using the SerialEM software package[3]. For dual-axis tomography, images were collected at 1° intervals as samples were tilted +/- 62°. The grid was then rotated 90° and a second tilt-series was acquired about the orthogonal axis. Tomograms were calculated, analyzed and modeled using the IMOD software package[4, 5] on MacPro and iMac Pro computers (Apple, Inc).

Presumptive SARS-CoV-2 virions were identified from tomographic reconstructions of tissue samples by observing structures resembling virions described in cryo-electron tomography studies of purified SARS-CoV-2 and SARS-CoV-2 in infected cells[6-9] and comparing to identified virions within SARS-CoV-2–infected cultured cells (Supplementary Figure 6). We used the following criteria for SARS-CoV-2 virion identification in tissues: (*i*) Structures that were spherical in 3D and not continuous with other adjacent structures with ~60-120 nM diameters, (*ii*) Spherical structures with densities corresponding to a distinct membrane bilayer, internal puncta consistent with ribonucleoproteins[6], and densities corresponding to surface spikes on the external peripheries of the spheres. Particles resembling virions were examined in 3D by tomography prior to assignments (Supplementary Movies 1 and 2). We note that the inner vesicles of multivesicular bodies (MVBs) have been mis-identified as SARS-CoV-2 by electron microscopy[10]. We therefore compared measurements of MVB inner vesicles and presumptive coronavirus virions from what we identified as intracellular exit compartments within the same tomogram (unpublished results) with our previous tomographic reconstructions of MVBs[11, 12].

We distinguished virions inside a cytoplasmic exit compartment from the inner vesicles of an MVB based on differences in size (MVB inner virions are generally smaller in diameter than coronaviruses) and the presence of surface spikes and internal puncta (MVB inner vesicles do not present surface spikes or internal puncta).

Cell Culture Experiments and Virus Isolation

African green monkey kidney epithelial cells (Vero E6) were originally purchased from American Type Culture Collection (ATCC). Cells were maintained in Dulbecco's modified Eagle's medium (DMEM) w/ L-glutamate, sodium pyruvate (Corning) supplemented with 10% fetal bovine serum (FBS), 100 U penicillin/ml, and 100 mg streptomycin/ml. For all experiments, the cells were always maintained in monolayers.

Several attempts were made to isolate live infectious particles from these biopsies. Briefly, biopsies were collected and stored in PBS until homogenization. Following homogenization and centrifugation (10,000 × g, 20 min, 4°C), the resulting supernatant tissue supernatant was inoculated onto Vero E6 monolayer maintained in optimal virus growth media for SARS-CoV-2 virus (DMEM w/ L-Glutamate, Sodium Pyruvate, 2% FBS, 100 U Penicillin/ml, and 100 mg Streptomycin/ml, 10 mM Non-Essential Amino Acids, 1 mM Sodium Pyruvate and 10 mM HEPES). Vero E6 cells were incubated at 37 °C, 5% CO2 for a week and monitored daily for potential cytopathic effect (CPE).

Cell culture supernatants were also collected and assessed for the presence of infective particles by plaque assay. Briefly, ten-fold serial dilutions were performed in infection media for SARS-CoV-2 and inoculated onto confluent Vero E6 cell monolayer in 6-well plate. After one-hour adsorption, supernatants were removed, and cells monolayers were overlaid with minimum

essential media (MEM) containing 2% FBS and purified agar (OXOID) at a final concentration of 0.7%. Cells were then incubated for 3 days at 37°C. Cells were fixed overnight with 10% formaldehyde for the inactivation of potential SARS-CoV-2 virus. Overlay was removed and cells were washed once with PBS. A 2% crystal violet solution was used for plaque visualization and count. Experiments were performed under BSL3 conditions.

Viral SARS-CoV-2 RNA Detection in Intestinal Biopsy Tissue

To detect SARS-CoV-2 RNA from intestinal biopsies, a modified version of the CDC 2019-nCoV real-time RT-qPCR was used. Primers and probes were commercially available (Integrated DNA Technologies, cat. 10006713, RUO Kit). SARS-CoV-2 primer and probe sets consisted of two 2019-nCoV-specific sets (N1, N2). A third primer set was used to detect host cellular RNaseP. Reactions were run using the QuantiFast Pathogen RT-PCR +IC Kit (QIAGEN, cat. 211454). Assays were run using USA/WA-1/2020 SARS-CoV-2 RNA as a positive control and nuclease-free water as a non-template control in a 384-well format. A plasmid containing the genome sequence of the N protein (Integrated DNA Technologies, cat. 10006625, RUO Kit) was used to calculate genome copy number of from their respective CT (cycle threshold) using the linear equation from the respective plasmid standard curve. Limit of detection was established as 1-10 copies per μL. Reactions were performed in duplicate using the following cycling conditions on the Roche LightCycler 480 Instrument II (Roche Molecular Systems, 05015243001): 50°C for 20 min, 95°C for 1 sec, 95°C for 5 min, followed by 45 cycles of 95°C for 15 sec and 60°C for 45 sec. Limit of detection for SARS-CoV-2 was determined by using a commercially available plasmid control (Integrated DNA Technologies, cat. 10006625).

Biopsy collection and processing for Mass cytometry (CyTOF)

Biopsies were transferred to 10 ml of 'dissociation buffer' (1M HEPES(Lonza), 5μM EDTA(Invitrogen), 10% FBS in HBSS buffer (Gibco)). The tubes were kept in a shaker (180 rpm, 37°C) for 20 min and then gently vortexed. Cell suspensions were collected after passing the biopsies through 100μm cell strainers. A second round of EDTA dissociation was performed as detailed above. The cell suspension was centrifuged at 1800 rpm to pellet the epithelial fraction and kept on ice. The remaining tissue was transferred to fresh tubes containing a 'digestion buffer' (2% FBS, 0.005g Collagenase type IV per sample (Sigma), 100 μl DNAse-I (Sigma) in RPMI). Tubes were placed in the shaker (180 rpm, 37°C) for 40 min and thereafter gently vortexed. The digested tissues were filtered through 100 μm cell strainers followed by another round of filtration through 40μm cell strainers. Cell suspensions were centrifuged at 1800 rpm to obtain lamina propria mononuclear cells. Both epithelial cell (EC) and lamina propria (LP) pellets were then resuspended into 500 μl of RPMI (Gibco) containing 10% FBS+ 1μl Rh103 +1μl IdU and incubated at 37°C for 20 min. 5 ml RPMI (+10%FBS) was added to each tube and spun at 1800 rpm to pellet cells. 700 μl of Prot1 stabilizer (SmartTube Inc.) was added to each tube and transferred to cryovials and incubated at room temperature for 10 min. Cryovials were immediately transferred to -80°C until the sample was acquired for mass cytometry as detailed below.

Blood collection and processing for CyTOF

Briefly, 15ml of Lymphosep® - Lymphocyte Separation Medium (MP Bio.) was added to each 50 ml centrifugation tube. Blood was diluted with PBS to bring the volume up to 30ml and diluted blood was layered gently over Lymphosep®. Tubes were then centrifuged at 2000 rpm

for 20 mins with the brakes and acceleration off. After centrifugation, the buffy coat containing PBMCs was transferred to another tube and was centrifuged at 1800 rpm to pellet the cells. Pellets were resuspended in PBS and tubes were centrifuged at 1800 rpm. Finally, the pellets were resuspended in the freezing medium (10% DMSO + 44% FBS in RPMI) and cryopreserved at -80 °C.

CyTOF processing and data acquisition

Cells were processed as previously described by *Geanon et al*[13]. Briefly, EC and LP SmartTube proteomic stabilized samples were thawed in a 10°C water bath and washed with Cell Staining Buffer (Fluidigm). To facilitate data acquisition and doublet removal, multiple samples were also barcoded using Fluidigm Pd barcoding kits and then washed and pooled for data acquisition. Immediately prior to data acquisition, samples were washed with Cell Staining Buffer and Cell Acquisition Solution (Fluidigm) and resuspended at a concentration of 1 million cells per ml in Cell Acquisition Solution containing a 1:20 dilution of EQ Normalization beads (Fluidigm). The samples were then acquired on a Helios Mass Cytometer equipped with a wide-bore sample injector at an event rate of <400 events per second. After acquisition, repeat acquisitions of the same sample concatenated and normalized using the Fluidigm software, and barcoded samples were de-multiplexed using the Zunder single cell debarcoder.

CyTOF Data analysis

De-barcoded files were uploaded to Cytobank for analyses. Immune cells were identified based on Ir-193 DNA intensity and CD45 expression; Ce140+ normalization beads, CD45-low/Ir-193-low debris and cross-sample and Gaussian ion-cloud multiplets were excluded from subsequent

downstream analysis. CyTOF antibody panel is detailed in Supplementary Data File 1. Major immune cell types were identified using automated Astrolabe approach, the result of which largely correlated well with our manual gating approaches. The impact of each tested condition on relative staining quality was evaluated in two ways: 1) overall correlations were determined by calculating the Pearson's correlation coefficients for the median expression of each marker across each defined immune subset; and 2) a staining index was calculated using defined populations showing the highest and lowest expression levels of each marker: SI = (Medianpos - Medianneg) / 2 X Std.Devneg. It is already been described that SmartTube-based fixation protocols take into account previously described mass cytometry artifacts such as cell-cell multiplets, isotopic spillover or oxidation, or mass cytometer instrument configuration[13].

Statistical Analysis for CyTOF

Pre-gated viable CD45+ cells were first clustered and annotated using the Astrolabe Cytometry Platform (Astrolabe Diagnostics, Inc.), which involves using a hierarchy-based FlowSOM algorithm for labeling cell populations in individual samples. These Astrolabe Profiling clusters from each tissue type were then meta-clustered across all samples utilizing Clustergrammer2's interactive heatmap as a method to interrogate antibody expression across every cluster and curate and assign cell population categories. Single sample clusters were also visualized using UMAP. Pairwise comparisons were performed on the frequencies of each identified cell population between the patient cohorts (COVID-19 vs. control, COVID-19 severe vs. control, COVID19-asymptomatic/mild/moderate vs. control) to determine fold change, p-values and FDR adjusted p-values using the Benjamini-Hochberg[14] method to account for multiple comparisons.

RNA Sequencing

Library preparation and sequencing

Directional RNA-seq libraries were prepared from 50 ng of total RNA from EC and LP samples with the TruSeq® Stranded Total RNA prep with Ribo-Zero kit (Cat no. 20020599). Paired-end (100 bp) sequencing was performed for DNA libraries on an Illumina NovaSeq instrument on a NovaSeq S1 Flowcell, with an average yield of 39 million PE reads/sample.

RNA-seq analysis

Base-calling and quality scoring of sequencing data were done through Illumina's Real-Time Analysis (RTA) software. RNA-seq data processing and reference mapping were done with custom analysis scripts combining publicly available tools as previously described[15] with modifications as follows, reads were mapped to a custom reference that combined the human hg38 reference genome (Release 34, GRCh38.p13) and the SARS-CoV-2 genome (RefSeq NC_045512) for simultaneous quantification of host and virus transcripts.

Differential gene expression (DGE) analysis was performed with the Bioconductor edgeR package[16] using as input a combined matrix of mapped paired-end read raw counts, with genes in rows and samples in columns. Prior to DGE analysis, gene counts were converted to fragments per kb per million reads (FPKM) with the RSEM package with default settings in strand-specific mode[17].

Genes with less than 1 FPKM in at least 50% of the samples were removed. The remaining gene counts were then normalized across samples using the weighted trimmed mean of M-values (TMM) method[18]. The dispersion was estimated by fitting a generalized linear

model (GLM) as implemented in edgeR, sex was fitted as a covariate on a per-patient paired design. Pairwise comparisons were performed between sample groups (i.e., between tissue sections, and between cases and controls). Significant expression differences were selected based on eBayes adjusted p values corrected for multiple testing using the Benjamini-Hochberg method ($q \leq 0.05$).

Gene Ontology and Pathway Enrichment Analysis

KEGG pathway and gene ontology (GO) biological process (BP), molecular function (MF), and/ or cellular component (CC) enrichment analyses were performed using the gProfileR R v0.6.8 package[19]. The background gene set was restricted genes with detected expression (defined as genes with expression levels above 1 FPKM in at least 50% of samples). Genes with differential expression were ranked by log 2 fold change and used as an ordered query. P values were corrected using the g:SCS algorithm to account for multiple comparisons.

Cell-type deconvolution and gene signature enrichment analysis

For cell-type deconvolution of the bulk RNA-seq data, Gene Set Enrichment Analysis (GSEA) of differentially expressed genes of cases vs controls comparisons was performed against cell type gene-expression single-cell signatures from intestinal mucosa[20] and gene-expression signatures from ileal dendritic cell (DCs) subsets[21]. Similarly, differentially expressed genes were tested for enrichment of gene signatures associated with an antiviral response, inflammation, and cytokine signaling in acutely infected post-mortem tissue with SARS-CoV-2[22] , were tested for significant ($p \leq 0.05$) enrichment using Fisher's exact tests and using Bonferroni correction for multiple comparisons.

Additionally, GSEA[23] was carried out on a rank ordered list of the infected EC versus control molecular analysis. The ranking metric used was logFC * -logP value, however, the results were similar when logFC metric was also used (data not shown). For the COVID-19 associated datasets, we curated two signatures from infected organoids[24]: hSIOs-COVID-19: human small intestinal organoids (hSIOs) grown in either i) Wnt high expansion (EXP) medium (at adjP<0.05) or ii) differentiation (DIF) medium (at adjP<0.1). The standard GSEA settings were used, namely 'meandiv' for normalization mode, 'weighted' enrichment statistic, and '1000' permutations. GSEA using the Hallmark database (v7.1[25]) was also performed with the same settings.

Computational analyses

Multivariate model based on Discovery Cohort

For this analysis, we considered 570 patients with clinical descriptors including as age, gender, race/ethnicity, BMI, comorbidities (including hypertension, diabetes, chronic lung disease (including asthma and COPD), heart disease (including coronary artery disease, atrial fibrillation and heart failure), and GI symptoms. A multivariate logistic regression was utilized to model severity and mortality as function of each of the GI symptoms and clinical variables including race, age, gender, BMI, heart and lung diseases and hypertension.

In particular, race was stratified as White (Caucasian), Black (African-American), Hispanic and others; lung disease was set equal to 1 if the patient was either affected by COPD or asthma and zero otherwise; heart disease was set equal to 1 if the patient was either affected by coronary artery disease, atrial fibrillation or heart failure and 0 otherwise. The severity indicator was set equal to 1 for severe and severe with EOD patients and 0 for mild and moderate COVID-19 patients; mortality was set equal to 1 for deceased patients and 0 otherwise.

Significant association were determined based on 95% confidence interval (CI) based on 1000 bootstrap iterations. At each bootstrap iteration, patients were sampled with replacements and logistic regressions were estimated considering as outcome severity and mortality. Then, 95% CI of coefficients and odds ratio were estimated across bootstrap iterations.

External Validation Cohort

For this analysis, we considered 228 patients with clinical data such as age, gender and GI symptoms as described in *Aghemo et al*[1]. A multivariate logistic regression was utilized to model mortality, ICU admission and the composite outcome of ICU admission or mortality as function of presence or absence of diarrhea and clinical variables including age, gender, BMI, heart disease, COPD, diabetes and hypertension. Heart disease was set equal to 1 if the patient was either affected by coronary artery disease or atrial fibrillation and 0 otherwise. CI of odds ratio were computed based on 1000 bootstrap iterations as above.

In 270 patients from this cohort treatment data was available. Treatments included hydroxychloroquine, antiviral treatments including lopinavir-ritonavir and darunavir-cobicistat, tocilizumab, steroids, antibiotics including ceftriaxone, azithromycin, piperacillin-tazobactam, statins, angiotensin-converting-enzyme (ACE) inhibitors and angiotensin II receptor blockers (ARBs). Using this data, we performed fisher's exact test to determine whether any treatments were associated with diarrhea. Additionally, we computed 95% CI of odds ratio based on 1000 bootstrap iterations.

Predictive performance based on the Internal Validation Cohort

For this analysis, we considered 233 patients with clinical data including age, BMI, and GI symptoms. In order to evaluate the predictive performance of each model, bootstrapping was performed. Specifically, at each bootstrap iteration, we randomly sampled patients in the Discovery Cohort with replacement and estimated a logistic regression to model each outcome as function of a particular GI symptom, age and BMI. In this analysis, only age and BMI were adjusted for since they were the only variables significantly associated with both outcomes across different GI symptoms models in the Discovery Cohort (Figure 5B, Supplementary Table 9). Then, the estimated model was utilized to predict the outcome of patients in the Internal Validation Cohort. This procedure was repeated for 1000 bootstrap iterations. For each iteration, Receiving Operating Characteristic (ROC) curve and area under the curve (AUC) were computed. For comparison purposes, the distribution of AUC across 1000 bootstrap iterations from the predictive model based on age and BMI only was considered. Figure 5D shows the boxplot of AUC values across 1000 bootstrap iterations. Then, considering the following model

outcome = f(age + bmi + any GI symptom) [Model 1]

we evaluated the effect of each variable on the outcome by computing the reduction in AUC obtained after removing one variable at a time. For this purpose, the AUC of model [Model 1] was compared to the following three models

outcome = f(age + bmi) [Model 2]

outcome = f(age + any GI symptom)[Model 3]

outcome = f(bmi + any GI symptom)[Model 4]

for 1000 bootstrap iterations. Following the strategy above, at each bootstrap iteration, patients were sampled with replacement. Figure 5E shows the 95% confidence intervals of difference in AUC between [Model 1] and [Model 2], [Model 3] and [Model 4] (i.e., AUCModel1 -

AUCModel2, AUCModel1 - AUCModel3, AUCModel1 - AUCModel4) across 1000 bootstrap iterations. The difference in AUC was computed considering both mortality and severity as the outcome.

Average treatment effect (ATE)

The average treatment effect (ATE) for the Mount Sinai Cohort (MSH) combining Discovery and Internal Validation Cohorts and the External Validation Cohort were calculated via the TMLE package in R[26]. For the MSH cohort, ATE was calculated for each GI symptom using as outcomes disease severity and mortality. The marginal effect was calculated after adjusting for covariates such as age, race, BMI, gender, diabetes, lung disease, heart disease and hypertension. For the External Validation Cohort, ATE was calculated for diarrhea on ICU admission, mortality and the composite of ICU admission and mortality. The marginal effect was calculated after adjusting for covariates such as age, BMI, gender, diabetes, lung disease, heart disease and hypertension.

Quantification of SARS-CoV-2 nasopharyngeal viral loads

SARS-CoV-2 viral loads were determined as detailed in Pujadas et al[27]. Briefly, viral RNA was extracted from the NP swab specimen followed by real time RT-PCR using N2 primers. Only specimens with $N2_{Cpt} < 38$ were included. SARS-CoV-2 viral RNA was calculated with the delta CT method and a standard curve. Viral loads are presented as log base 10 transformed uncorrected N2 value + 1000 (constant added before transformation)[27]. For patients with multiple NP swabs available, the first swab was used for analysis.

ELLA Cytokine panel

The ELLA platform is a method for rapid cytokine measurement using microfluidics ELISA assays. The assay measured TNF-α, IL-6, IL-8, and IL-1β, previously validated by the Mount Sinai Human Immune Monitoring Center (HIMC) using plasma from multiple myeloma patients and recently reported for large cohort of COVID-19 patients admitted to MSH.

Multiplexed proteomic assay (Olink)

For analysis of circulating cytokines, we used a multiplexed proteomic inflammation panel (Olink), which consists of 92 inflammation-related proteins quantified by an antibody-mediated proximity extension-based assay. Samples with normalized protein expression values below the limit-of-detection in >75% of samples were excluded from further analysis. For the remainder of analytes, any sample under the limit of detection was assigned a value of the limit-of-detection divided by the square root of 2. The log2 fold-change over the median healthy control protein expression was then calculated, and the Benjamini-Hochberg procedure was used to adjust P values for multiple testing.

Consensus Clustering of Olink Data

For this analysis, we considered 238 samples with GI symptoms annotation. Consensus clustering was performed based on the abundance of 92 cytokines across all 238 samples. Consensus clustering was performed using the R packages ConsensusClusterPlus based on z-score normalized data. Specifically, markers were partitioned into six clusters using the K-means algorithm, which was repeated 1000 times. Then, markers in each cluster were considered in order to derive cluster z-score signatures via package GSVA. Based on these signatures, the association between different clusters and GI symptoms were derived via logistic regression with

outcome corresponding to each GI symptom. Figure 6C shows the signed FDR (-log10 scale). P-values were adjusted via Benjamini-Hochberg. The pathway analysis for the clusters described above was carried out considering the entire KEGG and HALLMARK databases.

Supplementary References

1. Aghemo A, Piovani D, Parigi TL, et al. COVID-19 Digestive System Involvement and Clinical Outcomes in a Large Academic Hospital in Milan, Italy. Clin Gastroenterol Hepatol 2020;18:2366-2368 e3.
2. Schneider CA, Rasband WS, Eliceiri KW. NIH Image to ImageJ: 25 years of image analysis. Nat Methods 2012;9:671-5.
3. Mastronarde DN. Automated electron microscope tomography using robust prediction of specimen movements. J Struct Biol 2005;152:36-51.
4. Mastronarde DN, Held SR. Automated tilt series alignment and tomographic reconstruction in IMOD. J Struct Biol 2017;197:102-113.
5. Mastronarde DN. Correction for non-perpendicularity of beam and tilt axis in tomographic reconstructions with the IMOD package. J Microsc 2008;230:212-7.
6. **Yao H, Song Y, Chen Y, Wu N, Xu J,** et al. Molecular Architecture of the SARS-CoV-2 Virus. Cell 2020.
7. **Ke Z, Oton J, Qu K,** et al. Structures and distributions of SARS-CoV-2 spike proteins on intact virions. Nature 2020.
8. **Klein S, Cortese M, Winter SL,** et al. SARS-CoV-2 structure and replication characterized by in situ cryo-electron tomography. bioRxiv 2020.
9. **Turoňová B, Sikora M, Schürmann C**, et al. In situ structural analysis of SARS-CoV-2 spike reveals flexibility mediated by three hinges. Science 2020;370:203-208.
10. Calomeni E, Satoskar A, Ayoub I, et al. Multivesicular bodies mimicking SARS-CoV-2 in patients without COVID-19. Kidney Int 2020;98:233-234.
11. He W, Ladinsky MS, Huey-Tubman KE, et al. FcRn-mediated antibody transport across epithelial cells revealed by electron tomography. Nature 2008;455:542-6.
12. Ladinsky MS, Huey-Tubman KE, Bjorkman PJ. Electron tomography of late stages of FcRn-mediated antibody transcytosis in neonatal rat small intestine. Mol Biol Cell 2012;23:2537-45.
13. **Geanon D, Lee B,** Kelly G, et al. A Streamlined CyTOF Workflow To Facilitate Standardized Multi-Site Immune Profiling of COVID-19 Patients. medRxiv 2020.
14. Benjamini Y, Hochberg Y. Controlling the False Discovery Rate: A Practical and Powerful Approach to Multiple Testing. Journal of the Royal Statistical Society. Series B (Methodological) 1995;57:289-300.

15. **Holmes G, Gonzalez-Reiche AS, Lu N, Zhou Z,** et al. Integrated Transcriptome and Network Analysis Reveals Spatiotemporal Dynamics of Calvarial Suturogenesis. Cell Rep 2020;32:107871.
16. **Robinson MD, McCarthy DJ,** Smyth GK. edgeR: a Bioconductor package for differential expression analysis of digital gene expression data. Bioinformatics 2010;26:139-40.
17. Li B, Dewey CN. RSEM: accurate transcript quantification from RNA-Seq data with or without a reference genome. BMC Bioinformatics 2011;12:323.
18. Robinson MD, Oshlack A. A scaling normalization method for differential expression analysis of RNA-seq data. Genome Biol 2010;11:R25.
19. Reimand J, Kull M, Peterson H, et al. g:Profiler--a web-based toolset for functional profiling of gene lists from large-scale experiments. Nucleic Acids Res 2007;35:W193-200.
20. **Smillie CS, Biton M, Ordovas-Montanes J,** et al. Intra- and Inter-cellular Rewiring of the Human Colon during Ulcerative Colitis. Cell 2019;178:714-730 e22.
21. Martin JC, Chang C, Boschetti G, et al. Single-Cell Analysis of Crohn's Disease Lesions Identifies a Pathogenic Cellular Module Associated with Resistance to Anti-TNF Therapy. Cell 2019;178:1493-1508 e20.
22. **Blanco-Melo D, Nilsson-Payant BE, Liu WC**, et al. Imbalanced Host Response to SARS-CoV-2 Drives Development of COVID-19. Cell 2020;181:1036-1045 e9.
23. **Subramanian A, Tamayo P,** Mootha VK, et al. Gene set enrichment analysis: a knowledge-based approach for interpreting genome-wide expression profiles. Proc Natl Acad Sci U S A 2005;102:15545-50.
24. **Lamers MM, Beumer J, van der Vaart J,** et al. SARS-CoV-2 productively infects human gut enterocytes. Science 2020;369:50-54.
25. Liberzon A, Birger C, Thorvaldsdottir H, et al. The Molecular Signatures Database (MSigDB) hallmark gene set collection. Cell Syst 2015;1:417-425.
26. Gruber S, van der Laan M. tmle: An R Package for Targeted Maximum Likelihood Estimation. Journal of Statistical Software 2012;51:1-35. https://www.jstatsoft.org/v051/i13.
27. **Pujadas E, Chaudhry F**, McBride R, et al. SARS-CoV-2 viral load predicts COVID-19 mortality. Lancet Respir Med 2020;8:e70.

Supplementary Figures and Tables

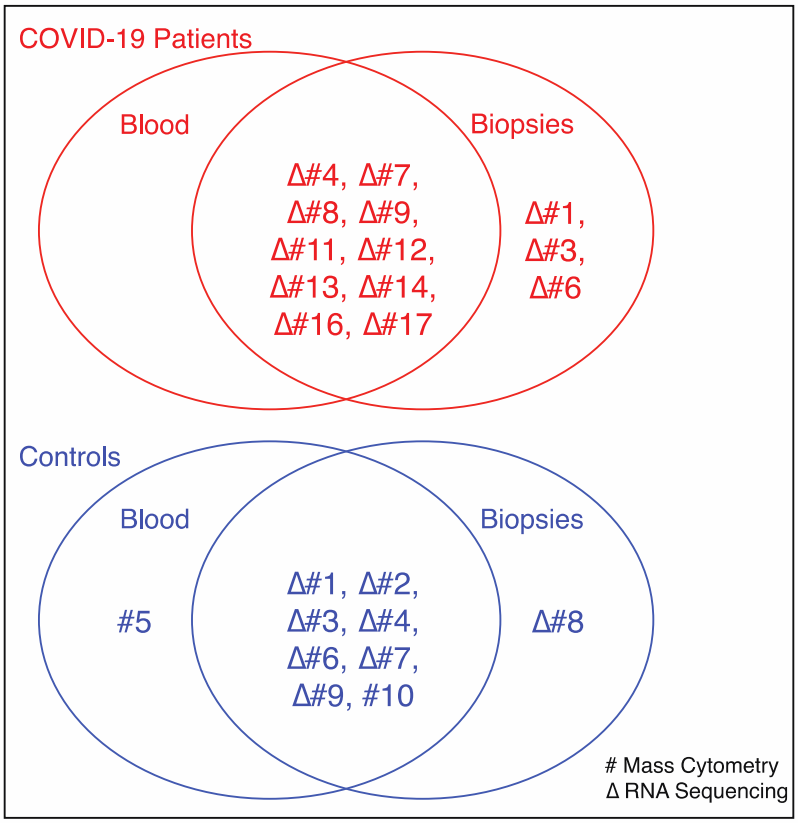

Assays	Sample	COVID-19 cases	Controls
Mass Cytometry	Biopsy	13	9
	Blood	10	9
RNA Sequencing	Biopsy	13	8
	Blood	N/A	N/A

Supplementary Figure 1. Sample allocation for different assays in COVID-19 patients and controls. Venn diagrams showing blood and biopsy samples used for mass cytometry (#) and RNA sequencing (Δ) in COVID-19 patients (red) and controls (blue). The numbers in the Venn diagrams refer to respective patient and control cases detailed Supplementary Table 2. The table summarizes the total number of blood and biopsy samples allocated for mass cytometry and RNA sequencing.

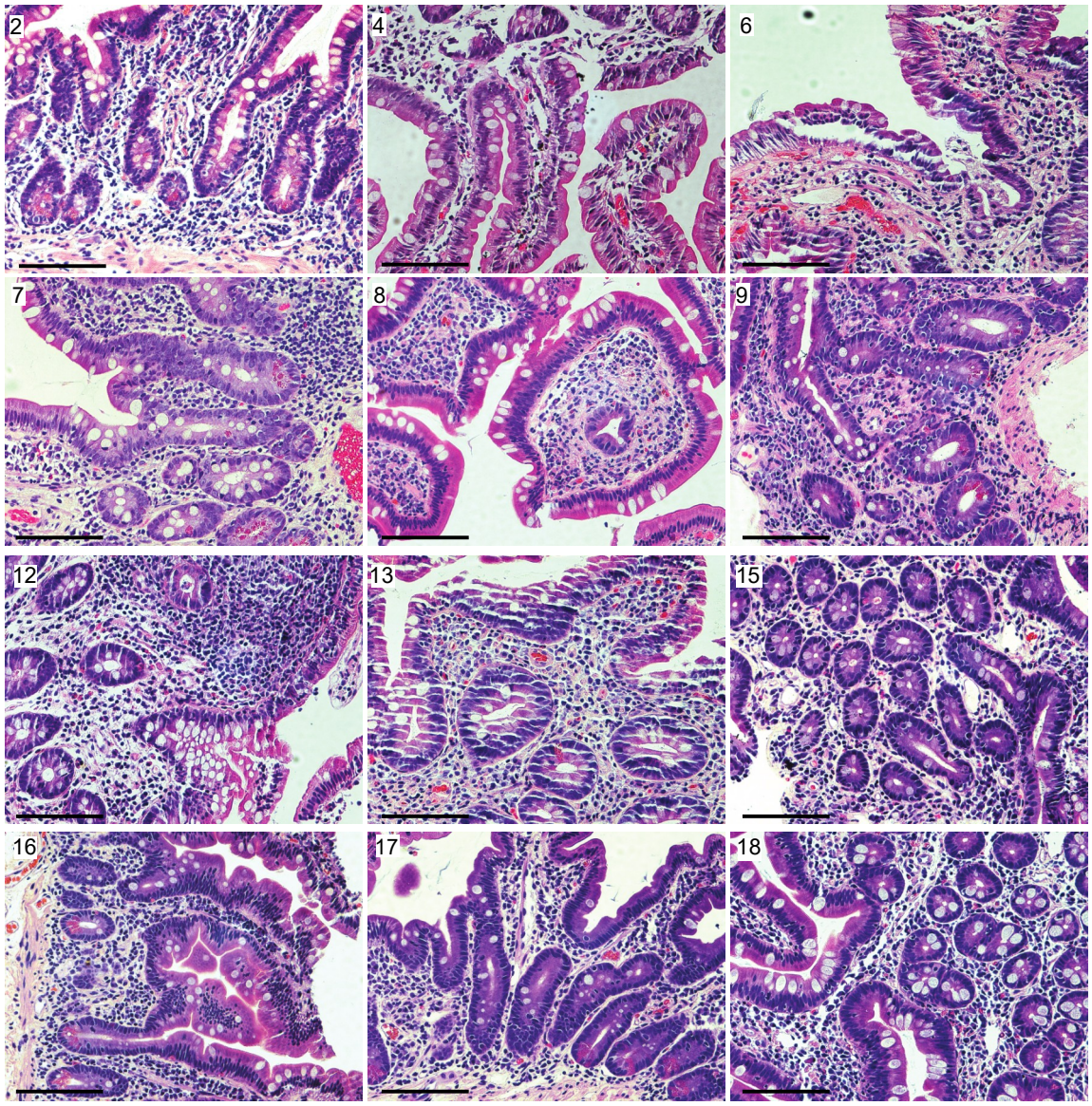

Supplementary Figure 2. Representative H&E staining of small intestinal biopsies of COVID-19 patients. Patient number in the top left corner corresponds with the patient number in Supplementary Table 2. All biopsies are duodenal with the exception of patient 12 which is from the terminal ileum. Scale bar; 100µm.

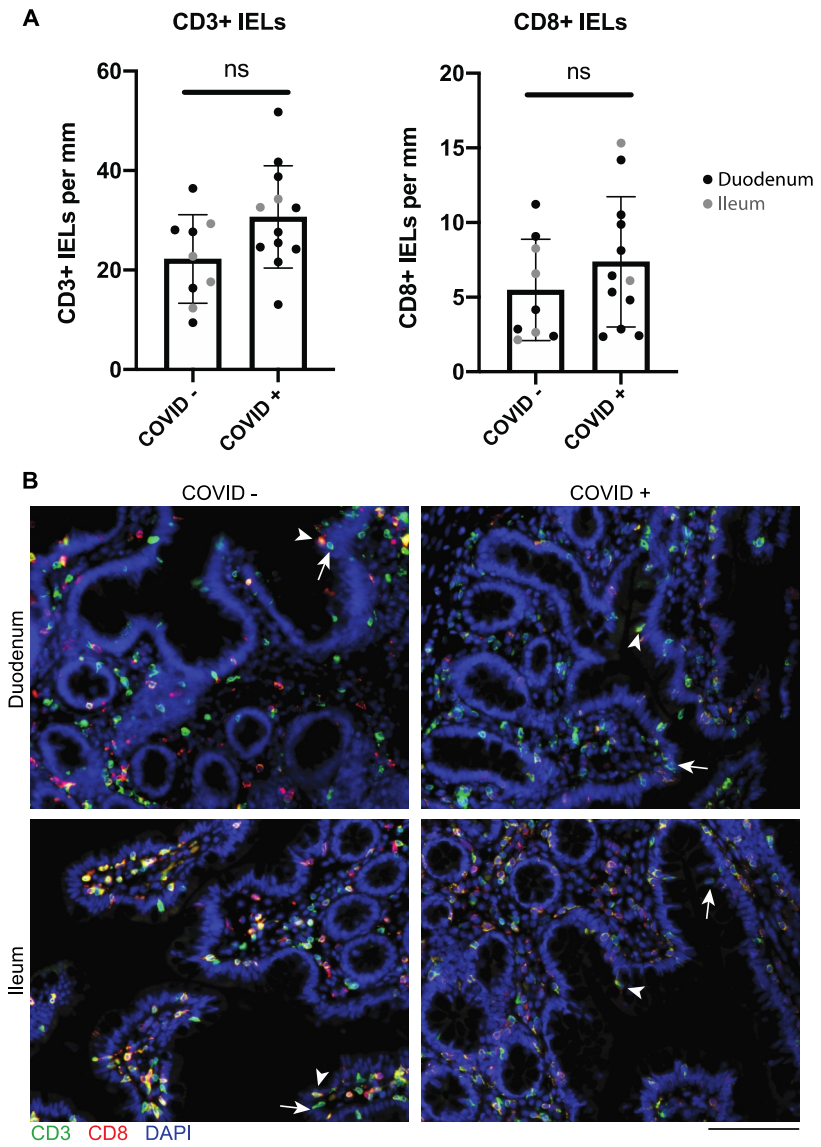

Supplementary Figure 3. Intraepithelial lymphocytes (IELs) are not increased in small intestinal biopsies from COVID-19 patients compared to controls. (**A**) CD3+ and CD8+ IELs per mm of epithelium in COVID-19 patients and uninfected controls in the duodenum (black) and ileum (gray). *P*-values generated from unpaired t-tests. (**B**) Representative IF images of small intestinal biopsies showing CD3 (green), CD8 (red) and DAPI (blue). Representative CD8+ IELs (arrow head) and representative CD8- IELs (arrow) are indicated. Scale bar; 100µm.

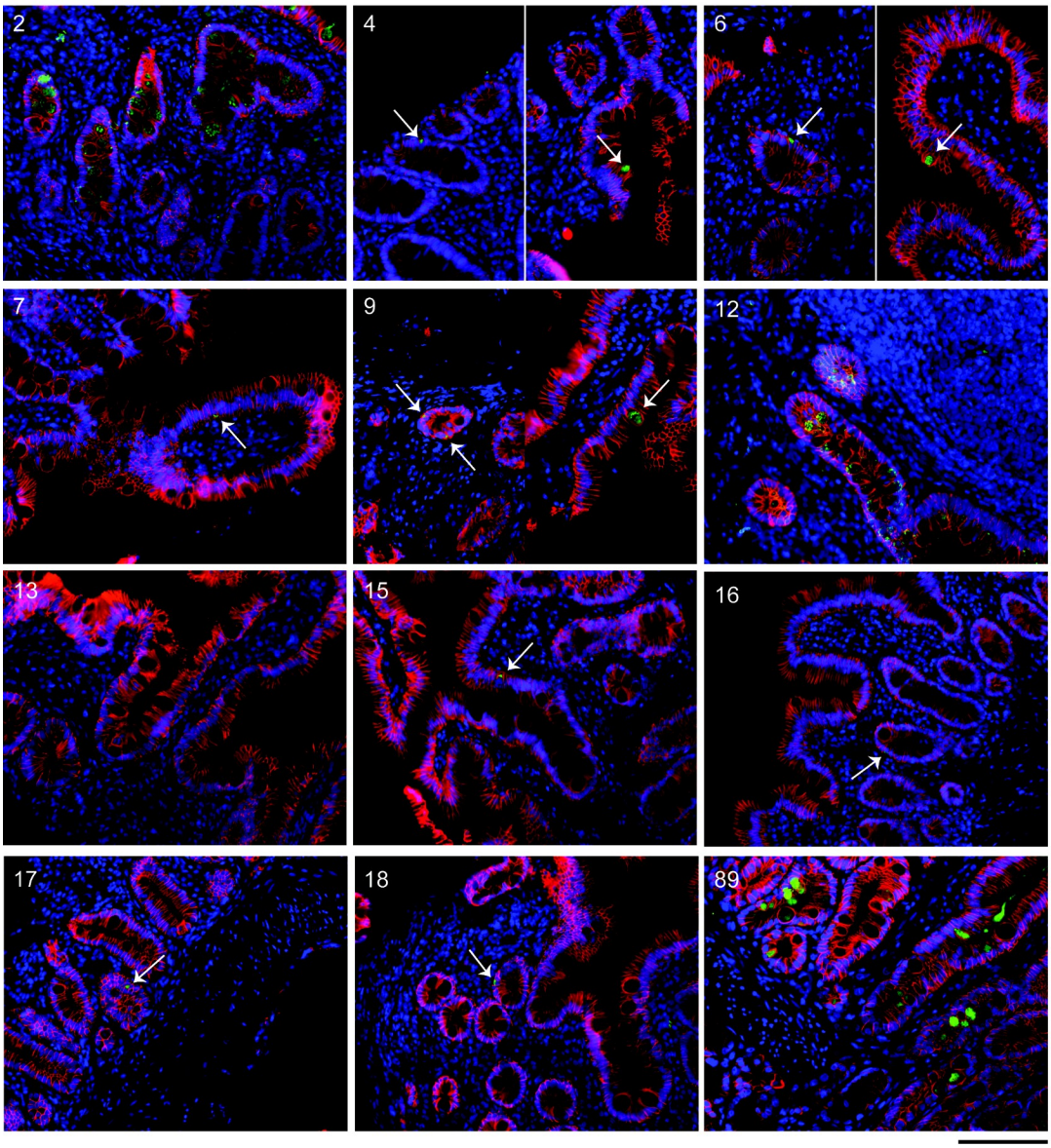

Supplementary Figure 4. Representative immunofluorescence (IF) images of small intestinal biopsies of COVID-19 patients. SARS-CoV-2 nucleocapsid (green), EPCAM (red) and DAPI (blue) in all COVID-19 patients where tissue was available for IF. Patient number in the top right corner corresponds with the patient number in Supplementary Table 2. All biopsies are duodenal with the exception of patient 12 which is from the terminal ileum. Patient 8 missing due to technical difficulties during IF staining. Scale bar; 100 µm.

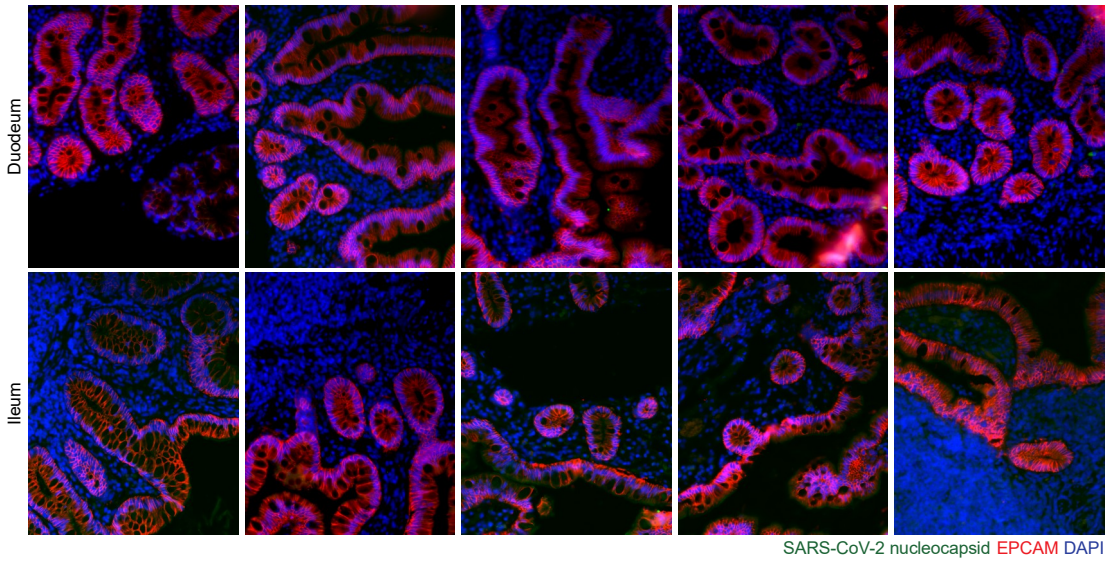

Supplementary Figure 5. Representative immunofluorescence images of small intestinal biopsies of control patients. SARS-CoV-2 nucleocapsid (green), EPCAM (red) and DAPI (blue) in duodenal biopsies (upper) and ileal biopsies (lower). Scale bar; 100 µm.

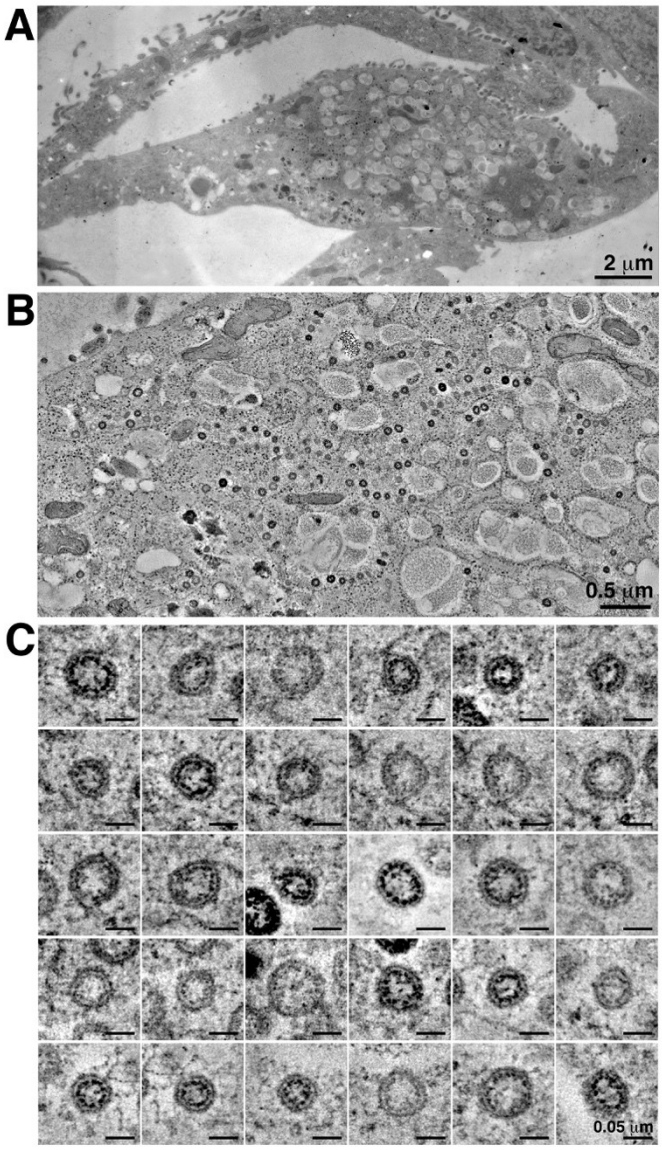

Supplementary Figure 6. Electron microscopy by high pressure freezing/freeze substitution fixation (HPF/FSF) of presumptive SARS-CoV-2 infection in culture Vero cells. (**A**) Montaged overview of an infected cell (150 nm section) (presented for comparison with analogous structures found in tissue samples (Figure 2 and Supplementary Movie 1), which could not be preserved under similar optimal conditions for EM). The cell exhibits large numbers of cytoplasmic vacuoles, surface blebbing and general cytopathogenicity. (**B**) Montaged tomographic reconstruction of the central portion of the cell shown in **A**. Large numbers of

presumptive SARS-CoV-2 virions are contained within cytoplasmic compartments, most are closely adjacent to the compartment's peripheries. (**C**) Gallery of 30 individual presumptive SARS-CoV-2 virions taken from the tomogram shown in **B**. Each example is displayed as an equatorial view with a tomographic thickness of 4.7 nm.

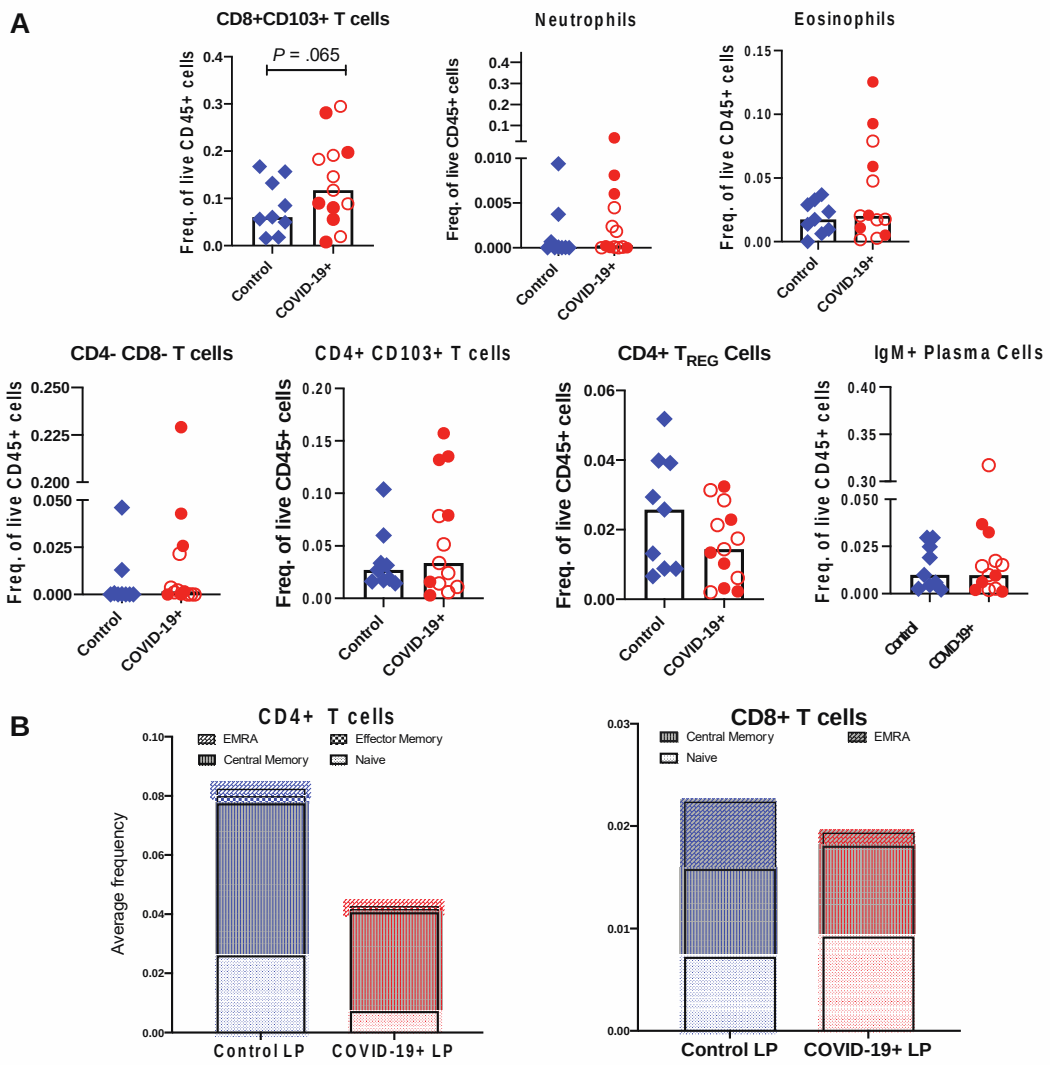

Supplementary Figure 7. Altered immune populations in the lamina propria of COVID-19 patients compared to controls. (**A**) Relative frequencies of lamina propria immune cells in controls and COVID-19 patients. Open red circles denote patients with asymptomatic/mild/moderate disease while filled red circles denote patients with severe COVID-19. The bar plots show median frequencies. (**B**) The stacked bar graphs show the distribution of average frequencies of naïve and memory CD4+ and CD8+ T cells in the lamina propria of COVID-19 patients and controls.

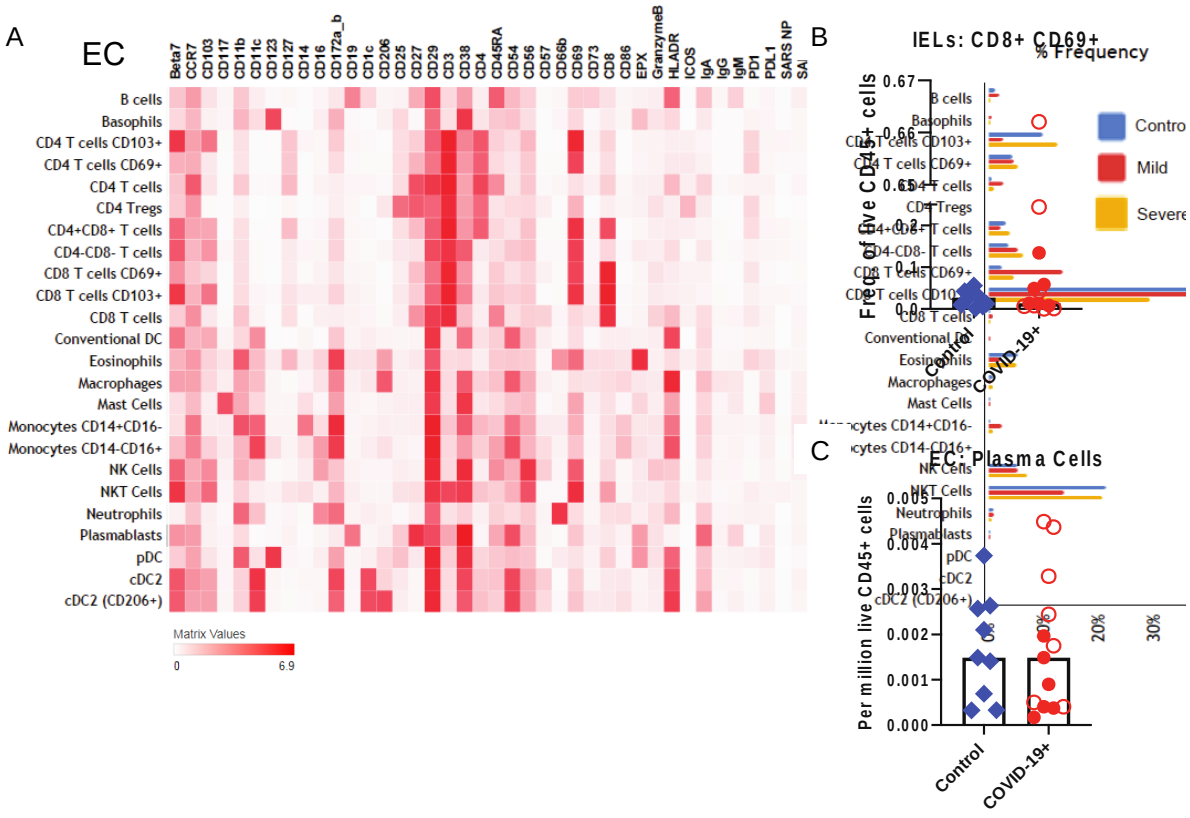

Supplementary Figure 8. Altered immune populations in the epithelial compartment (EC) of COVID-19 patients compared to controls. (**A**) The heat map shows clustering and distribution of different cell types in the EC. Relative frequencies of (**B**) intraepithelial lymphocytes (IELs) and (**C**) plasma cells in the EC of controls and COVID-19 patients. Open red circles denote patients with asymptomatic/mild/moderate disease while filled red circles denote patients with severe COVID-19. The bar plots show median frequencies.

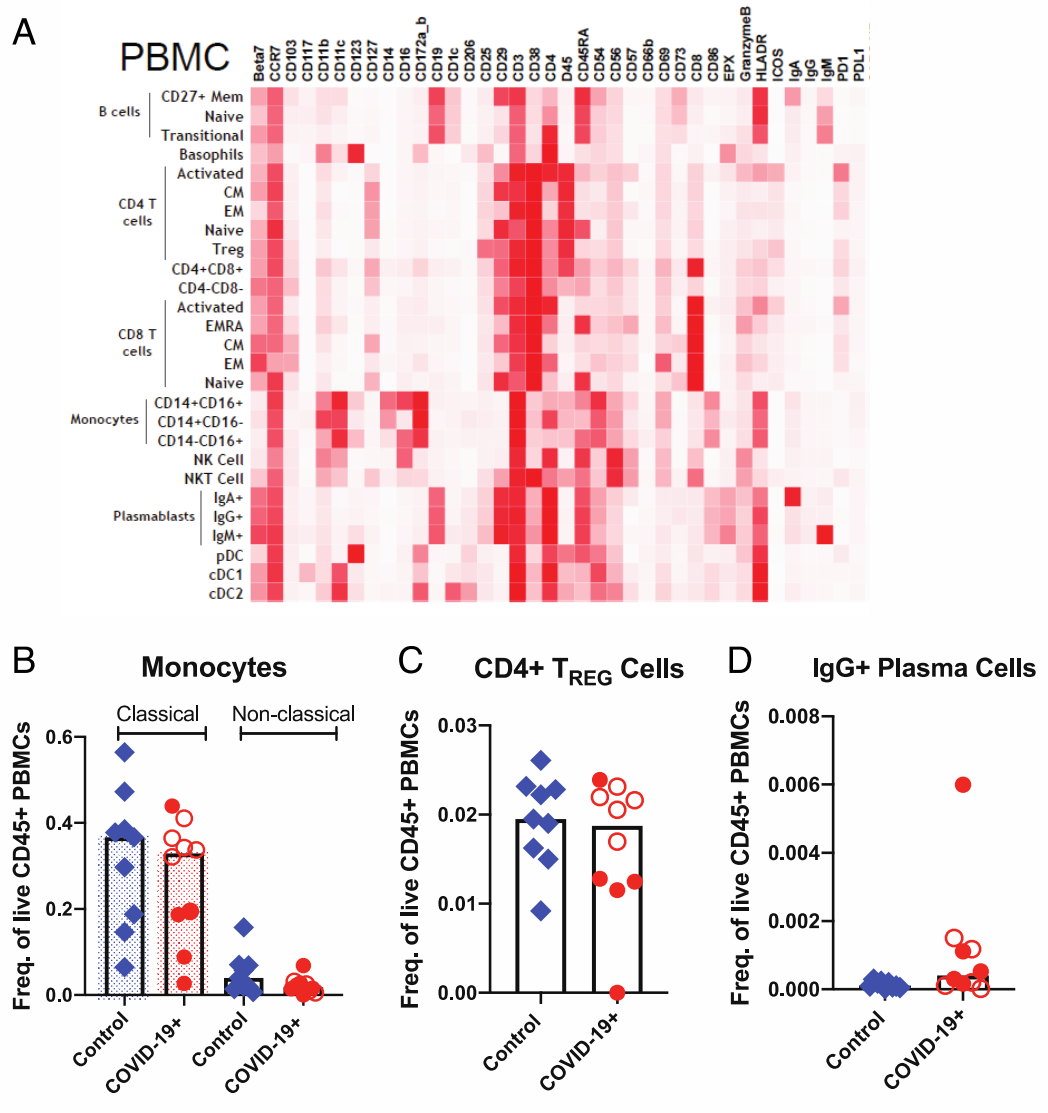

Supplementary Figure 9. Altered immune populations in the blood of COVID-19 patients compared to controls. (**A**) The heat map shows clustering and distribution of different immune cell types in the blood. Relative frequencies of (**B**) classical (dotted bars) and non-classical monocytes (open bars), (**C**) CD4+ regulatory T cells and (**D**) IgG+ plasma cells in the blood of controls and COVID-19 patients. Open red circles denote patients with asymptomatic/mild/moderate disease while filled red circles denote patients with severe COVID-19. The bar plots show median frequencies.

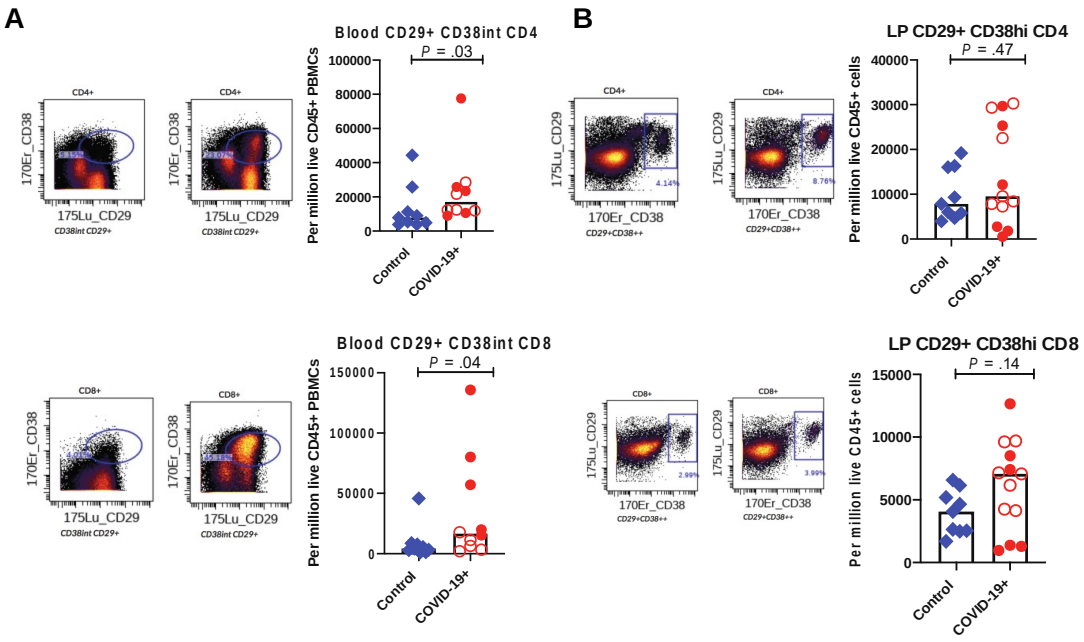

Supplementary Figure 10. Altered T cell populations in blood and intestinal biopsies of COVID-19 patients compared to controls based on supervised analysis. Representative CyTOF plots and bar plots comparing the frequencies of CD29+ CD38+ CD4+ and CD29+ CD38+ CD8+ T cells in (**A**) the blood and (**B**) lamina propria of controls (blue) and COVID-19 patients (red). Open red circles denote patients with asymptomatic/mild/moderate disease while filled red circles denote patients with severe COVID-19. The bar plots show median frequencies.

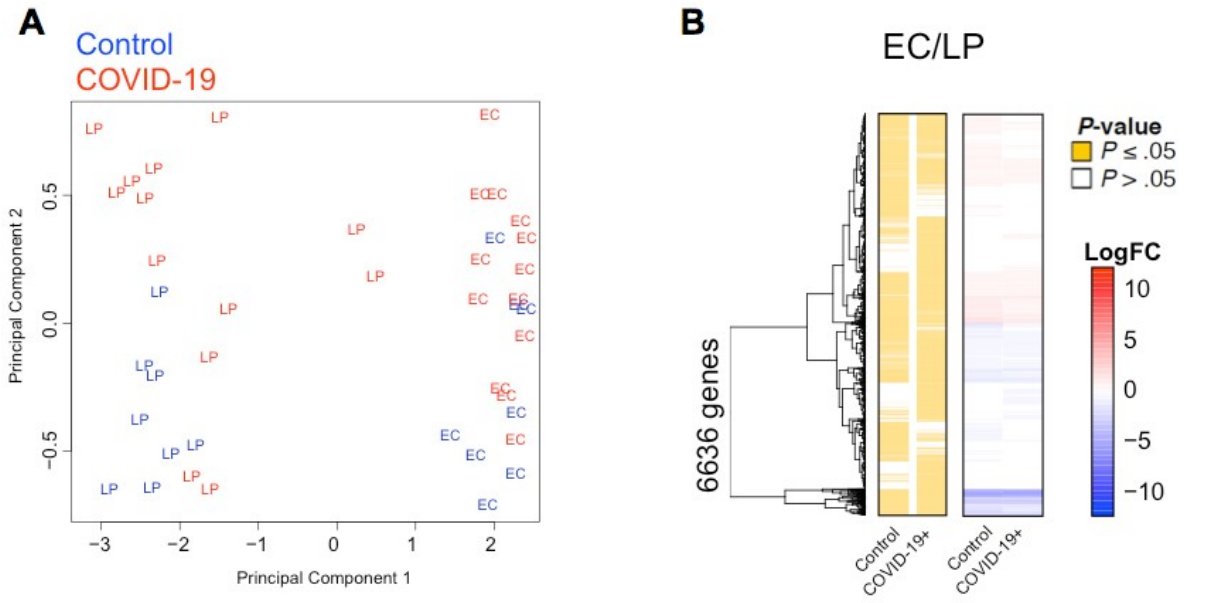

Supplementary Figure 11. Distinct expression profiles in the intestinal epithelial compartment (EC) and lamina propria (LP). (**A**) Principal Component Analysis (PCA) of EC and LP fractions of COVID-19 patients and controls. The two tissue fractions separate on the principal component 1 (x-axis). **(B)** Hierarchical clustering of average expression changes for 6636 genes (rows) characterizing the EC (red) or LP (blue) fractions (FDR ≤ 0.05) in the intestinal biopsies of COVID-19 patients and controls. The left panel indicates significant genes in yellow for each tissue compartment. The color bar (right panel) indicates the average log2 fold-change (FC).

A

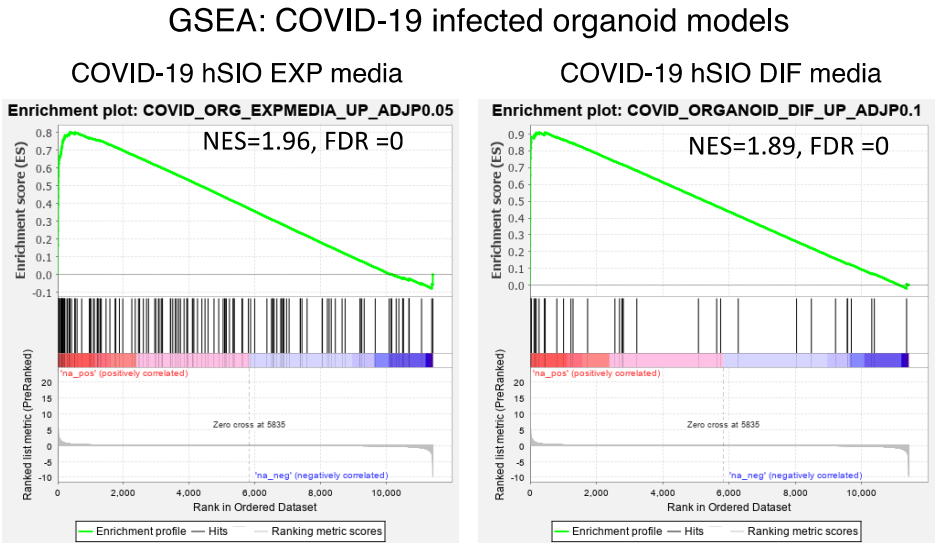

Rank ordered genes: Inf EC vs control (logFC*-logPvalue)

B

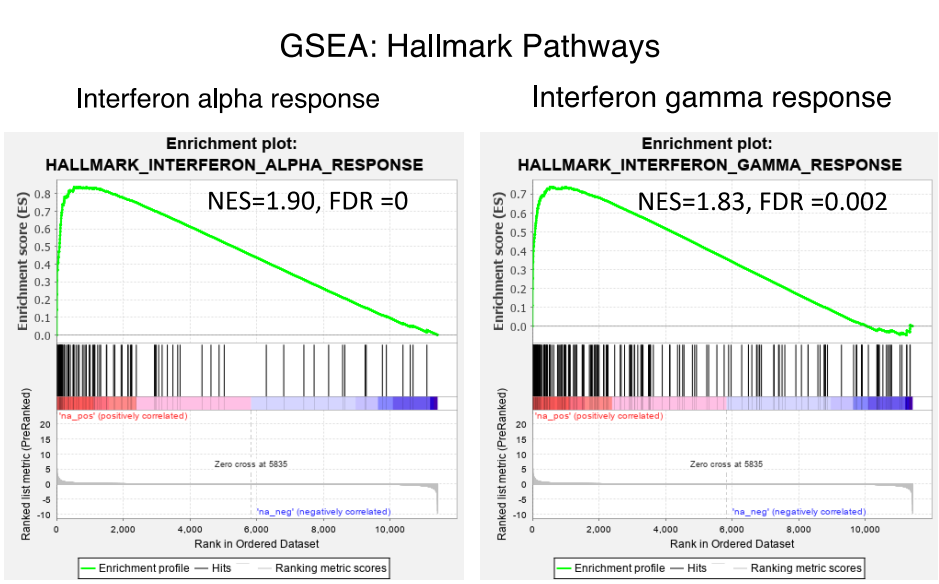

Rank ordered genes: Inf EC vs control (logFC*-logPvalue)

Supplementary Figure 12. Immune signatures in the epithelial compartment (EC) of COVID-19 patients. Gene Set Enrichment Analysis (GSEA) was performed using a rank ordered list of genes differentially expressed in the infected EC vs control EC. The metric for ranking was logFC*-logPvalue. (**A**) GSEA was performed on the rank ordered EC gene set using SARS-CoV-2 infected organoid datasets. The gene sets tested were molecular signatures curated

from SARS-CoV-2 infected organoid experimental datasets using human small intestinal organoids (hSIOs) grown in either i) Wnt high expansion (EXP) medium (at adj$P < .05$) or ii) differentiation (DIF) medium (at adj$P < .1$). Only gene sets significantly enriched (at FDR <0.05) are displayed. (**B**) GSEA was performed for the same rank ordered EC gene set using the Hallmark Pathway datasets. Two significantly enriched pathways were found to be associated with upregulated genes in infected EC relative to controls (at FDR<0.05). Normalized enrichment score (NES) and FDR values are as indicated.

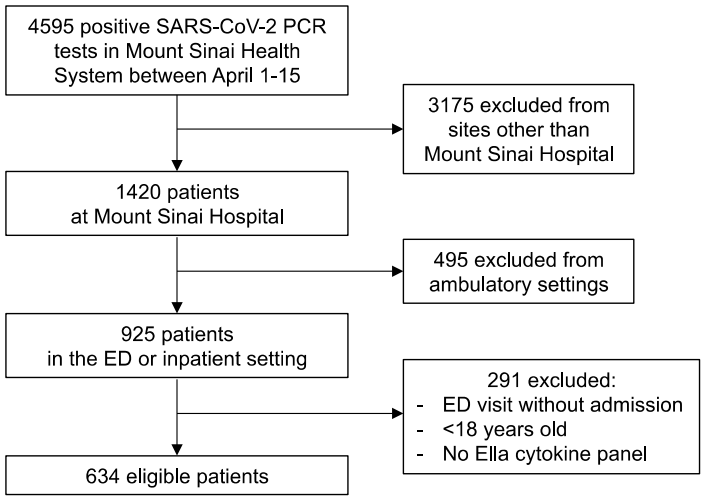

Supplementary Figure 13. Flow diagram of the Discovery Cohort. The diagram shows the total number of patients admitted to the Mount Sinai Health System between April 1-15, 2020 and the selection process that was adopted in order to select patients in the Discovery Cohort.

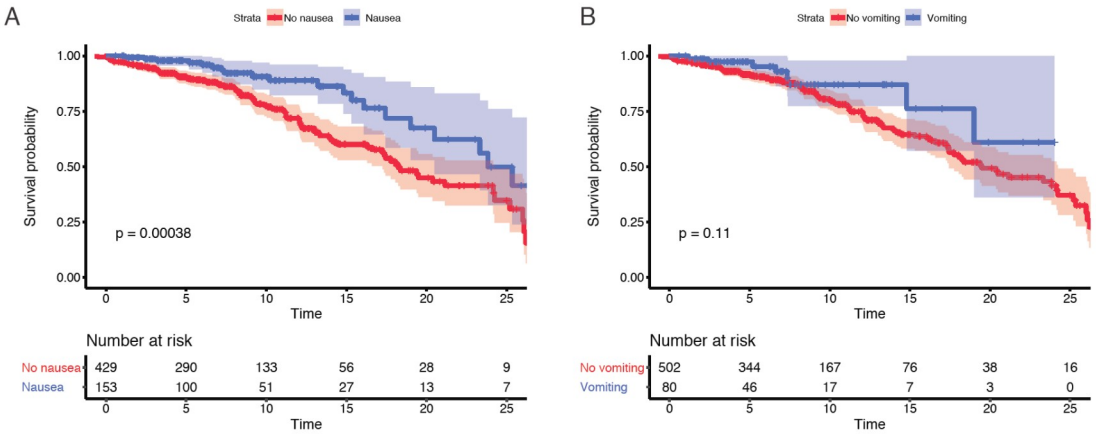

Supplementary Figure 14. Nausea and vomiting were associated with reduced mortality and severity. Kaplan-Meier curves for mortality stratified by (**A**) nausea and (**B**) vomiting for patients in the Discovery Cohort. *P*-values from log-rank test and 95% confidence intervals of Kaplan-Meier curves are shown. Below each Kaplan-Meier, the number of patients at risk for different time points are reported.

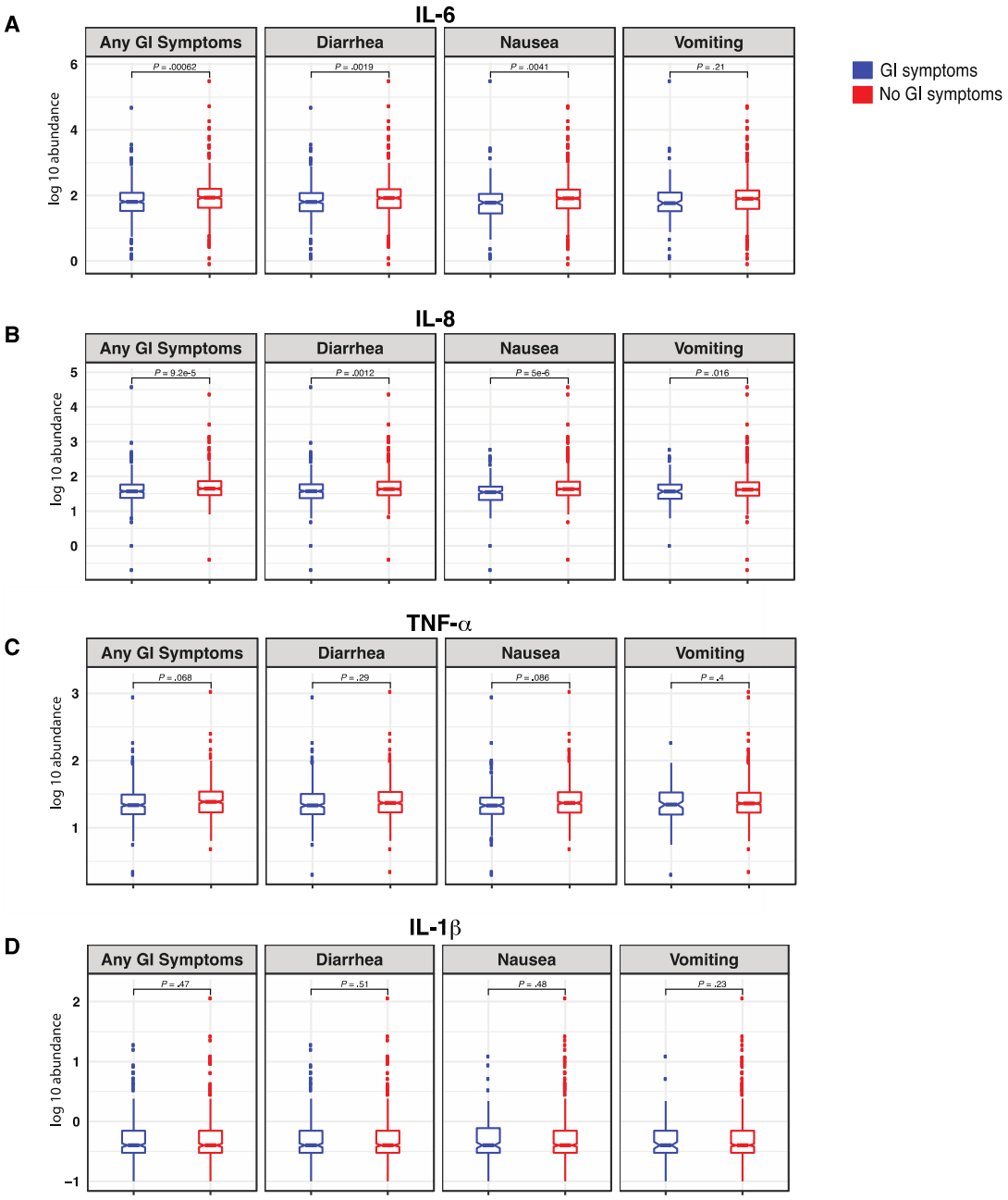

Supplementary Figure 15. COVID-19 patients with GI symptoms had reduced levels of circulating IL-6 and IL-8. (**A**) IL-6, (**B**) IL-8, (**C**) TNF-α and (**D**) IL-1β at the time of admission in patients with and without GI symptoms. Boxplots represent the median and interquartile range. *P*-values calculated using unpaired two-tailed t-test.

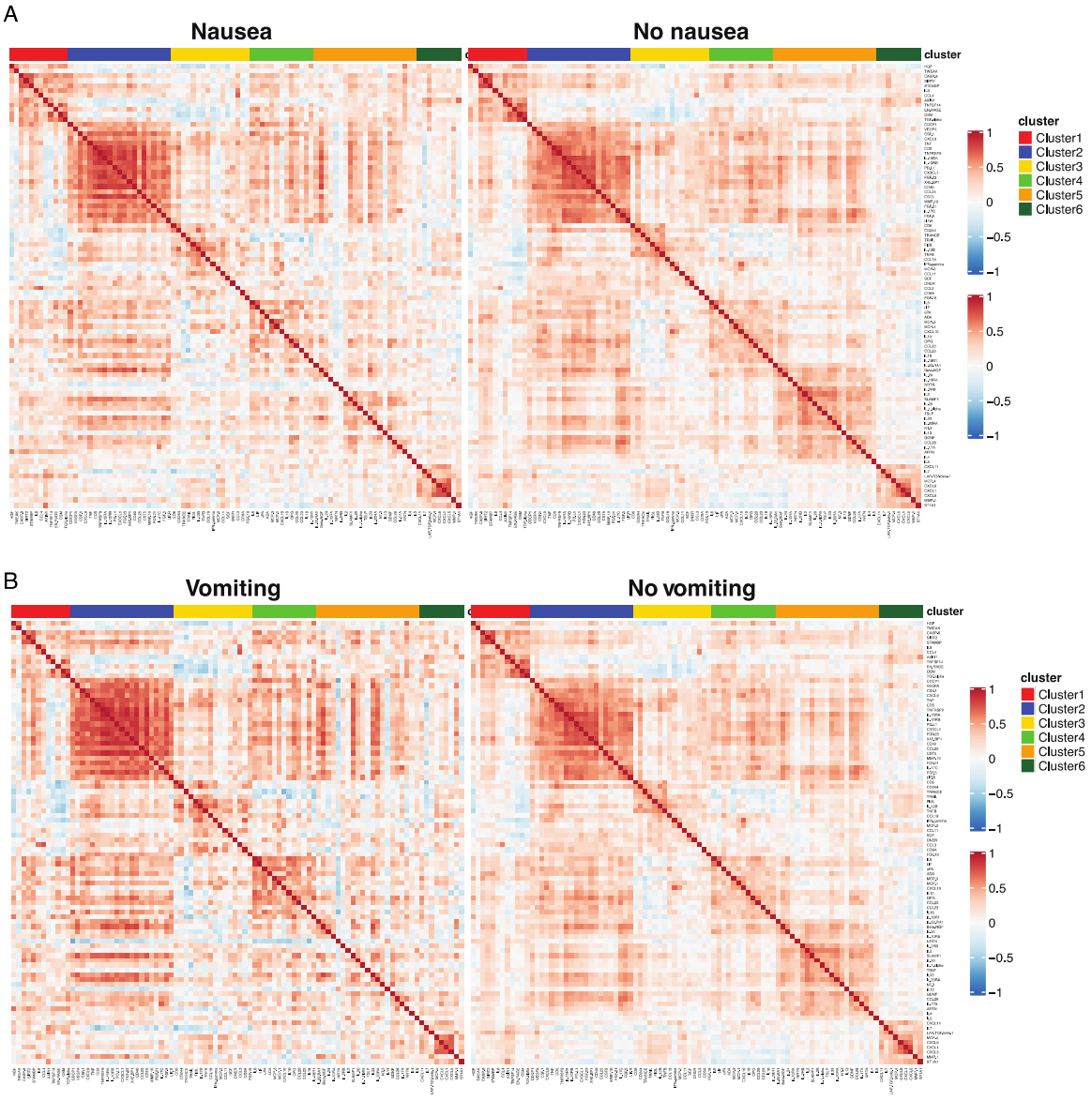

Supplementary Figure 16. Correlation matrix (Pearson's) for 92 markers contained in the Olink platform. (**A**) Correlation matrix across patients with nausea (left panel) compared to patients without nausea (right panel); and (**B**) patients with vomiting (left panel) compared to patients without vomiting (right panel). Cluster assignment derived using unsupervised consensus clustering is reported on the top of the heatmap.

Supplementary Table 1. Biopsy cohort characteristics

Characteristic	COVID-19 biopsy cases (n = 19)	Uninfected controls (n=10)	p-value
Age (mean years ± stdev*)	54 ± 20	65 ± 11	0.12
Male sex	12 (63%)	5 (50%)	0.69
Number of comorbidities § (mean ± stdev*)	1.9 ± 1.6	2.0 ± 1.1	0.93
Hospitalized patients	12 (63%)	6 (60%)	>0.99
COVID-19 characteristics			
Asymptomatic / mild / moderate COVID-19	12 (63%)	NA	NA
Severe COVID-19	7 (37%)	NA	NA
COVID-19 associated GI symptoms ^	3 (16%)	NA	NA

* stdev = standard deviation
§ = Hypertension (HTN), obesity (OB), diabetes mellitus (DM), asthma (A), chronic obstructive pulmonary disease (COPD), coronary artery disease (CAD), cancer (CX), transplant (TPX)
^ = GI symptoms defined as nausea, vomiting and /or diarrhea at the time of acute illness

Supplementary Table 2. Individual patient characteristics from biopsy cohort.

(included as separate excel)

Supplementary Table 3. Criteria for scoring disease severity in COVID-19 patients.

Severity Score	**Criteria**
Mild	SpO2>94% on room air AND no pneumonia on imaging
Moderate	SpO2<94% on room air OR pneumonia on imaging
Severe	High flow nasal cannula (HFNC), non-rebreather mask (NRBM), Bilevel Positive Airway Pressure (non-invasive positive airway ventilation), or Mechanical ventilation AND no pressor medications AND creatinine clearance > 30 AND ALT < 5x upper limit of normal
Severe with end organ damage (EOD)	High flow nasal cannula (HFNC), non-rebreather mask (NRBM), Bilevel Positive Airway Pressure (non-invasive positive airway ventilation), or Mechanical ventilation AND pressor medications OR creatinine clearance <30 OR new renal replacement therapy OR ALT > 5x upper limit of normal

Supplementary Table 4. Histopathological characteristics of COVID-19 patients.

Patient ID	Tissue	SARS-CoV-2 viral antigen detected by IF	Corona virion-like particles by EM	Increased IELs	Neutrophils	Other histologic abnormalities	Other potential reasons for inflammation
Case 1	NA	NA	NA	NA	NA	NA	NA
Case 2	Duodenum & Ileum	yes	NA	no	yes (ileum)	inflammation in ileum	transplant rejection
Case 3	Duodenum	NA	yes	yes	yes (mild)	none	HIV infection
Case 4	Duodenum	yes	yes	borderline	no	none	none
Case 5	Duodenum	NA	no	no	no	epithelial damage, villous blunting and reactive foveolar metaplasia	none
Case 6	Duodenum	yes	no	no	yes	epithelial damage and foveolar metaplasia	adenocarcinoma in the duodenum
Case 7	Duodenum	yes	NA	yes	yes (mild)	none	esophageal cancer
Case 8	Duodenum	NA	no	borderline	yes (mild)	none	none
Case 9	Duodenum	yes	yes	borderline	yes (mild)	epithelial damage	none
Case 11	Duodenum	NA	yes	no	no	none	none
Case 12	Ileum	yes	yes	no	no	none	none
Case 13	Duodenum	no	yes	borderline	no	none	stage IV pancreatic cancer
Case 14	Duodenum	NA	NA	NA	NA	NA	NA
Case 15	Duodenum	yes	no	borderline	no	none	choledocholithiasis
Case 16	Duodenum	yes	no	no	no	none	biliary stricture
Case 17	Duodenum	yes	no	no	no	none	none
Case 18	Duodenum	yes	no	patchy	yes (mild)	none	biliary stricture c/f cholangiocarcinoma
Case 88	Duodenum & Ileum	NA	yes	no	no	none	none
Case 89	Duodenum & Ileum	NA	NA	no	no	none	none

IF = immunofluorescence; EM = electron microscopy; IEL = intraepithelial lymphocytes
Histologic information in reference to tissue used for IF unless not available in which case inflammatory changes as documented in EM report
NA when tissue not available and/or technique not able to be performed

Supplementary Table 5. Histopathological characteristics of pre-pandemic controls.

Patient ID	Age	Sex	Number of comorbidities §	Indication	Medications	Tissue for IF
Control 1	55	M	0	epigastric pain	famotidine, ranitidine, azelastine-fluticasone, ipratropium bromide, levocetirizine, azelastine, omeprazole	Duodenum
Control 2	66	F	0	abdominal pain	none	Duodenum & Ileum
Control 3	82	F	4	dysphagia	fluticasone-salmeterol, guaifenesin, albuterol, sennosides, Montelukast, losartan, amlodipine, acetaminophen, glipizide, atenolol, atorvastatin	Duodenum
Control 4	79	F	4	abdominal pain	losartan, aspirin, ferrous sulfate, metformin, omeprazole, pravastatin	Duodenum
Control 5	79	F	2	weight loss	spironolactone, apixaban, folic acid, torsemide, fluticasone	Duodenum
Control 6	33	M	3	iron deficiency anemia	metformin, hydrochlorothiazide, enalapril	Ileum
Control 7	56	M	3	abdominal pain	divalproex, atorvastatin, benazepril, carvedilol, linagliptin, ondansetron, lamotrigine, lithium, rabeprazole, risperidone, alprazolam, oxycodone, glimepiride, allopurinol	Ileum
Control 8	42	M	1	rectal bleeding	none	Ileum
Control 9	51	F	0	CRC screening	acyclovir, acetaminophen	Ileum
Control 10	23	F	0	abdominal pain	none	Ileum

IF = immunofluorescence
§ = Hypertension (HTN), obesity (OB), diabetes mellitus (DM), asthma (A), chronic obstructive pulmonary disease (COPD), coronary artery disease (CAD), cancer (CX), transplant (TPX)

Supplementary Table 6. Discovery Cohort basic demographics, clinical characteristics and outcomes. For age, the mean ± standard deviation is listed. For categorical variables, the number of patients followed by the percent of patients in parentheses is listed.

	Discovery Cohort (n=634)
Age (years)	64.0 ± 15.7
Male	369 (58.2)
Race/ethnicities	
Hispanic	177 (27.9)
African-American	161 (25.4)
White	137 (21.6)
Asian	35 (5.5)
Other	124 (19.6)
Comorbidities	
HTN	229 (36.1)
Diabetes mellitus	141 (22.2)
Obesity (BMI>30)*	211 (37.1)
Chronic lung disease	59 (9.3)
Heart disease	111 (17.5)
Chronic kidney disease	95 (15.0)
Cancer	66 (10.4)
HIV	11 (1.7)
IBD	7 (1.1)
Disease severity	
Mild	54 (8.5)
Moderate	361 (56.9)
Severe	158 (24.9)
Severe with EOD	61 (9.6)
Outcomes	
ICU admission	110 (17.4)
Mortality	151 (23.8)
GI symptoms	
Nausea	157 (24.8)
Vomiting	82 (12.9)
Diarrhea	245 (38.6)
Any GI symptoms	299 (47.2)

*BMI information available on 568/634 patients

Supplementary Table 7. COVID-19 disease severity and mortality in patients with and without GI symptoms in the Discovery Cohort. Fisher's exact test used to calculate p-values.

GI symptom	Severity	GI symptom		p-value
		Presence (n)	Absence (n)	
Nausea	Mild	16	38	
	Moderate	102	259	
	Severe	32	126	
	Severe EOD	7	54	0.0112
Vomiting	Mild	10	44	
	Moderate	56	305	
	Severe	11	147	
	Severe EOD	5	56	0.0156
Diarrhea	Mild	26	28	
	Moderate	152	209	
	Severe	52	106	
	Severe EOD	15	46	0.0102
Any GI symptoms	Mild	31	23	
	Moderate	188	173	
	Severe	63	95	
	Severe EOD	17	44	0.0003

GI symptom	Mortality	GI symptom		p-value
		Presence (n)	Absence (n)	
Nausea	Non-survivor	21	130	
	Survivor	136	347	0.0003
Vomiting	Non-survivor	8	143	
	Survivor	74	409	0.0008
Diarrhea	Non-survivor	39	112	
	Survivor	206	277	0.0002
Any GI symptoms	Non-survivor	47	104	
	Survivor	252	231	<0.0001

Supplementary Table 8. Basic demographics in survivors and non-survivors in the Discovery Cohort. For age, the mean ± standard deviation and an unpaired two-tailed t-test was performed. For categorical variables, the number of patients followed by the percent of patients in parentheses is listed and the Fisher's exact test or the Chi-square test was used as appropriate.

	Survivors (n=483)	**Non-survivors (n=151)**	**p-value**
Age (years)	61.3 ± 15.2	72.6 ± 14.1	**<0.0001**
Male	287 (59.4)	82 (54.3)	0.30
Disease severity			
Mild	48 (9.9)	6 (4.0)	
Moderate	318 (65.8)	43 (28.5)	
Severe	95 (19.7)	63 (41.7)	
Severe with EOD	22 (4.6)	39 (25.8)	**<0.0001**

Supplementary Table 9. Confidence intervals of odds ratio based on 1000 bootstrap iterations for severity, mortality and ICU admission in the Discovery Cohort.

Severity	**2.5%**	**50%**	**97.5%**
(Intercept)	0.015	0.071	0.320
Any GI Symptom	0.378	0.559	0.844
baseline.GenderMale	0.939	1.380	2.090
baseline.Age	1.004	1.016	1.031
baseline.DIABETES	0.600	0.995	1.729
baseline.BMI	1.009	1.039	1.069
baseline.RACE_ETHNICITY_BLACK OR AFRICAN-AMERICAN	0.293	0.503	0.876
baseline.RACE_ETHNICITY_HISPANIC	0.688	1.188	2.035
baseline.RACE_ETHNICITY_OTHER	0.771	1.286	2.245
baseline.HTN	0.636	0.990	1.543
baseline.Lung.Disease	0.272	0.562	1.063
baseline.Heart.Disease	0.673	1.095	1.842
	2.5%	**50%**	**97.5%**
(Intercept)	0.013	0.060	0.259
Diarrhea	0.433	0.653	0.978
baseline.GenderMale	0.963	1.413	2.124
baseline.Age	1.005	1.017	1.033
baseline.DIABETES	0.604	1.012	1.747
baseline.BMI	1.008	1.037	1.067
baseline.RACE_ETHNICITY_BLACK OR AFRICAN-AMERICAN	0.300	0.521	0.920
baseline.RACE_ETHNICITY_HISPANIC	0.707	1.215	2.098
baseline.RACE_ETHNICITY_OTHER	0.777	1.311	2.280
baseline.HTN	0.634	0.977	1.529
baseline.Lung.Disease	0.267	0.546	1.042
baseline.Heart.Disease	0.686	1.113	1.826
	2.5%	**50%**	**97.5%**
(Intercept)	0.013	0.058	0.271
Nausea	0.329	0.563	0.880
baseline.GenderMale	0.932	1.364	2.089
baseline.Age	1.005	1.018	1.032
baseline.DIABETES	0.609	1.015	1.738
baseline.BMI	1.007	1.036	1.065
baseline.RACE_ETHNICITY_BLACK OR AFRICAN-AMERICAN	0.322	0.543	0.946
baseline.RACE_ETHNICITY_HISPANIC	0.749	1.264	2.169
baseline.RACE_ETHNICITY_OTHER	0.816	1.340	2.338
baseline.HTN	0.615	0.950	1.477
baseline.Lung.Disease	0.248	0.516	0.980
baseline.Heart.Disease	0.676	1.091	1.830
	2.5%	**50%**	**97.5%**
(Intercept)	0.012	0.054	0.236
Vomiting	0.190	0.399	0.732
baseline.GenderMale	0.938	1.395	2.107
baseline.Age	1.006	1.018	1.032
baseline.DIABETES	0.615	1.032	1.744
baseline.BMI	1.006	1.036	1.065
baseline.RACE_ETHNICITY_BLACK OR AFRICAN-AMERICAN	0.330	0.558	0.962
baseline.RACE_ETHNICITY_HISPANIC	0.766	1.286	2.191
baseline.RACE_ETHNICITY_OTHER	0.802	1.337	2.307
baseline.HTN	0.610	0.950	1.511
baseline.Lung.Disease	0.261	0.526	0.981
baseline.Heart.Disease	0.703	1.123	1.886

Mortality	**2.5%**	**50%**	**97.5%**
(Intercept)	0.000	0.003	0.022
Any GI Symptom	0.335	0.544	0.861
baseline.GenderMale	0.679	1.049	1.703
baseline.Age	1.036	1.053	1.074
baseline.DIABETES	0.527	0.930	1.605
baseline.BMI	1.010	1.043	1.081
baseline.RACE_ETHNICITY_BLACK OR AFRICAN-AMERICAN	0.529	1.035	1.959
baseline.RACE_ETHNICITY_HISPANIC	0.867	1.597	2.899
baseline.RACE_ETHNICITY_OTHER	0.450	0.878	1.630
baseline.HTN	0.600	1.007	1.665
baseline.Lung.Disease	0.342	0.778	1.577
baseline.Heart.Disease	0.652	1.154	2.028
	2.5%	**50%**	**97.5%**
(Intercept)	0.000	0.003	0.017
Diarrhea	0.388	0.638	0.985
baseline.GenderMale	0.702	1.076	1.737
baseline.Age	1.038	1.055	1.076
baseline.DIABETES	0.531	0.945	1.608
baseline.BMI	1.007	1.041	1.079
baseline.RACE_ETHNICITY_BLACK OR AFRICAN-AMERICAN	0.562	1.071	2.020
baseline.RACE_ETHNICITY_HISPANIC	0.901	1.640	2.898
baseline.RACE_ETHNICITY_OTHER	0.468	0.900	1.709
baseline.HTN	0.595	1.001	1.665
baseline.Lung.Disease	0.333	0.752	1.561
baseline.Heart.Disease	0.660	1.166	2.020
	2.5%	**50%**	**97.5%**
(Intercept)	0.000	0.003	0.019
Nausea	0.255	0.490	0.886
baseline.GenderMale	0.669	1.041	1.719
baseline.Age	1.038	1.055	1.075
baseline.DIABETES	0.528	0.938	1.623
baseline.BMI	1.006	1.040	1.077
baseline.RACE_ETHNICITY_BLACK OR AFRICAN-AMERICAN	0.591	1.112	2.116
baseline.RACE_ETHNICITY_HISPANIC	0.956	1.718	3.085
baseline.RACE_ETHNICITY_OTHER	0.474	0.916	1.703
baseline.HTN	0.579	0.960	1.571
baseline.Lung.Disease	0.313	0.699	1.457
baseline.Heart.Disease	0.655	1.155	2.007
	2.5%	**50%**	**97.5%**
(Intercept)	0.000	0.002	0.016
Vomiting	0.116	0.364	0.753
baseline.GenderMale	0.690	1.070	1.759
baseline.Age	1.038	1.055	1.076
baseline.DIABETES	0.558	0.970	1.652
baseline.BMI	1.006	1.040	1.077
baseline.RACE_ETHNICITY_BLACK OR AFRICAN-AMERICAN	0.609	1.145	2.144
baseline.RACE_ETHNICITY_HISPANIC	1.004	1.746	3.086
baseline.RACE_ETHNICITY_OTHER	0.463	0.907	1.697
baseline.HTN	0.586	0.974	1.620
baseline.Lung.Disease	0.318	0.717	1.489
baseline.Heart.Disease	0.670	1.186	2.025

ICU admission	**2.5%**	**50%**	**97.5%**
(Intercept)	0.03	0.17	1.11
Any GI Symptom	0.46	0.75	1.19
baseline.GenderMale	1.23	2.00	3.26
baseline.Age	0.98	0.99	1.01
baseline.DIABETES	0.91	1.70	3.23
baseline.BMI	0.98	1.02	1.05
baseline.RACE_ETHNICITY_BLACK OR AFRICAN-AMERICAN	0.26	0.57	1.20
baseline.RACE_ETHNICITY_HISPANIC	0.79	1.50	2.95
baseline.RACE_ETHNICITY_OTHER	0.48	0.98	1.99
baseline.HTN	0.34	0.61	1.08
baseline.Lung.Disease	0.15	0.63	1.45
baseline.Heart.Disease	0.20	0.51	0.97
	2.5%	**50%**	**97.5%**
(Intercept)	0.02	0.16	1.10
Diarrhea	0.45	0.76	1.25
baseline.GenderMale	1.23	2.00	3.27
baseline.Age	0.98	0.99	1.01
baseline.DIABETES	0.89	1.70	3.25
baseline.BMI	0.98	1.02	1.05
baseline.RACE_ETHNICITY_BLACK OR AFRICAN-AMERICAN	0.26	0.56	1.19
baseline.RACE_ETHNICITY_HISPANIC	0.78	1.50	2.96
baseline.RACE_ETHNICITY_OTHER	0.48	0.98	1.98
baseline.HTN	0.34	0.61	1.09
baseline.Lung.Disease	0.15	0.62	1.44
baseline.Heart.Disease	0.20	0.52	0.99
	2.5%	**50%**	**97.5%**
(Intercept)	0.02	0.14	0.95
Nausea	0.45	0.85	1.42
baseline.GenderMale	1.24	2.00	3.33
baseline.Age	0.98	0.99	1.01
baseline.DIABETES	0.91	1.74	3.31
baseline.BMI	0.98	1.02	1.05
baseline.RACE_ETHNICITY_BLACK OR AFRICAN-AMERICAN	0.27	0.60	1.25
baseline.RACE_ETHNICITY_HISPANIC	0.81	1.54	3.00
baseline.RACE_ETHNICITY_OTHER	0.49	0.99	1.97
baseline.HTN	0.33	0.59	1.06
baseline.Lung.Disease	0.14	0.60	1.40
baseline.Heart.Disease	0.20	0.51	0.98
	2.5%	**50%**	**97.5%**
(Intercept)	0.02	0.15	0.98
Vomiting	0.16	0.53	1.08
baseline.GenderMale	1.21	1.98	3.26
baseline.Age	0.98	0.99	1.01
baseline.DIABETES	0.92	1.74	3.31
baseline.BMI	0.98	1.02	1.05
baseline.RACE_ETHNICITY_BLACK OR AFRICAN-AMERICAN	0.27	0.60	1.26
baseline.RACE_ETHNICITY_HISPANIC	0.82	1.55	3.01
baseline.RACE_ETHNICITY_OTHER	0.48	0.99	1.96
baseline.HTN	0.34	0.61	1.07
baseline.Lung.Disease	0.15	0.62	1.43
baseline.Heart.Disease	0.20	0.52	0.99

Supplementary Table 10. Age, gender and mortality in an External Validation (Italian) Cohort stratified by presence or absence of diarrhea on admission. For age, the mean ± standard deviation and an unpaired two tailed t-test was performed. For categorical variables, the number of patients followed by the percent of patients in parentheses is listed and the Fisher's exact test or the Chi-square test was used as appropriate.

	Diarrhea on admission (n=80)	**No diarrhea on admission (n=207)**	**p-value**
Age (years)	60.6 ± 13.9	65.5 ± 13.3	**0.006**
Male	46 (57.5)	149 (72.0)	**0.024**
ICU admission	9 (11.3)	43 (20.8)	0.06
Mortality	8 (10.0)	49 (23.7)	**0.008**
Death or ICU admission	16 (20.0)	83 (40.1)	**0.001**

Supplementary Table 11. Association between diarrhea and treatment in External Validation Cohort using Fisher's exact test. Association between diarrhea and outcome

after adjusting for treatment based on External Validation Cohort. Quantile of odds ratio based on 1000 bootstrap iterations are reported.

Treatment	Fisher's exact p-value
Hydroxychloroquine	0.409
Lopinavir.ritonavir	0.466
Darunavir.cobicistat	0.473
Tocilizumab	1.000
Steroids	0.698
Ceftrixone	0.871
Azithromicin	0.209
Piperacillin.Tazobactam	0.837
Statins	0.609
ACE.inhibitors	0.052
ARBs	0.844

Outcome: Death	2.50%	50%	97.50%
(Intercept)	0.025	0.138	0.434
diarrhea	0.111	0.313	0.699
treatment.Hydroxychloroquine	0.170	0.706	2.965
treatment.Lopinavir.ritonavir	0.740	2.397	11.006
treatment.Darunavir.cobicistat	0.477	1.723	8.455
treatment.Tocilizumab	0.000	0.472	2.692
treatment.Steroids	0.000	1.626	7.849
treatment.Ceftrixone	0.415	1.079	3.740
treatment.Azithromicin	0.252	0.651	1.462
treatment.Piperacillin.Tazobactam	0.961	3.014	11.740
treatment.Statins	0.981	2.261	5.127
treatment.ACE.inhibitors	0.588	1.503	3.413
treatment.ARBs	0.502	1.389	3.645

Outcome: ICU	2.50%	50%	97.50%
(Intercept)	8.89E-10	1.15E-08	3.40E-08
diarrhea	0.122	0.407	1.083
treatment.Hydroxychloroquine	1.52E-09	0.093814	1.265738
treatment.Lopinavir.ritonavir	33992289	318000000	4.11E+16
treatment.Darunavir.cobicistat	9669004	96256078	1.13E+16
treatment.Tocilizumab	3.17E-08	1.93167	11.84107
treatment.Steroids	0.557	4.866	46.290
treatment.Ceftrixone	0.474	1.606	8.810
treatment.Azithromicin	0.264	0.719	1.756
treatment.Piperacillin.Tazobactam	0.097	0.807	6.591
treatment.Statins	0.140	0.580	1.655
treatment.ACE.inhibitors	0.192	0.683	2.022
treatment.ARBs	0.381	1.362	3.893

Outcome: ICU or Death	2.50%	50%	97.50%
(Intercept)	0.054	0.219	0.674
diarrhea	0.126	0.297	0.585
treatment.Hydroxychloroquine	0.000	0.144	0.729

treatment.Lopinavir.ritonavir	4.142	22.183	215000000
treatment.Darunavir.cobicistat	2.143	11.491	102000000
treatment.Tocilizumab	0.000	1.198	7.012
treatment.Steroids	1.424	8.464	75358718
treatment.Ceftrixone	0.559	1.304	4.167
treatment.Azithromicin	0.224	0.510	1.003
treatment.Piperacillin.Tazobactam	0.656	2.090	7.553
treatment.Statins	0.696	1.595	3.529
treatment.ACE.inhibitors	0.615	1.409	2.987
treatment.ARBs	0.668	1.642	4.449

Supplementary Table 12. Confidence interval of AUC (95%) based on 1000 bootstrap iterations for severity, mortality and ICU admission in the Internal Validation Cohort.

Severity	**2.50%**	**50%**	**97.50%**

Age + BMI	0.539	0.587	0.598
Age + BMI + Nausea	0.567	0.608	0.619
Age + BMI + Vomiting	0.558	0.607	0.618
Age + BMI + Diarrhea	0.574	0.630	0.651
Age + BMI + Any GI symptoms	0.605	0.640	0.651

Mortality	**2.50%**	**50%**	**97.50%**
Age + BMI	0.685	0.700	0.702
Age + BMI + Nausea	0.698	0.717	0.722
Age + BMI + Vomiting	0.702	0.719	0.724
Age + BMI + Diarrhea	0.697	0.718	0.726
Age + BMI + Any GI symptoms	0.708	0.727	0.736

ICU admission	**2.50%**	**50%**	**97.50%**
Age + BMI	0.534	0.560	0.599
Age + BMI + Nausea	0.496	0.523	0.650
Age + BMI + Vomiting	0.488	0.515	0.626
Age + BMI + Diarrhea	0.562	0.649	0.667
Age + BMI + Any GI symptoms	0.570	0.647	0.670

Supplementary Table 13. IL-6, IL-8, TNF-α, and IL-1β concentrations on admission in patients with and without GI symptoms. Benjamini adjusted p-values (signed - log10 scale) from t-test are reported. Association passing a 10% FDR are highlighted in yellow.

	Nausea	Vomiting	Diarrhea	Any GI Symptoms
IL-6	-1.958	-0.473	-2.226	-2.484
IL-8	-4.098	-1.440	-2.302	-3.133
TNF-α	-0.815	-0.311	-0.406	-0.864
IL-1β	-0.295	-0.473	-0.295	-0.295

Supplementary Table 14. Cluster assignment for each of the 92 Olink analytes.

Marker	Cluster
IL8	1
AXIN1	1
OSM	1
CCL4	1
TGF.alpha	1
TNFSF14	1
HGF	1
SIRT2	1
EN.RAGE	1

Marker	Cluster
MCP.3	4
OPG	4
uPA	4
IL6	4
MCP.1	4
IL18	4
IL.18R1	4
IL10	4
CCL23	4

CASP.8	1
TWEAK	1
STAMBP	1
VEGFA	2
CDCP1	2
IL.17C	2
CXCL9	2
CST5	2
FGF.23	2
FGF.5	2
LIF.R	2
FGF.21	2
IL.15RA	2
IL.10RB	2
PD.L1	2
MMP.10	2
TNF	2
CD5	2
X4E.BP1	2
CD40	2
CCL25	2
CX3CL1	2
TNFRSF9	2
CSF.1	2
CD8A	3
CD244	3
TRAIL	3
CD6	3
SCF	3
CCL11	3
CCL19	3
TRANCE	3
IL.12B	3
CCL3	3
Flt3L	3
DNER	3
IFN.gamma	3
FGF.19	3
MCP.2	3
TNFB	3

CXCL10	4
LIF	4
CCL20	4
ADA	4
GDNF	5
IL.17A	5
IL.20RA	5
IL.2RB	5
IL.1.alpha	5
IL2	5
TSLP	5
SLAMF1	5
IL.10RA	5
IL.22.RA1	5
Beta.NGF	5
IL.24	5
IL13	5
ARTN	5
IL.20	5
CCL28	5
IL33	5
IL4	5
NRTN	5
NT.3	5
IL5	5
IL7	6
LAP.TGF.beta.1	6
CXCL11	6
CXCL1	6
MCP.4	6
MMP.1	6
CXCL5	6
CXCL6	6
ST1A1	6

Supplementary Table 15. Olink analytes in patients with and without GI symptoms. P-values from t-test comparing patients with and without GI symptoms. Signed Benjamini-Hochberg adjusted p-value (-log10 scale) are reported.

	Any GI Symptoms	**Nausea**	**Vomiting**	**Diarrhea**
IL8	-1.315	-0.654	-1.345	-1.562
VEGFA	0.006	0.014	-0.356	-0.027
CD8A	-0.823	-0.175	0.193	-0.823
MCP.3	-0.524	-1.437	-0.422	-0.254
GDNF	-1.355	-1.345	-0.014	-1.490

CDCP1	-0.449	-0.309	-0.175	-0.524
CD244	-0.023	0.110	0.126	-0.017
IL7	1.345	0.175	-0.123	1.345
OPG	-2.183	-1.209	-0.014	-2.183
LAP.TGF.beta.1	0.356	-0.006	-0.626	0.407
uPA	-0.156	-0.009	0.126	-0.385
IL6	-1.063	-1.022	-0.254	-0.747
IL.17C	-1.209	-0.287	-0.023	-1.455
MCP.1	-0.175	-0.654	-0.458	-0.187
IL.17A	-2.183	-1.097	-1.419	-2.183
CXCL11	0.058	-0.195	-0.004	0.027
AXIN1	-0.009	-0.031	-1.209	-0.026
TRAIL	1.063	0.626	0.314	0.458
IL.20RA	-0.548	-0.573	-0.563	-0.618
CXCL9	-0.573	-0.367	0.023	-1.209
CST5	-0.626	-0.187	-0.004	-0.969
IL.2RB	-0.156	-0.028	0.009	-0.044
IL.1.alpha	0.046	-0.023	0.001	0.162
OSM	-0.178	-0.117	-0.175	-0.242
IL2	-0.341	-0.424	-0.287	-0.264
CXCL1	-0.058	-0.533	-0.733	-0.164
TSLP	0.009	0.001	-0.031	-0.009
CCL4	-0.287	-0.022	0.022	-1.355
CD6	-0.001	0.027	0.363	0.001
SCF	-0.245	-0.022	-0.114	-0.082
IL18	-0.254	-0.068	0.332	-0.434
SLAMF1	-0.618	-0.707	-0.190	-0.708
TGF.alpha	-1.087	-0.626	-0.675	-1.345
MCP.4	0.191	-0.175	-0.461	0.058
CCL11	-0.327	-0.440	-1.209	-0.260
TNFSF14	0.014	-0.014	-0.434	-0.012
FGF.23	-0.556	-0.058	0.036	-1.209
IL.10RA	0.027	0.218	-0.044	-0.026
FGF.5	-0.823	-0.164	-0.027	-1.365
MMP.1	0.110	0.156	-0.218	0.027
LIF.R	-0.347	-0.009	0.310	-0.358
FGF.21	-0.495	-0.003	0.056	-0.880
CCL19	-0.044	-0.227	-0.156	-0.175
IL.15RA	-1.345	-0.175	0.022	-2.177
IL.10RB	-1.355	-0.389	-0.079	-2.183
IL.22.RA1	-0.073	-0.022	-0.009	-0.254
IL.18R1	-0.208	-0.054	0.175	-0.156
PD.L1	-0.441	-0.195	0.031	-0.702
Beta.NGF	-0.573	-0.458	-0.022	-0.495
CXCL5	-0.014	-0.144	-0.424	-0.042
TRANCE	0.933	0.458	0.236	0.654
HGF	-0.626	-0.333	-0.009	-0.529
IL.12B	0.060	0.058	-0.009	0.038
IL.24	-0.536	-0.218	0.023	-0.618
IL13	-0.007	0.075	0.068	-0.126
ARTN	-1.209	-1.365	-0.618	-1.345
MMP.10	-1.562	-0.967	-0.156	-2.073
IL10	-0.379	-0.377	0.058	-0.270
TNF	-0.643	-0.175	-0.027	-0.932
CCL23	-0.023	-0.218	0.001	0.001
CD5	-0.823	-0.357	-0.036	-0.933
CCL3	-0.933	-0.553	-0.576	-1.490
Flt3L	0.031	-0.009	-0.377	-0.009

CXCL6	-0.156	-0.385	-0.347	-0.385
CXCL10	-0.001	-0.441	-0.012	0.031
X4E.BP1	-0.733	-0.211	0.064	-1.223
IL.20	-0.247	-1.022	-0.270	-0.195
SIRT2	-0.123	-0.164	-0.332	-0.162
CCL28	-2.183	-2.183	-0.737	-2.183
DNER	0.175	0.317	0.332	0.202
EN.RAGE	-0.357	-0.193	-0.166	-0.526
CD40	-0.823	-0.079	0.001	-1.490
IL33	-0.236	-0.164	0.023	-0.287
IFN.gamma	0.218	0.044	0.175	0.270
FGF.19	-0.458	-0.001	-0.036	-1.355
IL4	-0.020	-0.175	-0.027	-0.009
LIF	-1.345	-0.526	-0.573	-1.355
NRTN	0.001	-0.168	-0.036	-0.012
MCP.2	0.319	-0.327	-0.036	1.231
CASP.8	-0.438	-0.377	-0.264	-0.731
CCL25	-0.264	0.025	-0.075	-0.626
CX3CL1	-0.556	-0.164	-0.009	-0.810
TNFRSF9	-1.345	-0.175	-0.012	-2.029
NT.3	-0.012	-0.363	0.009	-0.122
TWEAK	-0.014	0.014	-0.113	-0.012
CCL20	-0.737	-0.576	0.187	-0.823
ST1A1	0.156	-0.025	-0.175	0.068
STAMBP	-0.201	-0.171	-0.175	-0.377
IL5	0.156	-0.009	0.156	-0.009
ADA	-0.259	-0.270	0.175	-0.434
TNFB	0.009	-0.009	-0.036	0.014
CSF.1	-0.458	-0.028	0.012	-0.450

Supplementary Table 16. List of antibodies used for microscopy studies.

Antigen	**Clone**	**Vendor**	**Catalogue number**	**Host**	**Conjugation**	**Dilution**
ACE2	Polyclonal	Abcam	ab15348	rabbit	Unconjugated	1:1000
EPCAM	SPM491	GeneTex	GTX34693	mouse	Unconjugated	1:100
SARS-CoV-2 nucleocapsid	Polyclonal	NA	NA	rabbit	Unconjugated	1:2000

CD3	polyclonal	Abcam	ab5690	rabbit	Unconjugated	1:500
CD8a	C8/468-C8/144B	Abcam	ab199016	mouse	Unconjugated	1:200
MUC2	SPM512	Abcam	ab231427	mouse	Unconjugated	1:200
No known specificity (isotype control)	Polyclonal	Abcam	ab37415	rabbit	Unconjugated	variable
Yeast GAL4 (isotype control)	15-6E10A7	Abcam	ab170190	mouse	Unconjugated	variable
Mouse IgG H&L	Polyclonal	Abcam	ab150116	goat	Alexa Fluor 594	1:1000
Rabbit IgG H&L	Polyclonal	Abcam	ab150077	goat	Alexa Fluor 488	1:1000

Supplementary Movie 1. Montaged tomographic reconstruction of Golgi region of a goblet cell in apical epithelium of the terminal ileum of a COVID-19 patient. The movie begins with an overview of the goblet cell Golgi complex within a reconstructed volume of a 150 nm section. Intestinal epithelial cells border the goblet cell on the left and right side, and the apical portion of the epithelium is in the upper right, outside of the field of view. The movie progressively zooms

in to detail a membrane-bound compartment located at the trans-side of the Golgi stack. This compartment contains five presumptive SARS-CoV-2 virions that closely resemble the structures illustrated in Supplementary Figure 6 and in similar datasets of presumptive SARS-CoV-2 virions in SARS-CoV-2 infected cultured cells in Supplementary Movie 2.

Supplementary Movie 2. Tomographic reconstruction of SARS-CoV-2–infected cultured cells, prepared by high-pressure freezing and freeze-substitution fixation. The movie, which is presented for comparison with analogous structures found in tissue samples (Figure 2 and Supplementary Movie 1) that could not be preserved under similar optimal conditions, shows an overview of a central portion of an infected cell, featuring large numbers of presumptive SARS-CoV-2 virions within membrane-bound compartments, and then increases in magnification to show details of groups of presumptive virions and then individual presumptive virions themselves. Note the consistent presence of dense nucleocapsid puncta arranged within the core of each presumptive virion, membrane bilayers, and occasional surface spike densities visible through the volume.